Catechyl-lignin tissues in Vanilla orchid and Candlenut: structure/property studies

Eky Yenita Ristanti

Dissertation submitted to the faculty of the Virginia Polytechnic Institute and State University in partial fulfillment of the requirements for the degree of

Doctor of Philosophy

In

Sustainable Biomaterials

Charles E. Frazier, Chair

Justin R. Barone

Maren Roman

Young T. Kim

May 1st, 2023

Blacksburg, Virginia

Keywords: Catechyl-lignin, Structure/property studies, Seed coat, Nutshell, Glass transition temperature (T_g), Crystallinity, Morphology.

Catechyl-lignin tissues in Vanilla orchid and Candlenut: structure/property studies

Eky Yenita Ristanti

ABSTRACT

In 2012, a new type of lignin, catechyl (C)-lignin was found in the seed coat of vanilla orchid (*Vanilla planifolia*) and *Melocactus* cacti, and later in the nutshell of *Aleurites moluccana* (candlenut). This caffeyl alcohol homopolymer is the exclusive lignin in vanilla seed coat but separated in time and/or location with guaiacyl (G)-lignin in candlenut. Unlike conventional guaiacyl/syringyl (G/S-lignins) with alkyl-aryl ether linkages, intermonomer linkagsa in C-lignin are connected by benzodioxane linkages which are stiffer than alkyl-aryl ether linkages. C-lignin is unusually stable against acid-catalyzed cleavage. Tissues with C-lignin are expected to exhibit high glass transition temperature (T_g) compared to tissues with G/S/H-lignin. C-lignin also probably shows high crystallinity due to its highly linear-homopolymer structure.

The ability of some seed coats/nutshells in angiosperms to synthesize a new type of lignin is another level of lignin evolution. However, the role of C-lignin related to the function of the seed coat is unclear while it exhibits different behaviors to the regular G/S/H-lignin. These points motivated us to conduct cell-wall structure/property studies in the context of plant evolution, using microscopy, X-ray diffraction (XRD) and dynamic mechanical analysis (DMA).

Light and electron microscopes were used to identify cell's size and type of intact and macerated vanilla seed coat and candlenut shell. Vanilla seeds are tiny, sized approximately 300μm and the surface is covered with dark-colored seed coat. Candlenut is slightly smaller than walnut, with uneven, hard, dark brown shell covering the nut. Microscopy observations indicated that both seed coat and nutshell are dominated by highly lignified cells, known as sclereids. The types of

sclereids in vanilla seed coat and candlenut shell are different; vanilla seed coat has ostoesclereid-type cells, while candlenut shell has macrosclereid-type cells.

XRD was used to study tissue with C-lignin crystallinity by comparing diffractograms of vanilla seed coat and candlenut shell to Southern Yellow Pine wood diffractograms. The Southern Yellow Pine wood diffractogram corresponds to a typical native cellulose in higher plants, that is cellulose I allomorph. Diffractogram XRD analysis on vanilla seed coat and candlenut shell shows similarities to Southern Yellow Pine native cellulose, suggesting that cellulose is the contributor for crystallinity in seed coat and nutshell, and this also indicated that tissues with C-lignin is not crystalline. Crystallinities of vanilla seed coat and candlenut shell determined using peak deconvolution methods were about half of Southern Yellow Pine crystallinity.

DMA was used to measure T_g in vanilla seed coat and candlenut shell. Measurements were conducted in solvent-submersion mode using organic plasticizers to reduce the Tg to non-damaging temperatures. DMA measurement of vanilla seed coat and candlenut shell is challenging due to specimen size and shape. Specimen preparation for DMA measurement included seed coat purification for vanilla and cutting/milling for candlenut shell followed by specimen saturation in plasticizers. Compressive-torsion DMA was used to allow tiny specimens gripping. Vanilla seed coats exhibited higher glass transition temperature compared to wood, while candlenut shells exhibited various T_gs depending on specimen type/size.

Catechyl-lignin tissues in Vanilla orchid and Candlenut: structure/property studies

Eky Yenita Ristanti

GENERAL AUDIENCE ABSTRACT

Lignin is a complex organic material that constructs higher plant cell walls. Lignin provides stiffness and strength and is the landmark of plant evolution to terrestrial life. Typically, lignin in hardwood/softwood has guaicayl and/syringyl (G/S) units derived from coniferyl/sinapyl alcohols. ln 2012, a new type of lignin, catechyl (C)-lignin, was found in the seed coat of vanilla orchid (*Vanilla planifolia*) and *Melocactus* cacti, and later in the nutshell of *Aleurites moluccana* (candlenut). C-lignin is derived from caffeyl alcohol and is exclusive in vanilla seed coat but coexists with guaiacyl (G)-lignin in candlenut shells. This new type of lignin exhibits different behavior than G/S-lignin due to its chemical structure, which indicates that C-lignin is perhaps a very stiff material. C-lignin's roles are not well known and therefore, these are merit for structure/property studies in the context of plant evolution as bio-inspired new materials. Microscopy, x-ray diffraction (XRD), and dynamic mechanical analysis (DMA) were used to study the structure/property of plant tissues exhibiting C-lignin in their seed coat/nutshell. Understanding the structure/property of tissues with C-lignin is significant for developing the future use of C-lignin.

Acknowledgements

First and foremost, I would like to express my sincere gratitude to my advisor, Dr. Charles E. Frazier for his guidance, training and learning opportunities, and support during this last four years. I am very grateful to join your group and meet wonderful people there.

Secondly, I would like to sincerely appreciate my committee members – Dr. Justin Barone, Dr. Maren Roman, and Dr. Young-Teck Kim for their suggestions that helped me to gain insights into my research. I also would like to express my great appreciation to Dr. Audrey Zink-Sharp who has trained me with both light and electron microscopes.

It has been such a great time to be part of Sustainable Biomaterials. I have known and been helped by so many people here. I owe gratitude to Debbie Garnand, Shanon Lenahan, David Jones, Matt Hopkins, Angie Riegel, Trish Colley, and Mimi Harrison.

I also want to thank people who have trained and helped me with sample characterization – McAlister Council-Trouche from Virginia-Maryland College of Veterinary Medicine, Dr. Rituraj Borgohain and Patrick Finley from the Material Characterization Lab (MCL)-ICTAS, Dr. Narasimhamurthy Shanaiah from the NMR facility, and Dr. Jonathan Angle from the Nanoscale Characterization and Fabrication (NCFL)-ICTAS.

I am very fortunate to work with past and present members of Plant Polymer Group – Niloofar Shivyari, Dr. Lu Fang, Mitchell Patrowich, Sara Yazdi, Dr. Bhawna Soni, Ryan Gray, Mark Cashman, Emilie Kohler, and JC Stant. They are all very reliable and have been my place to ask for help and suggestions. I also want to thank Dr. Kim's students, Soohyung Lee and Belladini Lovely for their help.

I have never imagined doing a PhD in the US if it was not sponsored by Fulbright. I would like to express my gratitude to Fulbright-Aminef team in Jakarta and my IIE advisors in the US. My sincere gratitude is also dedicated to Dr. Lynn Thiesmeyer and Dr. Wanglin Yan from Keio University who have written my recommendation letters for my Fulbright scholarship application.

I have been part of the Ministry of Industry, the Republic of Indonesia since 2008. I am very grateful that they have been very supportive during my study, and I want to thank my colleagues for taking over my jobs and responsibilities.

I am very thankful to be surrounded by nice people who brighten my days: the past and present members of Indonesian students' association (Permias) Bela, Tian, Owen, Gladys, Kharisa, Hardi, Belladini, Dini, Adhis and many more; Fulbright-Indonesia Awardees 2018 (especially Hanif for XRD discussion and Ida for always listening to my complaint and calming my panic attack); my first roommates, Adriana and Jeanine, that have made the first semester less stressful; and my Zumba instructors and friends at Blacksburg Community Center.

Finally, I would like to thank my family (Mom, Dad, and my sister, Lia) for always cheering me on during my ups and downs. I am forever grateful.

Table of Contents

Chapter 1
Introduction

1. 1 Motivation and Research Outline

Over decades, scientists have learned lignin structure, biosynthesis, and reactions. Lignin chemistry is an interesting field to look up to, since there are many aspects about lignin that are not well understood. Traditional lignin from softwood and hardwood have been known to be a complex copolymer with β-O-4 linkages dominated the structures and made up of three primary monolignols known as p-coumaryl, coniferyl, and sinapyl alcohol. The role of these traditional lignin also has been known to provide mechanical support, conduct water, and protect cells from pathogens.

A new type of lignin derived exclusively from caffeyl alcohol was unexpectedly discovered in 2012, known as catechyl lignin (C-lignin). C-lignin is a linear homopolymer which is connected by benzodioxane intermonomer linkages; making rotation is restricted compared to guaiacyl structure. This new type of lignin was found in seed coats of vanilla orchid (*Vanilla planifolia*) and some cacti. Later, it is reported that C-lignin was also found in some Euphorbiaceae and Cleomaceae seed coats together with guaiacyl/syringyl lignin. Surprisingly, C and G lignin is not copolymerized in the seed coat of Euphorbiaceae and Cleomaceae, indicating that both lignins are deposited at a different time.

C-lignin is believed to be the type of lignin favored in biorefinery due to its acid resistance thus it will not repolymerized. The acid resistance is probably one of C-lignin properties that has been known up to now. Current research mostly focused on attempts to understand the mechanism of C-lignin biosynthesis in the seed coat. In the projection of future applications of C-lignin, there

is not enough study on material structure-properties relationships, while several studies have moved forward on lignin applications for carbon fiber production and in catechol monomers production via hydrogenolysis.

The overarching aim of this study is to understand lignin structure-properties relationships in the context of evolution. Main work of this study is dedicated to study rheology of *in situ* non-conventional catechyl lignin in vanilla (*Vanilla planifolia*) seed coat and candlenut (*Aleurite* moluccanus) shell and the correlation with plant evolution which are covered in Chapter 2 and Chapter 3. Chapter 4 is aimed to study hydroxymethylated resorcinol (HMR)-lignocellulose components (lignin and pectin) interactions in softwoods.

1.2 Literature Review

1.2.1 Lignin Definition and Occurrence

Lignin was first recognized by Anselme Payne in early 1838 as a material with higher carbon content than that in cellulose of a nitric acid treated wood which called as “encrusting material”. It was F. Schulze who firstly introduced “lignin” term in 1865 and in 1890, E. Bamberger reported that the material called “lignin” contained methoxyl groups which were not found in pure cellulose.[1]

Lignin definition has developed as better understanding in its structure and properties is revealed. The most accepted concept about lignin is that it is an amorphous, polyphenolic material derived from an enzyme-mediated dehydrogenative polymerization of three phenylpropanoid monomers: coniferyl (1), synapyl (2), and p-coumaryl alcohol (3) alcohols as shown in Figure 1.[2]

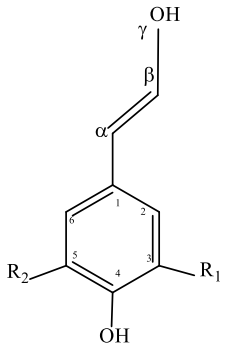

(1). $R_1 = OCH_3$, $R_2 = H$

(2). $R_1 = R_2 = OCH_3$

(3). $R_1 = R_2 = H$

Figure 1.1 *Phenylpropanoid unit*

Lignin is the second most-abundant polysaccharides after cellulose. Lignin, a phenolic rich compound, is found in spermatophytes and pteridophytes, except in some aqueous species. Lignin is present at the highest concentration in the secondary cell wall, especially in certain tissues such as the fibers, xylem vessel and tracheid. In the primary cell wall of the same tissues, the abundances of lignin are smaller and in some other cell types, the presence of lignin corresponds to stress.[3]

The concept that lignin originated from polymerization of coniferyl alcohol has been introduced from the late 19th century and early 20th century, but the metabolism processes that resulted in coniferyl alcohol were not known until 1960s. Coniferyl alcohol and other monolignols are the derivatives of phenylalanine obtained through general phenylpropanoid pathway as an initial step of metabolism process. The toxic and unstable monolignols undergo glycosylation on their phenolic hydroxyl group and result in monolignol glycosides.[4]

The role of lignin in plants is significant to help plants survive in land ecosystem. Lignin gives stiffness and strength to the stem, making plants structure strong enough to adapt with terrestrial landscape. The presence of lignin in the xylem vessel supports water and solutes transport by waterproofing the cell wall.[5] Lignin also acts as protection to infection. Plant cell wall responses to microbial infection involve multiple biochemical pathways, such as phenylpropanoid metabolism. Phenylpropanoid depositions is the significant indicator of defense against pathogen.[6-8]

Lignin interacts with cellulose, hemicellulose, and other polysaccharides within the cell wall.[9] Lignin and hemicellulose are amorphous while cellulose forms partially crystalline microfibrils.[10] Cellulose is a linear polymer chains of β-1,4 linked glucose residues, naturally appears as appears as crystalline cellulose. Cellulose crystallinity is affected by the arrangement of glucan chains, which thought to be spontaneously incorporated into cellulose.[11, 12] Hemicellulose is heterogenous polysaccharides, characterized by a β-1,4 linked backbone in which C1 and C4 are in equatorial position. Hemicellulose can be comprised of pentoses (xylose, arabinose), hexoses (mannose, glucose, galactose), and sugar acids.[13]

1.2.2 Evolution of Lignin

The oldest unequivocally identifiable land plants existence is about ~500 years ago.[14] The land plants arose from green algae, *Chlorophyta,* indicated by the similarity of cell wall chemistry and the identical photosynthetic pigments.[8, 14, 15] Land colonialization by plants has caused a necessity for plants to adapt with the new environment by changing their physiologies and structures.[16] This adaptation resulted in the development of some important metabolisms to synthesis lignin, flavonoids, cutins, and plant hormones in vascular plants from primary metabolism in algae.[17]

Plant evolution which took place for almost 1800 million years can be categorized into four phases[18]:

(1). *The Biochemical Phase (prior Ordovician period, 510-480 mya)*. The evolution stage was highlighted by the establishment of essential biochemical pathways in cyanobacteria and algae h previously living in an aqua environment.

(2). *The Anatomical Phase (Ordovician, 488.3-443.7 mya– Silurian period, 443-416 mya)*. The harsh environment during this period was more challenging than competition with other, leading to the evolution of tissue types and alternation generation that characterizes pteridophytic life history.

(3). *The Morphological Phase (Devonian period)*. The migrated plants were already settled in the terrestrial land. The further arrangement on their tissue types engendering more complex morphological form.

(4). *The Behavioral Phase (Carboniferous, 359.2-299 mya – Permian, 299-251 mya).* Characterized by a more established ecosystem in which each ecosystem component such as

individual plants, abiotic environment, biotic environment contributed to the ecosystem dynamic.

Methods to classify the vascular plants were also developed as more recent findings and evidence revealed. Initially, cladistics analysis, which uses similarity of derived character (synapomorphies) to group clades and the criterion of parsimony (reducing character state changes) were used to rearranging phylogeny. Later, advanced molecular biology provides more reliable methods to study phylogeny. Classification of bryophytes, lycopsids, and zosterophylls into one of crown-group vascular plants; knowledge that progymnosperms are the pioneer of seed plants; coniferophytes give rise to platyspermics seed ferns; and that angiosperms and Gnetales are related, are based on morphological and molecular evidence.[19, 20]

There are adequate cell structures and chemical evidence to support the claim that Chlorophyta is the progenitor of vascular plants and Bryophytes.[21] The most powerful evidence is the similarity of photosynthetic apparatus. Chloroplast pigment in land plants can also be found in most green algae, but not in the other type of algae. The second evidence relates to the synthesis of land plant important components, lignin and sporopollenin. Some green algae can produce sporopollenin and enzymatic components resemble lignin-synthesize reaction in vascular plants compared to other algae class. Last, the existence of cellulose and hydroxyproline-rich protein in the cell wall and flagella-characteristic of green algae, although these compounds also exist in some other algae. More specifically, the green algae group which is believed to give rise to the vascular land plants and bryophytes, are a group of green algae which contains the Charales and some members of the class Prasinophyceae due to similarity in the mechanism of nuclear and cell division, the structure of flagellate motile cells, the nature and subcellular location of glycolate oxidizing enzyme and apparently, they also have similar enzyme involved in urea breakdown.[22]

The evolution of land plants has led to the great transformation on their anatomy and morphology. These transformations started in the cellular level to conduct essential biochemical processes that result in organic materials they need to survive in land environment. Cellulose and lignin are two critical cell wall components to support terrestrial adaptation.[23] Cellulose, existed as cellulose microfibril in the primitive cell walls, apparently retained in the modern land plant as cellulose enhance the mechanical properties required for terrestrial adaptation.[24] Lignins are commonly found in the xylem of Tracheophyta and rarely existed in non-vascular plants. Lignins in general are present in the vascular and mechanical tissues, but they can also exist in seeds, seed coats, epidermal cells, and in *Humulus* and *Liriodendron*, woody perianth. Pure lignin is accumulated in the middle lamella as a result of pure carbohydrate transition around the lumen.[25]

Phenylpropanoid metabolism is among the secondary metabolisms evolved during the transition of plant ancestors to the terrestrial land. It was the tracheophytes which developed the ability to store the phenylpropanoid polymer lignin into their cell walls. However, metabolic scaffold of monolignol biosynthesis has been established before the occurrence of tracheophytes.[26] Views on the evolution of lignin can be started with the enrollment of enzymes of primary metabolisms, such as phenylalanine ammonia-lyase (PAL), cinnamate 4-hydroxylase (C4H), 4-hydroxynnamoyl-CoA ligase (4CL), hydroxycinnamoyl transferase (HCT), *p*-coumaroyl shikimate 3'-hydroxylase(C3'H), caffeyl-CoA O-methyltransferase (CCoAOMT), (hydroxy)cinnamoyl-CoA reductase (CCR), and (hydroxy)cinnamyl alcohol dehydrogenase (CAD), to conduct secondary metabolisms.[27]

The next step to observe after identifying enzymes involved in lignin evolution is the transcriptional regulation of lignin biosynthesis. The transcriptional regulation of lignin is found to be the same to those regulating the biosynthesis other secondary wall components.[28] In

Arabidopsis, MYB46 regulates the formation of secondary cell wall and also upregulates two transcriptional factors, MYB58 and MYB63, that are dedicated for lignin biosynthesis in Arabidopsis. The lignin biosynthesis regulated by MYB58 and MYB63 is the S lignin biosynthesis and therefore it differs biosynthesis pathway of S lignin to G and H lignins.[29, 30] Regulation of secondary wall is complicated and involving many factors such as dual function regulators, combinatorial complexes, and cross talk between pathways.[31]

1.2.3 Lignin Biosynthesis

In the wood cells of vascular plants, lignification or lignin biosynthesis is started from the primary cell walls adjacent to the cell corner, and then continued to the intercellular layer primary wall and secondary wall before accumulated in the middle lamella.[32] Lignin compositions are different in the gymnosperms and angiosperms and commonly characterized based on nitrobenzene or cupric oxide oxidation products. Lignin oxidation with alkaline cupric oxide results in six vanillyl and syringyl phenols in the form of aldehydes, ketones, and carboxylic acids. Meanwhile, oxidation of lignin in the non woody vascular plants can also produce ferulic and *p*-coumaric acids.[33]

Lignin abundance in the cell walls varies in the cell wall itself, different taxa, and species. The middle lamella of angiosperms has 50-70% lignin content, while the secondary cell wall only has 20% lignin. Gymnosperms' middle lamella has the same amount of lignin as angiosperms, but the lignin content in the secondary cell wall is only 16-19%. Traditionally, the composition of lignin in angiosperms and gymnosperms are differentiated by their guaiacyl and syringyl proportion. Angiosperms (hardwood) are composed of almost a similar proportion of guaiacyl and syrinyl, while gymnosperms' lignin dominated by guaiacyl with small proportion of p-hydroxyphelyl.[29, 34]

Sakakibara[35] proposed structural model for softwood lignin based on degradation products of protolignin by hydrolysis with dioxane-water and catalytic hydrogenolysis. The hydrolysis and hydrogenolysis resulted in 28 units. Products obtained from hydrolysis are arylglycerol-/3-aryl ether, diarylpropane, and resinol type compounds. Pinoresinol was absent among hydrolysis products of softwood lignin, but a large quantity of syringaresinol could be obtained from hardwood lignin. However, lignin polymer structure's configurations arrangement in vivo is thought to be either full biochemically controlled or randomly assembled by exchanging monomeric precursor units.[36]

Lignin biosynthesis is a complex process that involved monolignol biosynthesis, transport, and polymerization.[37] Lignin biosynthesis has been studied using isotope-labeled lignin precursors and enzyme experiments.[38] Monolignol biosynthetic pathway aims to convert phenylalanine or tyrosine into one of three monolignols in the favor of enzymes such as cinnamate 4-hydroxylase, caffeate O-methyltransferase, and cinnamyl alcohol dehydrogenase.[4, 39] The process of monolignol biosynthesis occurs in these following steps[40]:

(1). Deamination of phenylalanine

(2). Hydroxylation reactions of aromatic ring

(3). Phenolic-O-methylation

(4). Conversion of side chain carboxyl group into an alcohol.

Hydroxylation and methylation reactions occur at the level of cinnamic acids; and conversion of p-coumaric, ferulic, and sinapic acid into corresponding monolignols by 4-coumarate:CoA ligase (4CL), CCR, and CAD has been found to be indisputable[41] and first revision to this pathway was made when expression of caffeoyl-CoA O-methyltransferase (CCoAOMT) was found to occur at the same time with lignin deposition in Zinnia's tracheids.[42]

Following monolignols biosynthesis is the process of transporting monolignols from synthesis sites inside the cell throughout cell membranes to reach secondary cell walls. Monomers transport will allow lignin monomers to diffuse across lipid bilayers and then attach to cell wall via crosslinking.[43] Liu and co-workers[44-45] summarized three possible model of lignin monomer transport mechanisms:

(1). Exocytosis that occurs via Endoplasmic Reticulum-Golgi-derived vesicles. This model was suggested based on autoradiographic and immunochemical studies.[46] But, Kaneda and co-workers' experiment on lodgepole pine,[47] which used radioactive [^{3}H] phenylalanine to detect locations of monolignols act on lignification, Golgi vesicles are not significantly involved in exporting monolignols.

(2). Passive diffusion of via hydrophobic reactions through the plasma membrane. This mechanism is proposed to accommodate the non-conventional lignin monomers found in transgenic plant cell wall. Lignin monomers is possibly transported through plasma membranes. Evidence for this mechanism is based on *in vitro* experiments using model membranes in which hydrophobic-hydrophilic interaction allows incubated monolignol-like compounds to partition through the membrane.[48] Recent finding regarding passive diffusion mechanism studied using lignin-related compounds (LRCs) also shows that passive diffusion through plant and microbial membrane is possible.[49]

(3). Active transport mediated by secondary active transporters. Tsuyama and co-workers[50] reported that transport activity of coniferin in membrane vesicles prepared from softwoods and hardwoods tissues is ATP-dependent. Later, Shimada and co-workers[51] reported that coniferin and p-glucocoumaryl alcohol transports in bamboo tissues are also mediated by vacuolar type

H^+-ATPase and H^+ gradient across membrane, implying contributions of electrochemical potential in the transport process.

Monomers transported into the cell wall undergo dehydrogenative polymerization and form radicals that originate from peroxidases and laccases. These radicals are relatively stable due to coupled electron delocalization that gives single electron-density to sites around the aromatic ring and the conjugated side- chain β-position. Following dehydrogenation and radical formation, monolignol radicals will dimerize, but mostly polymerize.[40]

Lignin polymerization is the final steps of lignin biosynthesis in which monolignols secreted from cells are activated by oxidation system in the cell wall (such as laccase/O_2 and peroxidase/H_2O_2). Lignin is polymerized via a combinatorial radical coupling process which allows coniferyl, sinapyl, and p-coumaryl alcohol.[52] Lignin polymerization results in variations of racemic polymers with varied in physicochemical features that lead to lignin content, structure, and compositional variations in different taxa, cell types, growth stages, and location across the cell wall. This explains why gymnosperms have more G-unit monolignol which dominated by β–5, 5–5, β–β carbon–carbon linkages while angiosperms have more ether type β–O–4 linkages of S-unit.[53]

1.2.4 Unusual Monolignols

Lignification process can deviate from the traditional way as recent studies on mutant and transgenic plants show an uncommon subunit, dihydroconiferyl alcohol. Mutation affects the lignification process and results in the variation of lignin.[54] Traditional definition of lignin as complex natural polymers from oxidative polymerization of hydroxycinnamyl alcohol needs to be redefined as it does not accommodate the finding of uncommon subunits.[55] Some examples of uncommon lignin found in the transgenic plants are lignin with reduced caffeic acid/5-

hydroxyferulic acid O-methyltransferase activity in genetically modified poplar[56], lignin without cinnamyl alcohol dehydrogenase in loblolly pine mutant[57], and unusual lignin in mutant Arabidopsis.[58]

Defining lignin accurately has been a difficult task since lignins cover a very diverse class of polymers. Ralph and co-workers[59] define lignin as natural polymer derived from 4-hydroxyphenyl-propanoids and peroxidase is involved in the polymerization process. The mechanism of lignification is controlled both chemically and physically. Key features in the lignin structures are the predominant units, kinetically determined stereochemistry, β – β -unit conundrums, β – 1 -structures and other natural lignin monomers that are usually ignored than the primary monolignols. Later, it is questioned what really control the lignification to result in a variation in lignin structures.[60]

Genetic engineered plants have improved in understanding of conventional lignin. There are currently more phenolics compounds now regarded as lignin monomers and form a racemic polymer through a radical polymerization.[61] Non-conventional sub units of lignin have long found in the grasses, kenaf, pine, and tobacco that distinguished them from the conventional lignin.[39] Kenaf lignin, for example, shows a 50% of its subunits are acetylated, which associated with a relatively high syringyl to guaiacyl ratio (6:1, compared with 1;1 in most angiosperms). Transgenic tobacco also shows a different lignin monomer composition. The variation of subunits indicated the diversity between taxonomic groups as well as within individual species. This also leads to a new perspective on how lignin structure-function correlated in the different plants.

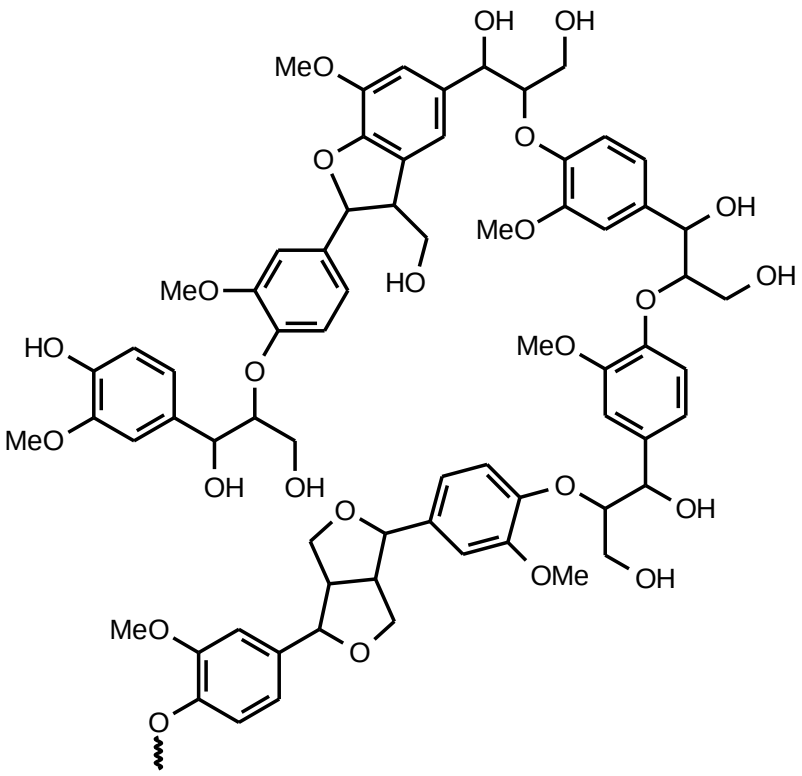

Figure 1.2 *Simplified gymnosperm's lignin structure*

1.2.5 Catechyl Lignin Discovery and Current State of Properties Knowledge

The existence of a homopolymer of caffeyl alcohol in the seed coat of both monocot and dicot was reported in 2011.[62] This type of lignin was found in the seed coats of vanilla orchid *Vanilla planifolia* as well as two other vanilla species, *Vanilla pompona* and *Vanilla tahitensis* but not in other seed coats of *Phalaeonopsis* orchid species. In other plants, the C-lignin was also found in the seed coat of *Euphorbiceae* (*Jathropa curcas*, *Vernicia fordii*, and *Aleurites moluccana*) and *Cleomaceae* (*Cleome hassleriana*). However, in *Euphorbiceae* and *Cleomaceae*, C-lignin exists together with G/S or G lignin.[63]

Cathecyl (C) and 5-hydroxyl guaiacyl (5-OH-G) units that probably come from polymerization of corresponding caffeyl and 5-hydroxy coniferyl alcohols are not found in conventional lignin. Analysis using NMR techniques revealed that C-lignin in vanilla seed coat is a linear polymer derived from caffeyl alcohol, linked by benzodioxane units, with linkage derived from β – O – 4-type end-wise radical coupling reaction of a caffeyl alcohol radical at the β-position with the radical of the catechol end unit, at the 4 – O – phenolic position.[62]

Analysis of C-lignin in the family Cactaceae[64] also found that the C-lignin isolated from the seed coat of *Melocactus salvadorensis* is a linear benzodioxane polymer. Analysis of cell wall from other vegetative tissue (stems, spines, spine base, stem/root interface) of this plant did not show the existence of C-lignin. Instead, these vegetative parts contain a predominantly G and S unit, with small amounts of H-units. There are not so many studies regarding C-lignin structure and properties. The potential pathway of C-lignin biosynthesis is studied by comparing lignin pathway genes in Arabidopsis to the *Vanilla planifolia* genes homologs potentially involved in the monolignol pathways.[65]

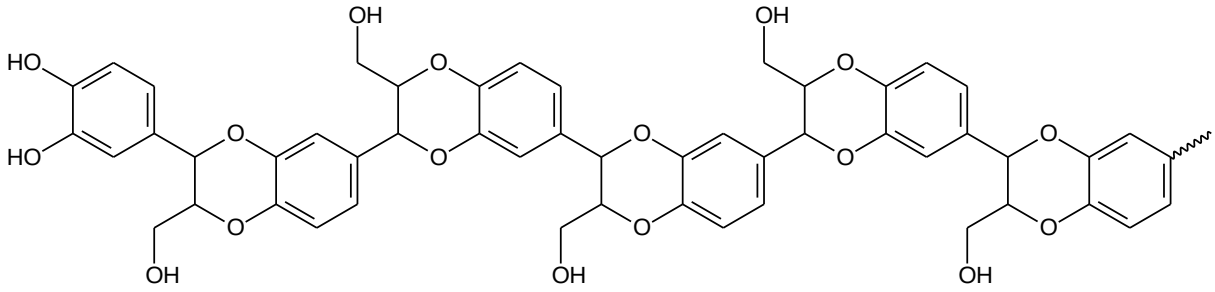

Figure 1.3 *Catechyl lignin structure*

1.2.6 Lignin Analytical Method

Isolation and Degradation

Variation in lignin structures makes chemical characterization difficult. Milled wood lignin (MWL) is considered to be the best preserved native lignin structure and reactivity.[66] Isolation of MWL involves several steps starting from particle size reduction using a Wiley mill, followed by rotary or ball-milling, and extraction with dioxane:water. Duration of milling affects MWL yield.[67] Other methods used to isolate lignin are Braun lignin[68] and cellulolytic enzyme lignin (CEL).[69] Braun lignin is low yield and molecular weight, but high in phenol content.[70] (CEL) was reported to be able to give higher yield with less degradation than MWL.[71]

Lignin content in biomass can be determined quantitatively and qualitatively using a wide range of wet chemistry to various spectroscopy methods.[72] Quantitative method determined lignin as acid soluble lignin (ASL) and acid insoluble lignin (Klason lignin). The procedure is preceded by acid hydrolysis of extractives free-biomass samples into monomeric form that is soluble in acid.[73] There are several standard procedures have been established to determine acid insoluble lignin in wood and pulp such as TAPPI Method T 222[74] and Laboratory Analytical Porcedure (LAP) on Determination of Structural Carbohydrates and Lignin in Biomass developed by National Renewable Energy Laboratory (NREL).[75]

Lignin building units are commonly characterized based on their nitrobenzene or cupric oxide oxidation products.[33] Nitrobenzene oxidation of lignin is an oxidative-cleavage reaction of lignin when heated with nitrobenzene in the presence of aqueous alkali.[76] Products of nitrobenzene oxidation are varied among species indicating different types of lignin monomers that includes vanillin, aldehydes, and acids.[77-79] Cupric oxide oxidation is more applicable in geochemical sample. Cupric oxide oxidation in lignin compounds in alkaline condition results in phenols in the

forms of aldehyde, vanillyl, syringyl ketones, and carboxylic acids.[80] In addition to nitrobenzene and cupric oxidation methods that used to characterize lignin monomers, acidolysis is an important method used to confirm the existence of β-O-4 and β-5 bonds in lignin.[81] Acidolysis is the term used when lignin or biomass sample is refluxed at 100°C with 0.2 M HCl in dioxane: water (9:1, v/v).[82]

Dynamic Mechanical Analysis (DMA)

DMA is an instrument used to measure the elasticity of material. The Weisenberg Rheogoniometer (~1950) and the Rheovibron (~1958) were among the first commercially available DMA instruments. The basic principle of DMA is to apply an oscillating force to a sample and analyze the material's response to the force. DMA is a more reliable tool to detect Tg in polymer compared to differential scanning calorimetry (DSC) or thermomechanical analysis (TMA) due to its sensitivity in detecting beta and gamma transitions.[83]

The applied strain (γ) and stress (σ) are given by,

$$\gamma(t) = \gamma_0 \sin(\omega t) \quad \text{(Eq. 1.1)}$$

$$\sigma(t) = G\,\gamma_0 \sin(\omega t) \quad \text{(Eq.1.2)}$$

DMA experiments are generally performed within linear viscoelastic region (LVR), wherein, when a sinusoidal stress is performed on a perfectly elastic solid, the resulting sinusoidal strain will perfectly follow the stress with a phase lag (δ) equal to zero or termed as in-phase. Meanwhile, when the same stress is applied to a viscous liquid, the corresponding strain will follow the stress with a phase lag (δ) of 90° or known as out-of-phase. Viscoelastic material response is in between $0° \leq \delta \geq 90°$ as illustrated in Figure 5.[84]

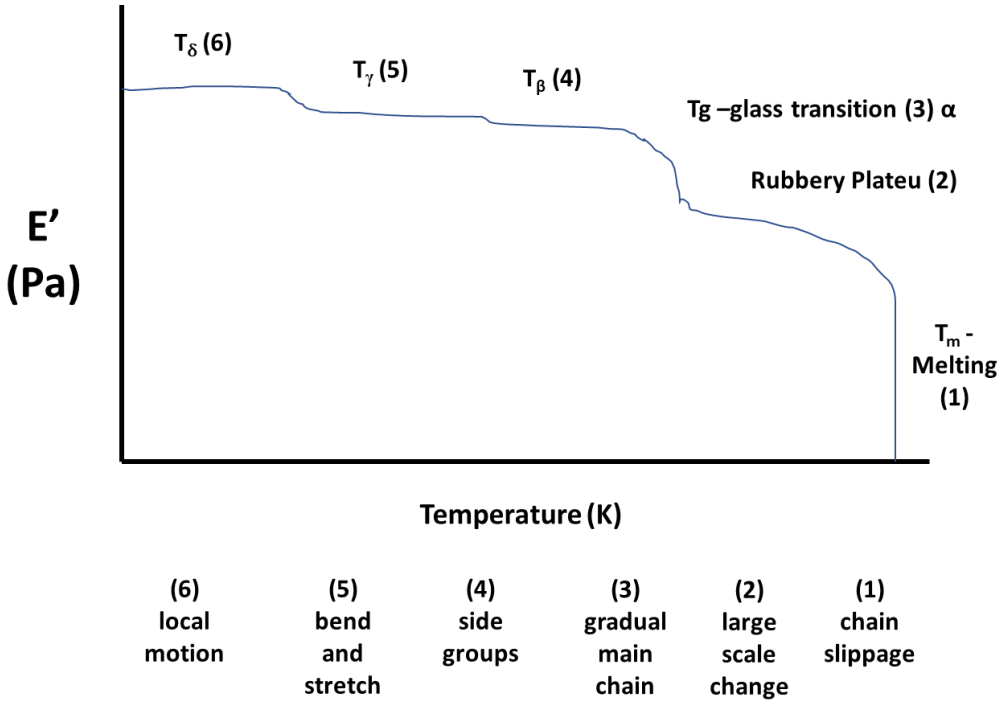

Figure 1.4 *Idealized temperature scan of a polymer (Adapted from Menard, 1999)*

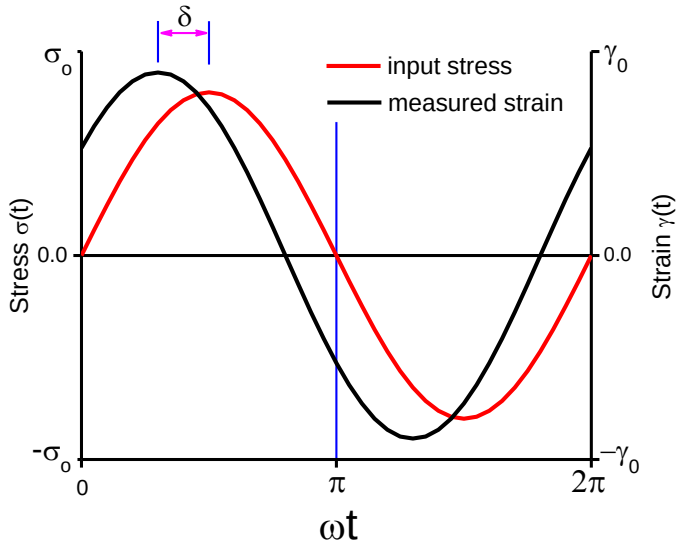

Figure 1.5 *Response of viscoelastic materials*

.

DMA measurement of lignocellulose materials benefit to understand organization of cellulose, hemicellulose, and lignin.[85] DMA response of lignocellulosic materials exhibit single major thermomechanical softening transition attributed to lignin.[86] Most of DMA analysis were done for lignocellulose with conventional lignin, such as wood, bamboo, and switchgrass.[87-89] Such materials are sensitive to moisture and thermorheologically complex. Solvent-submersion rheology using organic solvent has demonstrated effectiveness in reducing the T_g to non-damaging temperature.[87, 88] In addition to safety concern, lignocellulose materials such as fiber and grass are usually lack of mechanical integrity. DMA measurement in such materials will need specimen gripping to avoid slippage. Chowdhury and coworkers have demonstrated that tensile-torsion and compressive-torsion combined with solvent-submersion practically reliable to probe lignin glass transition in lignocellulosic materials. [90]

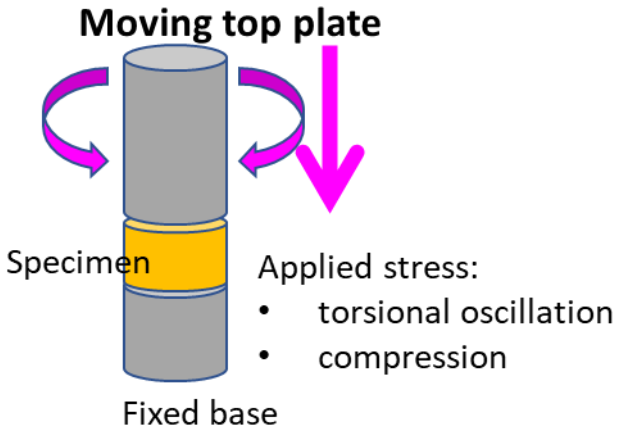

Figure 1.6 *Compressive-torsion DMA principle.*

Nuclear Magnetic Spectroscopy

Nuclear magnetic resonance (NMR) is a reliable technique to study lignin complex structure and interunit linkages. Various NMR techniques, either 1-Dimensional (1D) NMR or 2-Dimensional (2D) NMR have been used to analyze isolated lignin from various sources. Purified isolated lignin gives the best NMR spectra, but crude isolates and unfractionated cell wall materials can also be analyzed using different NMR techniques.[91-93] Due to the diversity and irregularity of interunit linkages in lignin polymers, lignin spectra appear broader and lacking distinctive characteristics compared to other comparable size natural polymers. Stereochemical complexity in lignin causes significant broadening due to the overlapping NMR signals in proton (^{1}H) spectroscopy, thus ^{1}H-NMR itself is not a very useful method for assigning lignin structure.[94]

Carbon (^{13}C) NMR has been used to identify qualitative (signal assignment) and quantitative (the relative abundance of substructures per aromatic ring) of non-acetylated lignin as well as acetylated lignin.[95] Aromatic carbon atoms in lignin have chemical shift between 104-160 ppm. Hardwood signals are characterized by intensive signals of carbon atoms 3/5 and 2/6 of syringyl units which are absent in softwood lignin. The Aliphatic region of lignin ^{13}C-NMR spectra has chemical shift between 50-90 ppm. The signals in the aliphatic region are methoxy signal, carbon atoms in β, α, and γ of β–O–4 linkages. ^{13}C-NMR shows relatively high intensity of signals correlated to β–O–4 and β–β in hardwood than in softwood, indicating that hardwood has more β–O–4 and β–β, while softwood shows high intensity of signal associated to β–5 linkage.[96]

The 2D ^{13}C,^{1}H-correlated NMR techniques such as heteronuclear single quantum coherence spectroscopy (HSQC) and heteronuclear multiple bond correlation spectroscopy (HMBC) are known to be the most reliable method to distinguish different lignin unit and interunit linkages that cannot be done using 1D-NMR such as dibenzodioxocine and spirodienone interunit linkages.

However, HSQC is not straight forward for quantification method. Sette and coworkers[97] reported a quick quantitative HSQC (QQ HSQC) that are highly reproducible to quantify C_9 unit in milled wood (MWL), enzymatic mild acidolysis (EMAL) and kraft lignins.

Microscopy

Various microscopy techniques have been introduced over decades to visualize lignin distribution and lignification in the cell wall of different plants.[98-100] Histological technique has been used over years and are still widely used. Histological staining for lignin can indicate the site and variation of lignin component in plant cell wall. Common histological stains used for staining lignin are acid phloroglucinol, chlorine-sulphite, Azure B, and diazotized sulphanilic acid. Most information on lignin staining methods reported is using wood tissues. Reactions of lignin phenolic compounds to histological stains are summarized on Table 2.1.[101]

Table 2.1 *Reactions of lignin phenolic compounds to histological stains (Adapted from Akin, D.E., 1989)*

Compound	**Histological Stain**			
	Acid Phloroglucinol	**Chlorine Sulphite**	**Azure B**	**Diazotized Sulfanilic Acid**
Syringaldehyde	Red	0	0	Orange
Ferulic acid	0	Pink	0	Red
Vanillin	Yellow (weak)	Yellow	0	Orange-Red
p-Coumaric Acid	0	0	0	Red-Orange
Methyl *p*-Coumarate	0	0	0	Red-Orange
Bermudagrass lignin	Yellow	Yellow	Blue-Green	Brown-Orange
Lignin-Carbohydrate Complex	Orange	Orange	0	Orange-Brown

Thin sectioned and stained samples are used for light microscopy examination. A compound light microscope has objective lens and ocular or eyepieces, which work together to create a total magnification, *M* of the image (M_{obj} x M_{oc}) ~ 40 to 1000-fold. In transmitted light microscopy, transmitted light is used to obtain information from the sample, in which, signal depends on the interaction between light and sample. The form of light-sample interaction can be light absorption, optical path, phase differences for scattered and un-scattered beams, phase gradients, or birefringence.[102] Reflected light microscopy is also known as incident light, epi-illumination, or metallurgical microscopy; it can be used to image specimen that remain opaque to a thickness of 30 microns. Reflected light microscopy is used in wide range fields, from metallurgy to biology, in which samples are unable to pass light. In reflected light microscopy, light is directed onto the specimen surface and returned to the microscope objective by specular or diffused reflection.[103]

Scanning electron microscopy (SEM) is used to analyze microstructure morphology and chemical composition. In SEM, image formation depends on the acquisition signals produced electron beams and specimen interactions, that categorized into elastic and inelastic interactions. Deflection of the incident electron by the specimen atomic nucleus or by outer shell of similar energy creates elastic scattering. Interactions between the incident electrons and the electrons and atoms of the sample that cause energy transfer by the primary beam electron creates inelastic scattering. Interaction between primary electron beam with secondary electron emission signal is the most widely used signal source in SEM. [104]

Microscopy examination of hard tissues usually required maceration to view structure of individual cells and to measure sectioned material. Several maceration techniques are available such as using acetic acid and sodium hypochlorite[105] and Jeffrey's fluid (1:1 aqueous nitric acid:aqueous chromic acid)[106]. Franklin used 1:2 v/v glacial acetic acid:hydrogen peroxide at 60°C

and atmospheric pressure to macerate wood-resin composite for 24-48h. Later, he modified his method by changing the proportion of glacial acetic acid:hydrogen peroxide into equal volume. This method is incidentally more useful for macerating wood for microscopic examination, because it gives a good and clean macerated.[107, 108]

Embedding is one of the various techniques to harden samples. Different types of embedding media have been used; paraffin wax is the oldest media and is still being used today. Other media such as Steedman's wax (polyester wax), glycol methacrylate, butyl methyl-methacrylate (BMM), spur resin, and LR White. LR White is a low viscosity acrylic resin, liquid at room temperature and penetrates well to the secondary vascular system. This resin is available in several grades of hardness and can be polymerized either by heating or adding accelerator for room temperature polymerization. [102]

X-Ray Diffraction (XRD)

XRD is a well-known method to determine crystallinity of partially crystalline materials. In the cell-walls of higher plants, hemicellulose and lignin are amorphous, while cellulose shows both crystalline and amorphous behavior. Crystallinity in lignocellulosic materials such as wood, is defined as the weight fraction of crystalline cellulose. Cellulose XRD patterns show reflections superimposed on the diffuse background. Due to the small size of cellulose crystallite and large amount of lignin amorphous constituent, it is difficult to separate the amorphous background intensity arisen from cellulose crystallite.[10] Cellulose has four different allomorphs that has been identified using XRD: celluloses I, II, III, and IV. Native cellulose I is the most abundant form in nature and to simultaneously crystallize in a one-chain triclinic structure I_α and a two-chain I_β. Regenerated or cellulose II has antiparallel arrangement in a two-chain unit cell. Cellulose I can

be converted into cellulose II by treating with 20% sodium hydroxide solution or known as mercerization. Cellulose III is obtained by treating native cellulose with dry liquid ammonia. Cellulose III_I is used to denote cellulose III that obtained from cellulose I and cellulose III_{II} if it is derived from cellulose II. Treating cellulose III with heat will result in cellulose IV. The same denotation is used to denote cellulose IV.[109]

Crystallographic index (CI) is a parameter used to determine the relative amount of crystalline material in cellulose. Besides XRD, solid state ^{13}C-NMR, infrared (IR) spectroscopy and Raman spectroscopy are also commonly used to determine cellulose crystallographic index. Park and co-worker (2010) compared three different methods to calculate CI of cellulose from XRD spectra. The first method is known as peak height method: CI was calculated from the height ratio between crystalline peak's peak intensity (intensity at crystallographic plane 002, I_{002} – amorphous intensity, I_{AM}) and total intensity (I_{002}) after being subtracted with background signal measured without cellulose. This method is less precise since this method only used peak at crystallographic plane at 002, while native cellulose usually shows at least four crystalline peaks. The second method is called the peak deconvolution method: individual crystalline peak is extracted by a peak-fitting program. The third method to calculate CI of cellulose is using ball-milled cellulose to subtract amorphous portion from the diffraction spectra. CI is calculated by dividing the remaining diffractogram area belongs to crystalline cellulose by the total area of the original diffractogram.[110]

1.2.7 Seed Coat Development

Seed coat (or testa) is developed from integument of ovule and its main role is to protect embryo by regulating moisture and surviving dispersals. Seed coats are usually dark in color due to pigmentation. Pigmentation in seed coat is the result of polyphenol and flavonoid. At the mature stage, seed surface (micromorphology) shows a characteristic pattern which is taxon specific.

Specification can be observed at the same plant taxon are cellular arrangement, cells shape, outline (straight, lobed, or irregularly curved) of anticlinal walls, surface relief of outer periclinal walls, sculptures of cuticle and epicuticular waxes, etc.[111] Mature seed coats accumulate lignin, polysaccharides, suberin, and cutin and therefore become steady.[112]

Seed coat tissue components consist of several layers which vary among species. In general, seed coat tissue has integument(s), parenchyma or nutrient layer, micropyle and hilum, and lens (strophiole).[113] Integuments are tissue layers covering the ovule, encasing the nucellus, and forming the micropyle. Angiosperms seed coat develops after fertilization from outer and inner integuments, comprises of testa and tegmen. Angiosperms have two integuments and therefore known as bitegmic, while gymnosperms have only one integument (unitegmic).[114]

Each layer of seed coat tissues comprises of different types of cells such as parenchyma cells, tannin cells, sclerenchyma cells, crystal cells, cork cells, and mucilage cells. Sclerenchyma is a lignified thick-walled cell presents in the form of sclereids and fibers. Sclereids can appear in isodiametric, palisade, or stellately lobed look, while fibers are usually exotegmic, but can also be found in the mesotesta such as in Annonaceae and Musaceae. Macrosclereids are the typical cell form in the outer layer of Leguminosae, Rhamnaceae , and Cannaceae; the inner layer of the testa of Geraniceae, and the outer layer of the tegmen of Cistaceae, Malvaceae, Tiliaceae, and Euphorbiaceae.[115]

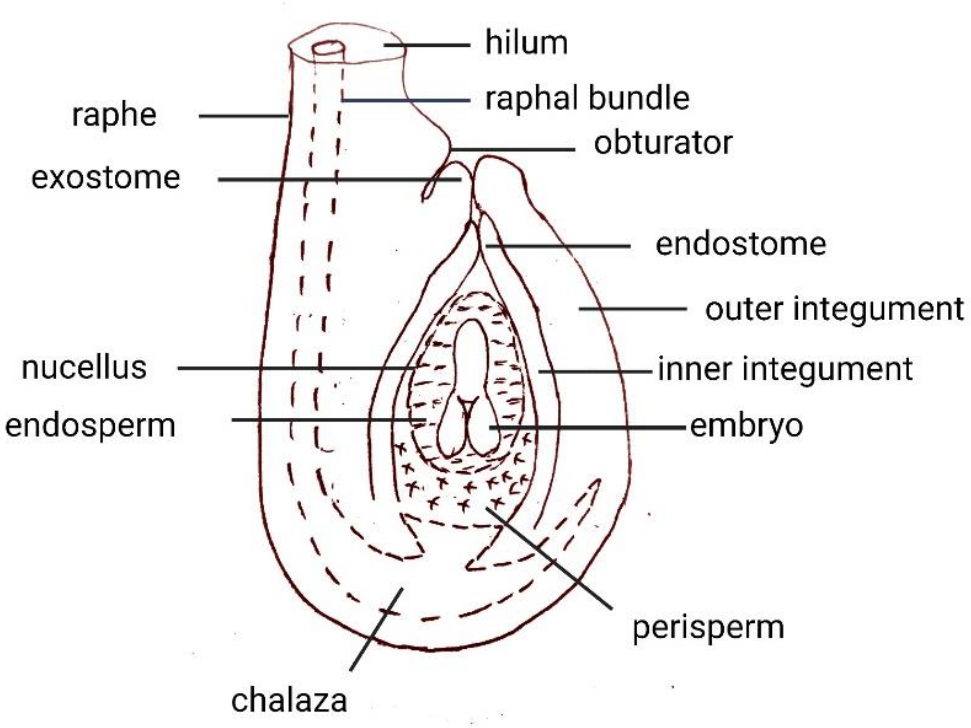

Figure 1.7 *General seed morphology (Adapted from Boesewinkel, F. D., & Bouman, F., 2017)*

1.2.8 Vanilla (*Vanilla planifolia*)

Vanilla planifolia or *Vanilla planifolia* Andr. belongs to Orchideae family (orchids), sub family of Vanilloideae (the vanilloid orchid) and known for its unusual features among orchids. This species has been domesticated for hundreds of years due to its distinct flavor and fragrance. The mature plant of *Vanilla planifolia* is a succulent climbing vine that initially grown rooted in the soil, but later becomes epiphytes to tree trunk and branches. This species also differs from other orchids in terms of flowers and pollination. The flower of *Vanilla planifolia* shed individual pollen grains while most orchids have their pollen loaded into complex pollinia. When pollinated, each flower will grow into a long slender fruit. The seeds of *Vanilla planifolia* are hard, crusty,

black in color and thus visible to the naked eye. Most orchids produce microscopic-sized seeds surrounded by a thin transparent seed coat.[116]

Vanilla planifolia is native to South America but has been grown in other parts of the world. The fruit of *Vanilla planifolia* is fleshy and usually described as "beans" due to its shape. After fertilization, the innermost layer's cells of the ovary wall develop into the cell cavity as nutritious unicellular hairs and secrete the vanillin. The innermost layer's cells grow from the entire inner surface of the ovary wall, except the placenta. In most orchids, seed coats are formed only from the outermost layer of the outer integument, whereas *Vanilla planifolia* has both inner and outer integuments. Both integuments contribute to the formation of the seed coat. During the embryo development, the epidermis of the seed coat or the outermost layer of the outer integument thicken massively until the cell cavity completely degraded. Later, the outermost layer of the outer integument becomes highly sclerotic in unspecific reticulation with brownish-black deposits until the surface is opaque and smooth.[117]

***Figure 1.8 Left** – Non-cultivated vanilla plant grows in home garden in rural area in Poso, Central Sulawesi, Indonesia; **Right** – bulk vanilla seed (right).*

1.2.9 Candlenut (*Aleurites moluccana*)

Candlenut is an evergreen arborescent plant of Euphorbiaceae family, with preferred scientific name is *Aleurites moluccana* (L.) Willd. Candlenut is native to Indo-Malaysia region and has widely distributed throughout Pacifics Islands. Candlenuts can reach 20 m height and 0.9 m trunk diameter. Its leaves are three-to-five nerved from the base, alternate, and simple with entire wavy margins. The flower is monoecious, both male and female flowers are in the same plant with greenish-white color. Candlenut fruit is oval to globular indehiscent drupe (stone fruit) sized 5–6 cm (2–2.4 in) in length by 5–7 cm (2–2.8 in) in width. The fruit is green to brownish in color with fleshy to leathery husk. Candlenut has an elliptical hard, black, rough shell similar in shape and texture to walnut, and sized about 2.5-3.5 cm (1–1.4 in) long.[118]

The word "candle" refers to its nature that burn easily when lit with fire. The kernel of candlenut is rich of lipid; it has been used since the ancient time for illumination, medicinal, and seasonings. The covering hard shell has been used for children's toys and ritual offerings. Candlenut wood is used for fuel and woodworking. Now days, candlenut kernel is mainly used as cooking ingredients within Indonesia and Malaysia, alternative drying oil to tung oil, and pharmaceutical (ointment, hair oil, toothpaste, cosmetics). The remaining shell is usually burned for fuel or produced into charcoal.[119]

Figure 1.9 *Images of candlenut tree grown in home garden in rural area in Sulawesi Island, Indonesia* ***(left)****, the tree trunk* ***(middle)****, and candlenut fruits* ***(right)****. Candlenut fruits are harvested by hand-picking of mature candlenut fallen to the grown.*

1.2.10 Hydroxymethylated Resorcinol (HMR)

Hydroxymethylated resorcinol (HMR) is a coupling agent prepared by reacting formaldehyde with resorcinol in 1.5 mole ratio at room temperature under mild alkaline condition. Structure of HMR is shown in Figure 11. Hydroxymethyl resorcinol was firstly developed by Forest Products Laboratory (FPL) to improve bonds to both epoxy and lignocellulosic wood and hence resistant to delamination.[120] HMR molecular size distribution and reactivity are controlled by the reaction time, that is the time between HMR solution preparation and the application to the wood surface. Application of HMR as thermosetting adhesive requires 4 hours reaction time, while epoxy adhesive requires 4-6 hours, but for some lower density wood species, 3-7 hours is the optimum reaction time.[121]

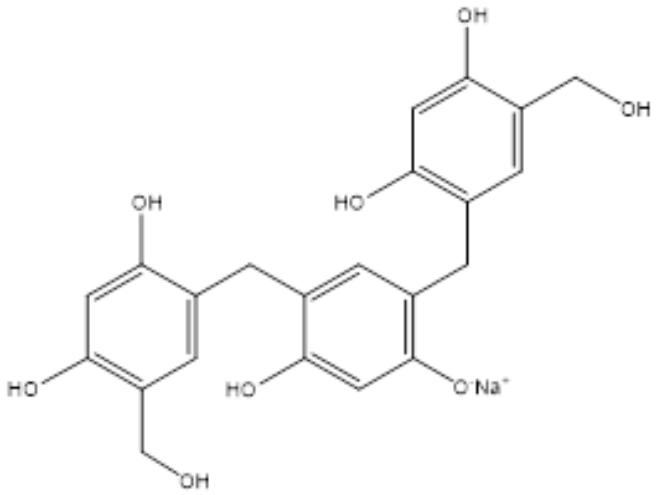

Figure 1.10 *Structure of HMR resin*

Mechanism of HMR formation during formaldehyde reaction with resorcinol under mild alkaline condition is described in Figure 10.[122] Reaction time has been a crucial factor for HMR efficacy. HMR is best prepared a few hours before being applied to the wood surface to maximize its efficacy. HMR reaction is relatively fast and the occurrence of chemical groups present in the dilute HMR solution during reaction has been studied by Christiansen study using ^{13}C-NMR.[123] Resorcinol has four signals from four aromatic carbon atoms which show up at 160.8 ppm for atom carbon C1 and C3; 106.1 ppm for C2; 110.2 ppm for C4 and C6; and at 133.4 ppm for C5 using DSS as internal standard for peak height. Observation at early reaction stage approximately 4 to 12 minutes after mixing using ^{13}C- enriched formaldehyde indicated that methylene was formed at early stage, dominated by hydroxymethyl groups through substitution at 4/6 and/or at 2-positions. The formation of 4-hydroxymethyl was six time more than 2-hydroxymethyl. 95% of formaldehyde was consumed within 1.7 h and 98% bound after 17 h.

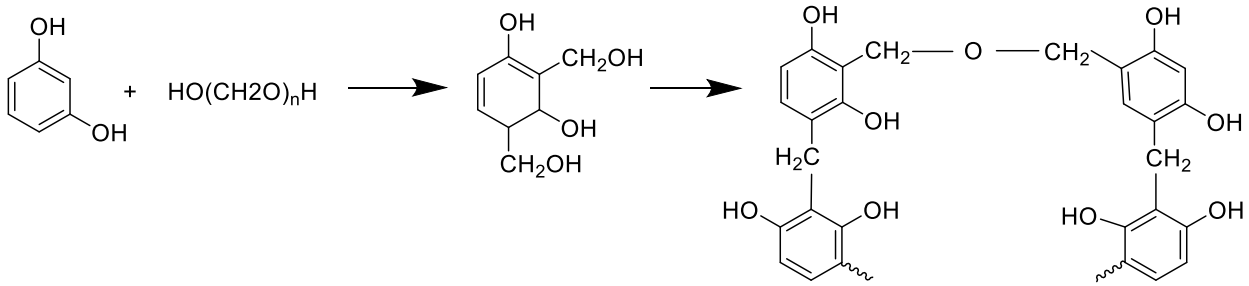

Figure 1.11 *Reaction of HMR polymerization*

The mechanism on how HMR improves durability of adhesive to wood has been hypothesized to be formation of ether linkages between hydroxymethyls group of HMR primer with the wood's or thermosetting adhesive's hydroxyls.[120] Christiansen tested the hypothesis on importance of crosslinking for HMR to improve bond durability by measuring the strength and stiffness of delaminated wood treated with HMR in which resorcinol has been partially substituted with 2-methylresorcinol to reduce crosslinking. The results indicate that higher resorcinol substitution, which reduces crosslinking, decreases bond durability.[124]

1.2.11 References

1. Adler, E., Lignin chemistry-past, present and future. *Wood Sci. Technol.* **1977,** *11*, 169-218.

2. Dence, C. W. L., S. Y. ,, Introduction. In *Methods in lignin chemistry*, Lin, S. Y., Dence, C. W. (Eds.), Ed. Springer Verlag: 1992; pp 3-17.

3. Wallace, G.; Fry, S. C., Phenolic Components of the Plant Cell Wall. In *International Review of Cytology Volume 151*, 1994; pp 229-267.

4. Whetten, R., Sederoff, R. , The lignin biosynthesis. *The plant cell wall* **1995,** *7*, 1001-1013.

5. Barcelo, A. R., Lignification in Plant Cell Walls. *International Review of Cytology* **1997,** *176*, 87-132.

6. Matern, U.; Grimmig, B.; Kneusel, R. E., Plant cell wall reinforcement in the disease-resistance response: molecular composition and regulation. *Canadian Journal of Botany* **1995,** *73* (S1), 511-517.

7. de Vries, S.; de Vries, J.; von Dahlen, J. K.; Gould, S. B.; Archibald, J. M.; Rose, L. E.; Slamovits, C. H., On plant defense signaling networks and early land plant evolution. *Commun Integr Biol* **2018,** *11* (3), 1-14.

8. Renault, H.; Werck-Reichhart, D.; Weng, J. K., Harnessing lignin evolution for biotechnological applications. *Curr Opin Biotechnol* **2019,** *56*, 105-111.

9. Kumar, M.; Campbell, L.; Turner, S., Secondary cell walls: biosynthesis and manipulation. *J Exp Bot* **2016,** *67* (2), 515-31.

10. Andersson, S.; Serimaa, R.; Paakkari, T.; Saranpää, P.; Pesonen, E., Crystallinity of wood and the size of cellulose crystallites in Norway spruce (Picea abies). *Journal of Wood Science* **2003,** *49* (6), 531-537.

11. Saxena, I. M.; Brown, R. M., Jr., Cellulose biosynthesis: current views and evolving concepts. *Ann Bot* **2005,** *96* (1), 9-21.

12. Taylor, N. G., Cellulose biosynthesis and deposition in higher plants. *New Phytol* **2008,** *178* (2), 239-52.

13. Scheller, H. V.; Ulvskov, P., Hemicelluloses. *Annual review of plant biology* **2010,** *61*, 263-289.

14. Rensing, S. A., Great moments in evolution: the conquest of land by plants. *Curr Opin Plant Biol* **2018,** *42*, 49-54.

15. Lowry, B., Lee, D., and Hebant, C., The origin of land plants: a new look at an old problem. *Taxon* **1980,** *29* (2/3), 183-199.

16. de Vries, J.; Archibald, J. M., Plant evolution: landmarks on the path to terrestrial life. *New Phytol* **2018,** *217* (4), 1428-1434.

17. Kenrick, P., Crane, P. R., The origin and early evolution of plants on land *Nature* **1997,** *384*, 33-39.

18. Bateman, R. M.; Crane, P. R.; DiMichele, W. A.; Kenrick, P. R.; Rowe, P.; Speck, T.; Stein, W. E., Early evolution of land plant: Phylogeny, Physiology, and Ecology of the Primary Terrestrial Radiation. *Anna. Rev. Ecol. Syst.* **1998,** *29*, 263-292.

19. Doyle, J. A., Phylogeny of vascular plants. *Annu. Rev. Ecol. Sys.* **1998,** *29*, 567-599.

20. Puttick, M. N.; Morris, J. L.; Williams, T. A.; Cox, C. J.; Edwards, D.; Kenrick, P.; Pressel, S.; Wellman, C. H.; Schneider, H.; Pisani, D.; Donoghue, P. C. J., The Interrelationships of Land Plants and the Nature of the Ancestral Embryophyte. *Curr Biol* **2018,** *28* (5), 733-745 e2.

21. Kenrick, P., The relationships of vascular plants. *Phil.Trans. R. Soc. Lond.* **2000,** *355*, 847-855.

22. Raven, J. A., The Evolution of Vascular Land Plants in Relation to Supracellular Transport Processes. In *Advances in Botanical Research* Woolhouse, H. W., Ed. Academic Press Inc.: London, 1977; Vol. V, pp 153-219.

23. Popper, Z. A., Evolution and diversity of green plant cell walls. *Curr. Opin. Plant. Biol.* **2008,** *11* (3), 286-92.

24. Duchesne, L. C., Larson, D. W., Cellulose and the evolution of plant life. *BioScience* **1989,** *39* (4), 238-241.

25. Siegel, S. M., The chemistry and physiology of lignin formation. *The Quarterly Review of Biology* **1956,** *31* (1), 1-18.

26. Weng, J. K.; Li, X.; Stout, J.; Chapple, C., Independent origins of syringyl lignin in vascular plants. *PNAS* **2008,** *105* (22), 7887-7992.

27. Weng, J. K.; Chapple, C., The origin and evolution of lignin biosynthesis. *New Phytol* **2010,** *187* (2), 273-85.

28. Zhong, R.; Ye, Z. H., Transcriptional regulation of lignin biosynthesis. *Plant Signal Behav* **2009,** *4* (11), 1028-34.

29. Novo-Uzal, E.; Pomar, F.; Gómez Ros, L. V.; Espiñeira, J. M.; Ros Barceló, A., Evolutionary history of lignins. *Advances in Botanical Research* **2012,** *61*, 309-350.

30. Uzal, E. N.; Gomez Ros, L. V.; Pomar, F.; Bernal, M. A.; Paradela, A.; Albar, J. P.; Ros Barcelo, A., The presence of sinapyl lignin in Ginkgo biloba cell cultures changes our views of the evolution of lignin biosynthesis. *Physiol Plant* **2009,** *135* (2), 196-213.

31. Grima-Pettenati, J.; Soler, M.; Camargo, E. L. O.; Wang, H., Transcriptional Regulation of the Lignin Biosynthetic Pathway Revisited: New Players and Insights. In *Lignins - Biosynthesis, Biodegradation and Bioengineering*, 2012; pp 173-218.

32. Higuchi, T., Biochemical Aspects of Lignification and Heartwood Formation. *bulletin of the Wood Research Institute Kyoto University* 1976, pp 180-199.

33. Hedges , J. I.; Mann, D. C., The characterization of plant tissues by their lignin oxidation products. *Geochimica et Cosmochimica Acta* **1979,** *43*, 1803-1807.

34. Obst, J. R., Guaiacyl and Syringyl Lignin Composition in Hardwood Cell Components. *Holzforschung* **1982,** *36*, 143-152.

35. Sakakibara, A., A structural model of softwood lignin. *Wood Sci. Technol.* **1980,** *14*, 89-100.

36. Lewis, N. G., A 20th century roller coaster ride: a short account of lignification. *Current Opinion in Plant Biology* **1999,** *2*, 153-162.

37. Liu, Q.; Luo, L.; Zheng, L., Lignins: Biosynthesis and Biological Functions in Plants. *Int J Mol Sci* **2018,** *19* (2).

38. Higuchi, T., Lignin biochemistry: Biosynthesis and biodegradation. *Wood Sci. Technol.* **1990,** *24*.

39. Whetten, R., MacKay, J.J., Sederoff, R., Recent advances in understanding lignin biosynthesis. *Annu. Rev. Plant Physiol. Plant Mol. Biol.* **1998,** *49*, 585-609.

40. Ralph, J.; Brunow, G.; Boerjan, W., Lignins. In *Encyclopedia of Life Sciences*, 2007.

41. Boerjan, W.; Ralph, J.; Baucher, M., Lignin biosynthesis. *Annu Rev Plant Biol* **2003,** *54*, 519-46.

42. Ye, Z. H.; Kneusel, R. E.; Matern, U.; Varner, J. E., An Alternative Methylation Pathway in Lignin Biosynthesis in Zinnia. *The Plant Cell* **1994,** *6*.

43. Perkins, M.; Smith, R. A.; Samuels, L., The transport of monomers during lignification in plants: anything goes but how? *Curr Opin Biotechnol* **2019,** *56*, 69-74.

44. Liu, C. J.; Miao, Y. C.; Zhang, K. W., Sequestration and transport of lignin monomeric precursors. *Molecules* **2011,** *16* (1), 710-27.

45. Liu, C. J., Deciphering the enigma of lignification: precursor transport, oxidation, and the topochemistry of lignin assembly. *Mol Plant* **2012,** *5* (2), 304-17.

46. Takabe, K., Cell walls of woody plants: autoradiography and ultraviolet microscopy. In *Wood formation in trees*, CRC Press: 2002; pp 179-198.

47. Kaneda, M.; Rensing, K. H.; Wong, J. C.; Banno, B.; Mansfield, S. D.; Samuels, A. L., Tracking monolignols during wood development in lodgepole pine. *Plant Physiol* **2008,** *147* (4), 1750-60.

48. Boija, E.; Lundquist, A.; Edwards, K.; Johansson, G., Evaluation of bilayer disks as plant cell membrane models in partition studies. *Anal Biochem* **2007,** *364* (2), 145-52.

49. Vermaas, J. V.; Dixon, R. A.; Chen, F.; Mansfield, S. D.; Boerjan, W.; Ralph, J.; Crowley, M. F.; Beckham, G. T., Passive membrane transport of lignin-related compounds. *Proc Natl Acad Sci U S A* **2019,** *116* (46), 23117-23123.

50. Tsuyama, T.; Kawai, R.; Shitan, N.; Matoh, T.; Sugiyama, J.; Yoshinaga, A.; Takabe, K.; Fujita, M.; Yazaki, K., Proton-dependent coniferin transport, a common major transport event in differentiating xylem tissue of woody plants. *Plant Physiol* **2013,** *162* (2), 918-26.

51. Shimada, N.; Munekata, N.; Tsuyama, T.; Matsushita, Y.; Fukushima, K.; Kijidani, Y.; Takabe, K.; Yazaki, K.; Kamei, I., Active Transport of Lignin Precursors into Membrane Vesicles from Lignifying Tissues of Bamboo. *Plants (Basel)* **2021,** *10* (11).

52. Tobimatsu, Y.; Schuetz, M., Lignin polymerization: how do plants manage the chemistry so well? *Curr Opin Biotechnol* **2019,** *56*, 75-81.

53. Mottiar, Y.; Vanholme, R.; Boerjan, W.; Ralph, J.; Mansfield, S. D., Designer lignins: harnessing the plasticity of lignification. *Curr Opin Biotechnol* **2016,** *37*, 190-200.

54. Baucher, M.; Halpin, C.; Petit-Conil, M.; Boerjan, W., Lignin: genetic engineering and impact on pulping. *Crit Rev Biochem Mol Biol* **2003,** *38* (4), 305-50.

55. Sederoff, R. R., MacKay, J. J., Ralph, J., Hatfield, R. D., Unexpected variation in lignin. *Current Opinion in Plant Biology* **1999,** *2*, 145-152.

56. Van Doorsselaere, J., Baucher, M., Chognot, E., Tollier, M. T., Petit-Konil, M., Leple, J. C., Pilate, G., Cornu, D., Monties, B., Van Montagu, M., Inze, D., Boerjan, W., Jouanin, L., A novel lignin in poplar tree with a reduced caffeic acid/5-hydroferulic acid O-methyltransferase activity. *The Plant Journal* **1995,** *8* (6), 855-864.

57. Ralph, J., MacKay, J. J., Hatfield, R. D., O'Malley, D. M., Whetten, R. W., Sederoff, R. R., Abnormal lignin in a Loblolly Pine mutant. *Science* **1997,** *277*, 235-238.

58. Franke, R., Hemm, M. R., Denault, J. W., Ruegger, M. O., Humphreys, J. M., Chapple, C., Changes in secondary metabolism and deposition of an unusual lignin in the ref8 mutant of Arabidopsis. *The Plant Journal* **2002,** *30* (1), 47-59.

59. Ralph, J.; Lundquist, K.; Brunow, G.; Lu, F.; Kim, H.; Schatz, P. F.; Marita, J. M.; Hatfield, R. D.; Ralph, S. A.; Christensen, J. H.; Boerjan, W., Lignins: Natural polymers from oxidative coupling of 4-hydroxyphenylpropanoids. *Phytochemistry Reviews* **2004,** *3*, 29-60.

60. Ralph, J.; Brunow, G.; Harris, P. J.; Dixon, R. A.; Schatz, P. F.; Boerjan, W., Lignification: are lignins biosynthesized via simple combinatorial chemistry or via proteinaceous control and template replication? In *Recent Advances in Polyphenol Research*, Daayf, F.; Lattanzio, V., Eds. Blackwell Publishing Ltd,: 2008; Vol. 1.

61. Ralph, J.; Lapierre, C.; Boerjan, W., Lignin structure and its engineering. *Curr Opin Biotechnol* **2019,** *56*, 240-249.

62. Chen, F.; Tobimatsu, Y.; Havkin-Frenkel, D.; Dixon, R. A.; Ralph, J., A polymer of caffeyl alcohol in plant seeds. *Proc Natl Acad Sci U S A* **2012,** *109* (5), 1772-7.

63. Tobimatsu, Y.; Chen, F.; Nakashima, J.; Escamilla-Trevino, L. L.; Jackson, L.; Dixon, R. A.; Ralph, J., Coexistence but independent biosynthesis of catechyl and guaiacyl/syringyl lignin polymers in seed coats. *Plant Cell* **2013,** *25* (7), 2587-600.

64. Chen, F.; Tobimatsu, Y.; Jackson, L.; Nakashima, J.; Ralph, J.; Dixon, R. A., Novel seed coat lignins in the Cactaceae: structure, distribution and implications for the evolution of lignin diversity. *Plant J* **2013,** *73* (2), 201-11.

65. Chen, F., Dixon, R., Vanilla planifolia-The Source of the Unexpected Discovery of a New Lignin. In *Handbook of Vanilla Science and Technology 2nd Edition*, Havkin-Frenkel, D., Belanger, F. C., Ed. John Wiley & Sons, Ltd.: 2019; pp 447-455.

66. Fujimoto, A.; Matsumoto, Y.; Chang, H.-M.; Meshitsuka, G., Quantitative evaluation of milling effects on lignin structure during the isolation process of milled wood lignin. *Journal of Wood Science* **2005,** *51* (1), 89-91.

67. Ikeda, T.; Holtman, K.; Kadla, J. F.; Chang, H.-M.; Jameel, H., Studies on the Effect of Ball Milling on Lignin Structure Using DFRC method. *J. Agric. Food Chem.* **2002,** *50*, 129-135.

68. Brauns, F. E., Native lignin1 I. Its isolation and methylation. *Journal of the American Chemical Society* **1939,** *61* (8), 2120-2127.

69. Chang, H. M.; Cowling, E. B.; Brown, W.; Adler, E.; Miksche, G., Comparative Studies on Cellulolytic Enzyme Lignin

and Milled Wood Lignin of Sweetgum and Spruce. *Holzforschung* **1975,** *29*, 153-159.

70. Lundquist, K., Isolation and Purification: Wood. In *Methods in lignin chemistry*, Lin, S. Y., Dence, C. W. (Eds.), Ed. Springer Verlag: 1992; pp 65-69.

71. Hu, Z.; Yeh, T.-F.; Chang, H.-m.; Matsumoto, Y.; Kadla, J. F., Elucidation of the structure of cellulolytic enzyme lignin. *Holzforschung* **2006,** *60* (4), 389-397.

72. Lupoi, J. S.; Singh, S.; Parthasarathi, R.; Simmons, B. A.; Henry, R. J., Recent innovations in analytical methods for the qualitative and quantitative assessment of lignin. *Renewable and Sustainable Energy Reviews* **2015,** *49*, 871-906.

73. Dence, C. W., Detection and Determination: The Determination of Lignin. In *Methods in lignin chemistry*, Lin, S. Y., Dence, C. W. (Eds.), Ed. Springer Verlag: 1992; pp 33-58.

74. TAPPI, TAPPI Method T222 om-02. In *Acid-insoluble lignin in wood and pulp (Reaffirmation of T 222 om-02)*, TAPPI Press: Atlanta, GA, 2006.

75. Sluiter, A.; Hames, B.; Ruiz, R.; Scarlata, C.; Sluiter, J.; Templeton, D.; Crocker, D., Determination of Structural Carbohydrates and Lignin in Biomass. Energy, U. D. o., Ed. National Renewable Energy Laboratory: Golden, Colorado, 2008.

76. Schultz, P.; Templeton, M. C., Proposed mechanism for lignin nitrobenzene oxidation. *Holzforschung* **1986,** *40*, 93-97.

77. Pew, J. C., Nitrobenzene Oxidation of Lignin Model Compounds, Spruce Wood and Spruce "Native Lignin. *J. Am. Chem. Soc* **1955,** *77* (10), 2831-2833.

78. Iiyama, K.; Lam, T. B. T., Lignin in wheat internodes. Part 1: The reactivities of lignin units during alkaline nitrobenzene oxidation. *Journal of the Science of Food and Agriculture* **1990,** *51* (4), 481-491.

79. Tamai, A.; Goto, H.; Akiyama, T.; Matsumoto, Y., Revisiting alkaline nitrobenzene oxidation: quantitative evaluation of biphenyl structures in cedar wood lignin (Cryptomeria japonica) by a modified nitrobenzene oxidation method. *Holzforschung* **2015,** *69* (8), 951-958.

80. Hedges, J. I.; Parker, L. P., Land-derived organic matter in surface sediments from the Gulf of Mexico. *Geochim. Cosmochim. Acta* **1976,** *40*, 1019-1029.

81. Adler, E.; Pepper, J. M.; Eriksoo, E., Action of Mineral Acid on Lignin and Model Substances of Guaiacylglycerol-beta-aryl Ether Type. *Industrial & Engineering Chemistry* **1957,** *49* (9), 1391-1392.

82. Lundquist, A., Characterization in Solution: Chemical Degradation Methods-Acidolysis. In *Methods in lignin chemistry*, Lin, S. Y., Dence, C. W. (Eds.), Ed. Springer Verlag: 1992; pp 289-298.

83. Menard, K. P., A practical introduction. *Dynamic Mechanical Analysis* **1999**.

84. Sun, N.; Das, S.; Frazier, C. E., Dynamic mechanical analysis of dry wood: Linear viscoelastic response region and effects of minor moisture changes. *Holzforschung* **2007,** *61* (1), 28-33.

85. Salmén, A.-M. O. a. L., Viscoelasticity of In Situ Lignin as Affected by Structure: Softwood vs. Hardwood. In *Viscoelasticity of Biomaterials*, Glasser, W. G.; Hatakeyama, H., Eds. Washington, DC, 1992; pp 133-143.

86. Olsson, A.-M.; Salmen, L., The effect of lignin composition on the viscoelastic properties of wood. *Nordic Pulp and Paper Research Journal* **1997,** *12*, 140-144.

87. Wan, G.; Frazier, T.; Jorgensen, J.; Zhao, B.; Frazier, C. E., Rheology of transgenic switchgrass reveals practical aspects of biomass processing. *Biotechnol Biofuels* **2018,** *11*, 57.

88. Chowdhury, S.; Fabiyi, J.; Frazier, C. E., Advancing the dynamic mechanical analysis of biomass: comparison of tensile-torsion and compressive-torsion wood DMA. *Holzforschung* **2010,** *64* (6).

89. Sun, F.; Wan, G.; Zhang, Y.; Frazier, C. E., Rheology of moso bamboo stem determined by DMA in ethylene glycol. *Holzforschung* **2019,** *73* (2), 171-179.

90. Chowdhury, S.; Frazier, C. E., Thermorheological complexity and fragility in plasticized lignocellulose. *Biomacromolecules* **2013,** *14* (4), 1166-1173.

91. Vanholme, R.; Demedts, B.; Morreel, K.; Ralph, J.; Boerjan, W., Lignin biosynthesis and structure. *Plant Physiol* **2010,** *153* (3), 895-905.

92. Mansfield, S. D.; Kim, H.; Lu, F.; Ralph, J., Whole plant cell wall characterization using solution-state 2D NMR. *Nat Protoc* **2012,** *7* (9), 1579-89.

93. Terrett, O. M.; Lyczakowski, J. J.; Yu, L.; Iuga, D.; Franks, W. T.; Brown, S. P.; Dupree, R.; Dupree, P., Molecular architecture of softwood revealed by solid-state NMR. *Nat Commun* **2019,** *10* (1), 4978.

94. Ralph, J.; Marita, J. M.; Ralph, S. A.; Hatfield, R. D.; Lu, F.; Ede, R. M.; Peng, J.; Quideau, S.; Helm, R. F.; Grabber, J. H.; Kim, H.; Jimenez-Monteon, G.; Zhang, C.; Jung, H. J. G.; Landucci, L. L.; MacKay, J. J.; Sederoff, R. R.; Chapple, C.; Boudet, A. M., Solution-state NMR of Lignins. In *Advances in Lignocellulosics Characterization*, Argyropoulos, D. S., Ed. TAPPI Press: Atlanta, GA., 1999; pp 55-108.

95. Wen, J. L.; Sun, S. L.; Xue, B. L.; Sun, R. C., Recent Advances in Characterization of Lignin Polymer by Solution-State Nuclear Magnetic Resonance (NMR) Methodology. *Materials (Basel)* **2013,** *6* (1), 359-391.

96. Nimz, H. H.; Robert, D.; Faix, O.; Nemr, M., Carbon-13 Spectra of Lignins, 8: Structural Differences between Lignins of Hardwoods, Softwoods, Grasses and Compression Wood. *Holzforschung* **1981,** *35*, 16-26.

97. Sette, M.; Wechselberger, R.; Crestini, C., Elucidation of lignin structure by quantitative 2D NMR. *Chemistry* **2011,** *17* (34), 9529-35.

98. Terashima, N.; Fukushima, K., Heterogeneity in formation of lignin XI: An autoradiographic study of the heterogeneous formation and structure of pine lignin. *Wood Sci. Technol.* **1988,** *22*, 259-270.

99. Fergus, B. J.; Goring, D. A. I., The Location of Guaiacyl and Syringyl Lignins in Birch Xylem Tissue. *Holzforschung* **1970,** *Bd. 24* (H. 4), 113-117.

100. Fergus, B. J.; Goring, D. A. I., The Distribution of Lignin in Birch Wood as Determined by Ultraviolet Microscopy. *Holzforschung* **1970,** *Bd. 24* (H. 4), 118-124.

101. Akin, D. E., Light Microscopy and Histology of Lignocellulose Related to Biodegradation. In *Physico-Chemical Characterisation of Plant Residues for Industrial and Feed Use*, Chesson, A. e. a., Ed. Springer: Dordrecht, 1989; pp 58-64.

102. Stylianou, A.; Gkretsi, V.; Sampaio, P.; Glosmann, M.; Walter, A., Transmission Light Microscopy. In *Imaging Modalities for Biological and Preclinical Research:*

A Compendium, Walter, A.; Manneheim, J. G.; Caruana, C. J., Eds. IOP Publishing Ltd.: 2021; Vol. 1, pp 1-18.

103. Abramowitz, M.; Davidson, M. W., Optical Microscopy. In *Encyclopedia of Imaging Science and Technology*

Hornak, J. P., Ed. 2002.

104. Zhou, W.; Apkarian, R. P.; Wang, Z. L.; Joy, D., Fundamentals of Scanning Electron Microscopy. In *Scanning Microscopy for Nanotechnology: Techniques and Applications*, 2007; pp 1-40.

105. Spearin We Fau - Isenberg, I. H.; Isenberg, I. H., The Maceration of Woody Tissue With Acetic Acid and Sodium Chlorite. (0036-8075 (Print)).

106. Schmid, R., Sonication and Other Improvements on Jeffrey's Technique for Macerating Wood. *Stain Technology* **1982,** *57* (5), 293-299.

107. Franklin, G. L., Preparation of Thin Sections of Synthetic Resins and Wood-Resin Composites, and a New Macerating Method for Wood. *Nature* **1945,** *13* (3924), 51.

108. Chaffey, N., Wood Microscopical Techniques. In *Wood Formation in Trees*, Chaffey, N., Ed. Harwood Academic Publishers: Singapore, 2001; pp 17-40.

109. Zugenmaier, P., Crystalline Cellulose and Derivatives: Characterization and Structures. In *Springer Series in Wood Science*, Timell, T. E.; Wimmer, R., Eds. Springer-Verlag Heidelberg, Germany, 2008.

110. Park, S.; Baker, J. O.; Himmel, M. E.; Parilla, P. A.; Johnson, D. K., Cellulose crystallinity index: measurement techniques and their impact on interpreting cellulase performance. *Biotechnol Biofuels* **2010,** *3* (10), 1-10.

111. Crang, R.; Lyons-Sobaski, S.; Wise, R., Fruit, Seeds, and Seedlings: The Seed Coat Surrounds the Embryo and Storage Tissues. In *Plant Anatomy: A Concept-Based Approach to the Structure of Seed Plants*, Springer: 2018; pp 667-669.

112. Sano, N.; Rajjou, L.; North, H. M.; Debeaujon, I.; Marion-Poll, A.; Seo, M., Staying Alive: Molecular Aspects of Seed Longevity. *Plant Cell Physiol* **2016,** *57* (4), 660-74.

113. Smykal, P.; Vernoud, V.; Blair, M. W.; Soukup, A.; Thompson, R. D., The role of the testa during development and in establishment of dormancy of the legume seed. *Front Plant Sci* **2014,** *5*, 351.

114. Matilla, A. J., Seed coat formation: its evolution and regulation. *Seed Science Research* **2019,** *29* (4), 215-226.

115. Boesewinkel, F. D. a. B., F., The Seed: Structure and Function. In *Seed development and germination*, Kigel, J.; Galili, G., Eds. CRC press: New York, 1995; Vol. 41, pp 1-21.

116. Cameron, K. M., Biology of Vanilla In *Handbook of Vanilla Science and Technology* Havkin-Frenkel, D.; Belanger, F., Eds. Blackwell Publishing, Ltd.: 2011; pp 241-254.

117. Swamy, B. G. L., On The Life-History of Vanilla Planifolia. *Botanical Gazette* **1947,** *108* (3), 449-456.

118. Elevitch, C. R.; Manner, H. I., Aleurites moluccana (kukui). In *Species Profiles for Pacific Island Agroforestry*, Elevitch, C. R., Ed. Permanent Agriculture Resources: 2006.

119. Koji, T., Kemiri (Aleurites moluccana) and forest resource management in eastern Indonesia: an eco-historical perspective. *アジア・アフリカ地域研究* **2002,** *2*, 5-23.

120. Vick, C. B. In *Hydroxymethylated Resorcinol Coupling Agent for Enhanced Adhesion of Epoxy and Other Thermosetting Adhesives to Wood*, Wood Adhesive, 1995.

121. Vick, C. B., More Durable Epoxy Bonds to Wood with Hydroxymethylated Resorcinol Coupling Agent. *Adhesives Age* **1997,** *40* (8), 24-29.

122. Gaca, K. Z., Parkinson, J. A., & Sefcik, J. , Kinetics of early stages of resorcinol-formaldehyde polymerization investigated by solution-phase nuclear magnetic resonance spectroscopy. *Polymer* **2017,** *110*, 62-73.

123. Christiansen, A. W., Resorcinol-Formaldehyde Reactions in Dilute Solution Observed by Carbon-13 NMR Spectroscopy. *J. Appl. Polym. Sci* **2000,** *75*, 1760-1768.

124. Christiansen, A. W., Chemical and mechanical aspects of HMR primer in relationship to wood bonding. *Forest products journal* **2005,** *55* (11), 73-78.

Chapter 2

Morphology of Vanilla (*Vanilla planifolia*) Seed Coat and Candlenut (*Aleurites moluccana*) Shell

Attribution

In this Chapter all work was conducted by E. Ristanti and except for EDS-IMGAES images were prepared by Nanoscale Characterization and Fabrication (NCFL), Virginia Tech Institute for Critical Technology and Applied Science.

2.1 Abstract

Vanilla (*Vanilla planifolia*) and candlenut (*Aleurites moluccana*) are angiosperms that, as of 2012, were found to exhibit a new type of lignin, "catechyl lignin", or C-lignin in the seed coat/nutshell. The new type of lignin is a linear homopolymer with benzodioxane intermonomer linkage, which is stiffer than alkyl-aryl ether linkage in guaiacyl/syringyl-lignin(G/S-lignin). C-lignin is found as the only lignin in vanilla seed coat, while in candlenut shell it is accompanied by G-lignin. Seed coat and nutshells are parts of seed that cover embryo, highly lignified, and hard to crack. The purpose of certain plants to develop C-lignin is unclear. In this study, we identified vanilla seed coat and candlenut shell cell size and type using reflected and transmitted light microscopes. Then, scanning electron microscope (SEM), energy dispersive X-ray spectroscopy-scanning electron microscope (EDS-SEM), and focused ion beam-scanning electron microscope (FIB-SEM) were used to image seed coats and nutshell's structure, elemental distribution, and specific-site of seed coat/nutshell respectively. Vanilla seeds, size approximately 300 μm and the

outer surface of macerated tissue shows osteosclereids type cell like *Pisum elatius.* Electron microscopy image of vanilla seed indicates that the surface is covered by elongated, rectangular-shaped cells, with undulated, curvature wall. Vanilla has calcium deposited almost equally in the outer and inner seed coat as well as the embryo. Candlenut shell density is 1.14 g/cm^3 on average, determined based on ASTM D2395. Candlenut shell consists of macroslereids type cell, which stretch along the shell thickness. Calcium deposition also observed in candlenut shell, but not distributed evenly.

2.2. Introduction

Reproductive adaptation is part of fundamental plant evolution to succeed terrestrial colonization that occur during Devonian.[1] Land plants have developed and differentiated reproductive anatomies into more complex and sophisticated organs than their ancestor, a unicellular green algal, that allow reproduction to occur in the harsh condition and over great distances.[2] Reproductive adaptations are varied among plants which can include sexual and asexual reproductive modes.[3] The most complex and diverse means of sexual reproduction in vascular plant is seed habit. Seed habit evolved from life history, i.e. the origin of male gametophyte to female gametophyte delivery, and from ovular, especially in the integumentary.[4]

The term seed refers to a "capsule" that consists of embryo surrounded by nutritive tissue (endosperm) and enclosed by protective seed coat.[5] Seed plants are categorized into two large groups: angiosperms and gymnosperms. In both angiosperms and gymnosperms, seeds develop from ovules. The ovule bears nucellus, which is encased by one integument in gymnosperms and two integuments in angiosperms. An ovule is also known as unfertilized, immature seed precursor surrounded by integument(s). The integument(s) later develops into *testa* (seed coat). In the mature

seed, the outer cell layer of outer integument forms a dead covering layer, while the inner cell layer remains alive.[6]

Hard encapsulation in seeds is provided by sclerenchyma (sclereids and fibers) that observed as tissue hardening.[7, 8] Tissue hardening in seeds and fruit is usually caused by lignification of secondary cell wall that takes place during differentiation and can also be induced by environmental changes such as lignin formation caused by pathogen attack, lack of nutrient availability, or drought.[9, 10] Lignification in the extra-axillary fibers and sclereids that compose sclerenchyma is controlled by the lignifying cells or called as Cell-Autonomous Lignification (CAL). Meanwhile, early lignification in vessels involve programmed cell death and later continued by neighboring cell to achieve full lignification or known as Non-Cell Autonomous Lignification (NCAL). [11]

Seed coat carries genetic characters of the mother plant as it derived from maternal tissues (integuments, chalaza, raphal tissue, and sometimes nucellus's layer). Seed coat serves several functions to the seed: nutrient transport, mechanical and chemical protection, function related to dehydration and imbibition, dispersals, and germination. In the seed coat, nutrient transport occurs through maternal tissue to the embryo sac. Seed coat is usually resistant to crushing and cracking, and not bright in color. Contributor to the mechanical strength of seed coats are sclerenchymatous elements, lignin, cellulose, and silicon that appears as $SiO_2.nH_2O$. Occurrence of crystal of Ca-Oxalate in both sclerenchyma and thin-walled cells probably also contribute to the mechanical strength of the seed coat. Tannin provides chemical defense against predator, which caused seed coat usually have dark color.[12, 13]

Fruits in angiosperms in general are divided into dry and fleshy fruit. Dry fruits are usually dispersed by physical forces, while fleshy fruit rely on animal consuming, such as bird

(ornithochory) and mammal (mammalocory). [14, 15] Both fruits types contain tissue layer originated from carpel ovary (collectively known as pericarp). Pericarp are differentiated into endocarp (innermost layer), mesocarp (intermediate layer), and exocarp (surface layer). Some fruits develop hardened endocarps and known as drupes that include some nuts such as pistachio, walnut, and almond. Endocarps function as seed protector and dispersal. Endocarps also role as connector during seed development. The hardening of endocarp occurs via secondary cell wall formation and lignification that is like in wood.[16, 17]

The hardening endocarp of dry fruit is known as nutshell. It consists of sclereids derived from lignification of primary meristem's parenchyma.[18] Nutshell appears as recalcitrant membrane or woody layer that covered seed and give mechanical strength to the seed.[19] Although many nutshells are harder to grind than wood, lignin composition in the nutshells are typical wood's lignin, the guaiacyl (G)-lignin that derived from coniferyl alcohol, and or syringyl (S)-lignin that derived from sinapyl alcohol. The hardness of nutshell is probably more caused by three-dimensional arrangement and cross-linking of the components, as observed in walnut shell.[19-22]

In 2012, a novel lignin was reported in the seed coat of vanilla orchid (*Vanilla planifolia*), and in some *Cactaceae*. This new type of lignin is known as Catechyl-lignin or C-lignin; a linear homopolymer of caffeyl alcohol.[23] C-lignin is the only lignin in vanilla-seed coat; but other plants exhibit seed coats (or nutshells) with both C-lignin and also G and/S-lignin, as in the candlenut (*Aleurites moluccanus*), jatropha (*Jatropha curcas*), cleome (*Cleome hassleriana*), castor tree (*Ricinus communis*), and tung tree (*Vernicia fordii*).[24]

Figure 2.1 *Candlenut (Aleurites moluccana). Seed in candlenut is covered by hard, dark brown in color nutshell. The nutshell is sometimes covered with white-yellowish flaky substance.*

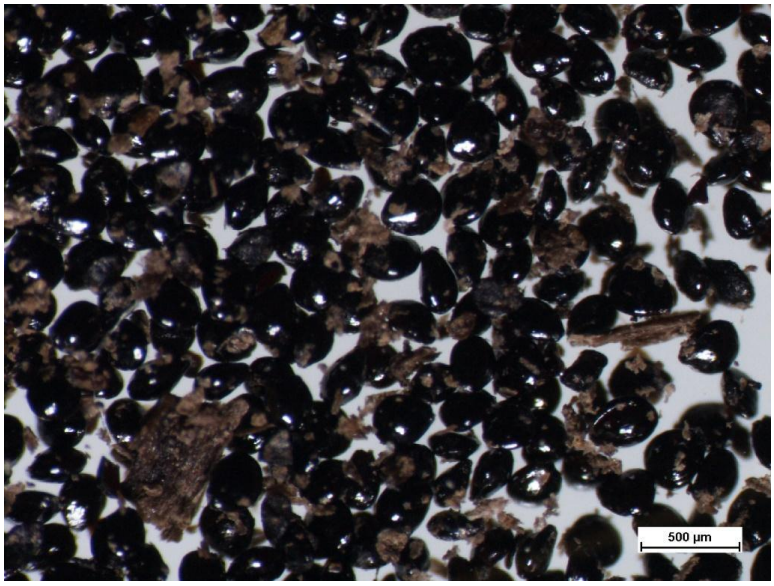

Figure 2.2 *Image of bulk vanilla (Vanilla planifolia) seeds. Vanilla seeds are tiny and black in color.*

To survive during dispersal that may include ingestion by birds and mammals, seed coat and nutshells must be resistant to gastrointestinal acid. C-lignins are unusually stable to acid-catalyzed cleavage due to the benzodioxane linkages.[25] But, this property likely does not explain C-lignin evolution, because many other species survive dispersal without having C-lignin in their seed coats or nutshells. To compare with, walnut (*Juglans regia*) shells have a hard, polylobate sclereids cells closely interlocked in 3D with their neighbors[21], but walnut shells do not exhibit C-lignin.[19]

Morphological study is required to identify the cell types and size of vanilla seed coat and nutshell that has C-lignin. In this study, we delignified vanilla seed coat and candlenut shell and used reflected and transmitted light microscope to determine cell type and size. We also conducted elemental composition distribution analysis using energy dispersive X-ray diffraction – scanning electron microscopy (EDS-SEM). Resin-embedded intact vanilla seed coat and candlenut shell cross-sectioned were used to produce images using reflected light and focused-ion beamed – scanning electron microscopy (FIB-SEM) on specific seed coat/nutshell sites.

2.3 Experimental

2.3.1 Materials

Vanilla seeds were obtained from Prof. Fang Chen (University of North Texas). Candlenut, due to limitation of availability within United States, were obtained from three sources: Prof. Fang Chen (University of North Texas), purchased from Hawaiian Art Shop (Hawaii), and from local plantation in Bukittinggi, West Sumatra, Indonesia. Chemicals: ethanol 190 Proof (Decon Lab), n-hexane, Safranin O (Fisher chemical), paraffin wax (Gulf Wax), glacial acetic acid, 30%

hydrogen peroxide (Sigma-Aldrich), epoxy resin L. R. White hard grade kit (Electron Microscopy Science), and DI water.

2.3.2 Methods

Seed and Nutshell Cleaning

Vanilla bean seed was washed with ethanol (3x20mL) and n-hexane (3x20mL) and air-dried overnight. Candlenut shells were separated from nuts by crushing with hammer, then removed the nut from the shell. Candlenut shells were used as it is.

Vanilla Embryo Isolation

Cleaned seeds (≈ 0.5g) were subjected to rotary-knife milling (1 minute pulse, 10-minutes break for a total milling time 5 minutes (A11 Basic Mill, beater blade A11.3; IKA–Werke, Staufen, Germany). Milled-seeds (≈ 0.1g) were added to a mixture of 1,2,4-tricholoro benzene, TCB,15mL):n-hexane (HXN, 15mL) (3:1, v/v), then centrifuges (5000 rpm, 15 minutes; Eppendorf 5804, Hamburg, Germany; the denser seed coats spun down to the tube bottom and the seeds embryo floats on the surface. Embryo were collected using spatula and dried overnight in a covered-petri dish at room temperature.

Determination of Vanilla Seed Size

Cleaned seed were spread onto filter paper-layered petri dish and observed in reflected light microscope SMZ 745T (Nikon, Tokyo, Japan). Images of vanilla seeds were captured using microscope camera DS-Fi1 (Nikon, Tokyo, Japan). Length of vanilla seeds were measured in NIS Elements Software ver. BR 4.11. Approximately 30 measurements were taken, and the seed size value was obtained from the average value of 30 measurements.

Determination of Candlenut Shell Relative Density

Candlenut shell disks (30 pieces) were collected by crushing whole candlenut. Each piece was weighed and recorded the mass. Each sample was coated with melted wax and measured the volume based on ASTM D2395 – Standard Test Methods for Density and Specific Gravity (Relative Density) of Wood and Wood-Based Materials **method B *Volume by Water Immersion***: *The initial mass of the specimen is measured. The specimen is submerged in a tank with a known volume of water and the change in volume of water is recorded. The volume of the specimen is equal to the volume of water displaced.*

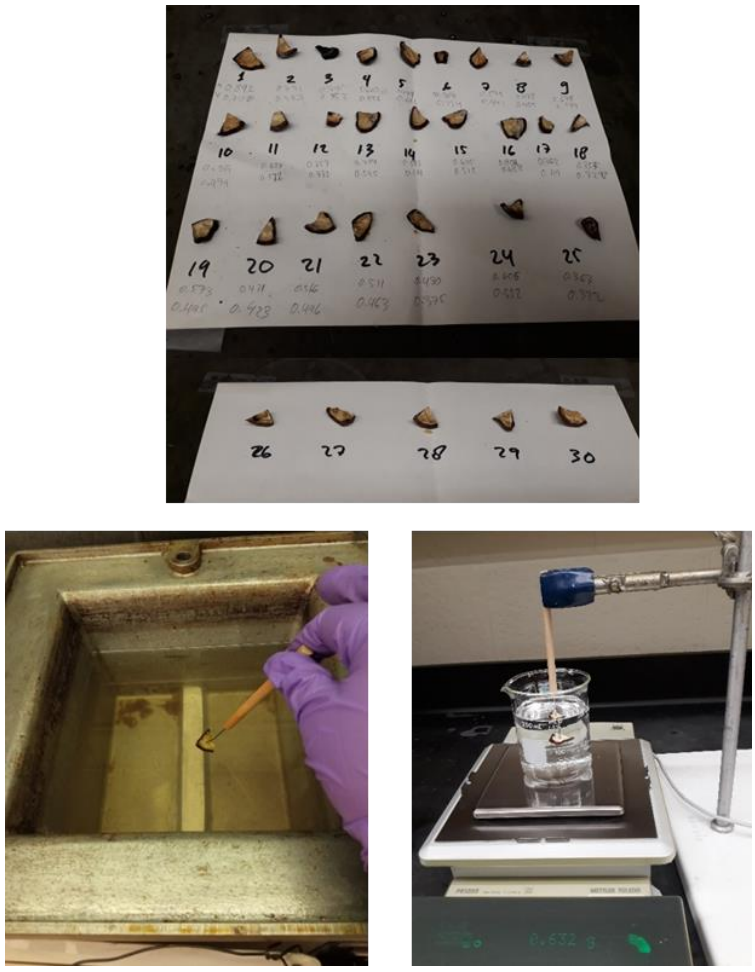

Figure 2.3 *Determination of candlenut shell relative density using water immersion method.*

Seed Coat Cell Size and Type Determination

Vanilla seed coat – approximately 0.05 gram of cleaned vanilla seed was macerated in 40 mL Franklin solution (glacial acetic acid:hydrogen peroxide, 1:1 v/v) at 60°C for 2/4/6h. Macerated seeds have a white-transparent appearance. Macerated seeds were removed from macerating solution by decantation and rinsed with water (3x10 mL). Macerated seeds were then transferred onto microscope slide, rinsed with water using spray bottle, and stained with Safranin-O. Samples were then observed in transmitted light microscope (Eclipse LV 100, Nikon, Tokyo, Japan). Images of macerated vanilla seed were captured using a microscope camera (DS-Fi1, Nikon, Tokyo, Japan). Dimensions of vanilla's seeds and cells were measured in NIS Elements Software ver. BR 4.11

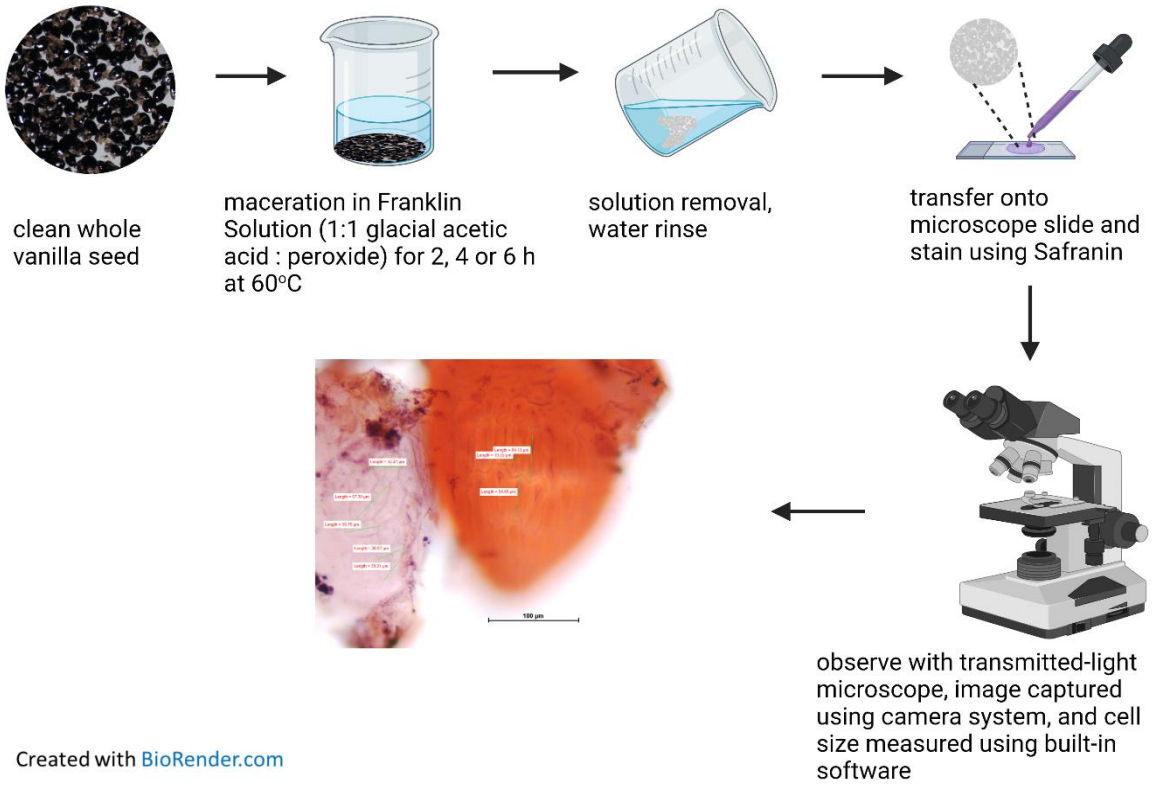

Figure 2.4 *Procedure to identify cell type and size in vanilla seed coat.*

Candlenut shell – candlenut shell was crushed using a hammer into small disk of approximately 10 x 5 mm (l x w) while maintaining nutshell original thickness. The nutshell disk was macerated in 40 mL Franklin solution (glacial acetic acid:hydrogen peroxide, 1:1 v/v) at 60°C for a total 18h (macerate 6h at 60°C then left soaked in Franklin solution at room temperature for 18h, repeat for 3 days using fresh Franklin solution). Macerated shell was removed from macerating solution by decantation and soaked in ethanol (30 mL) for 30 minutes. Ethanol was then removed and delignified shell was rinsed with water (3x10 mL). Macerated shell were then transferred onto petri dish filled with water. Single cell was separated from the whole delignified cell using dissecting needle. Several strands of single cells were transferred onto microscope slide, rinsed with water using spray bottle, and stained with Safranin-O. Cell diameter was observed in transmitted light microscope (Eclipse LV, 100 Nikon, Tokyo, Japan), while cell length was observed in reflected light microscope (SMZ745T, Nikon, Tokyo, Japan). Images of nutshell's cells were captured using microscope camera (DS-Fi1, Nikon, Tokyo, Japan). Diameter and length of candlenut shell's cell were measured in NIS Elements Software ver. BR 4.11.

Figure 2.5 *Hammer cracked candlenut to separate the shell and the nut.*

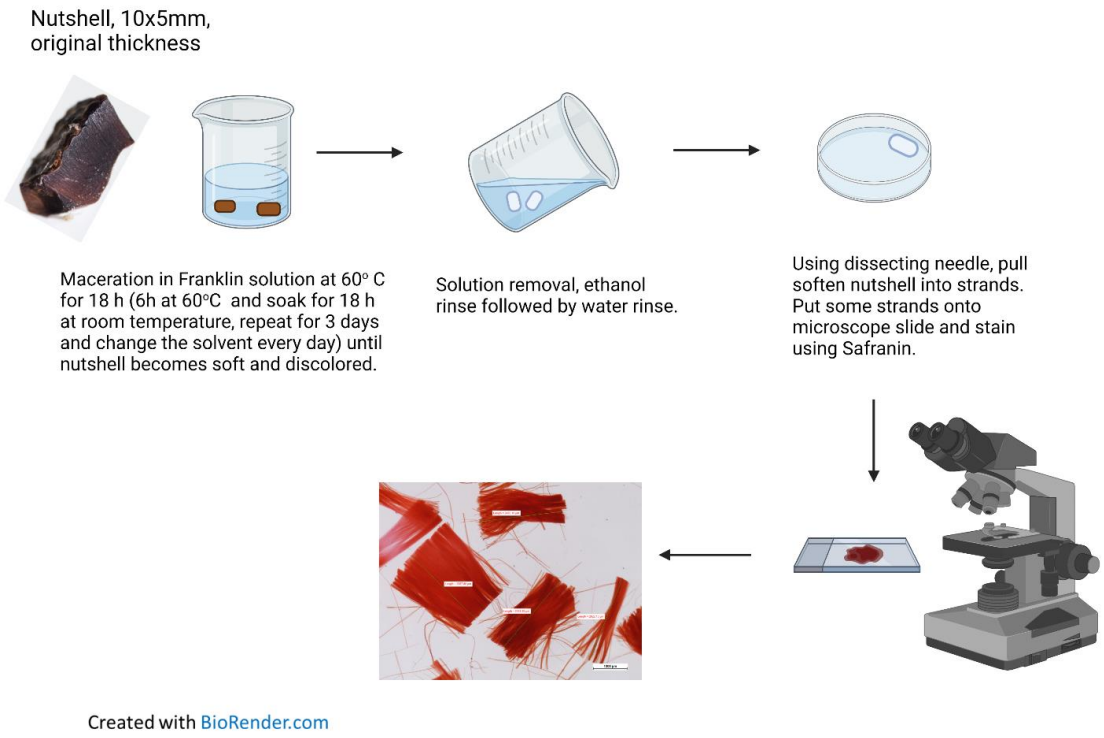

Figure 2.6 *Procedure to identify cell type and size in candlenut shell.*

SEM scanning

Vanilla seed – embryo and macerated tissue.

Samples (embryo and macerated tissue) were separately mounted onto SEM stub using double-sided copper tape and coated with gold in a sputter coater (Denton Vacuum, Moorestown, NJ, USA). The sputter instrument was set at gas pressure of of ≈50 mTorr, 40-50 mA. Samples were sputtered for 45 seconds and held back in the oven ≈50°C for at least overnight. Sample was mounted onto instrument sample holder and scanned in SEM instrument (NeoScope JCM 5000, JEOL Ltd., Tokyo, Japan) at operating voltage of 10 kV under vacuum.

Candlenut shell – intact disk and macerated.

Samples (intact candlenut shell disk and macerated) were dried in the oven ≈50°C overnight (Blue M, New Columbia, PA, USA) and mounted onto SEM bronze stub/pin mount with cross-section area (shell thickness)/outer layer/inner layer faced up, using double-sided copper tape, and coated with gold in a sputter coater (Denton Vacuum, Moorestown, NJ, USA). The sputter instrument was set at gas pressure of ≈50 mTorr, 40-50 mA. Samples were sputtered for 60 seconds and held back in the oven ≈50°C for at least overnight. Sample was mounted onto instrument sample holder.

Figure 2.8) and scanned in SEM instrument (NeoScope JCM 5000, JEOL Ltd., Tokyo, Japan) at operating voltage of 10 kV under vacuum. For isolated cell, some isolated cells were mounted onto SEM bronze stub, and arranged not to overlap each other using copper tape, then sputtered with gold for 60 seconds. Sample was mounted onto instrument sample holder and scanned in SEM instrument (NeoScope JCM 5000, JEOL Ltd., Tokyo, Japan) at operating voltage of 10 kV under vacuum.

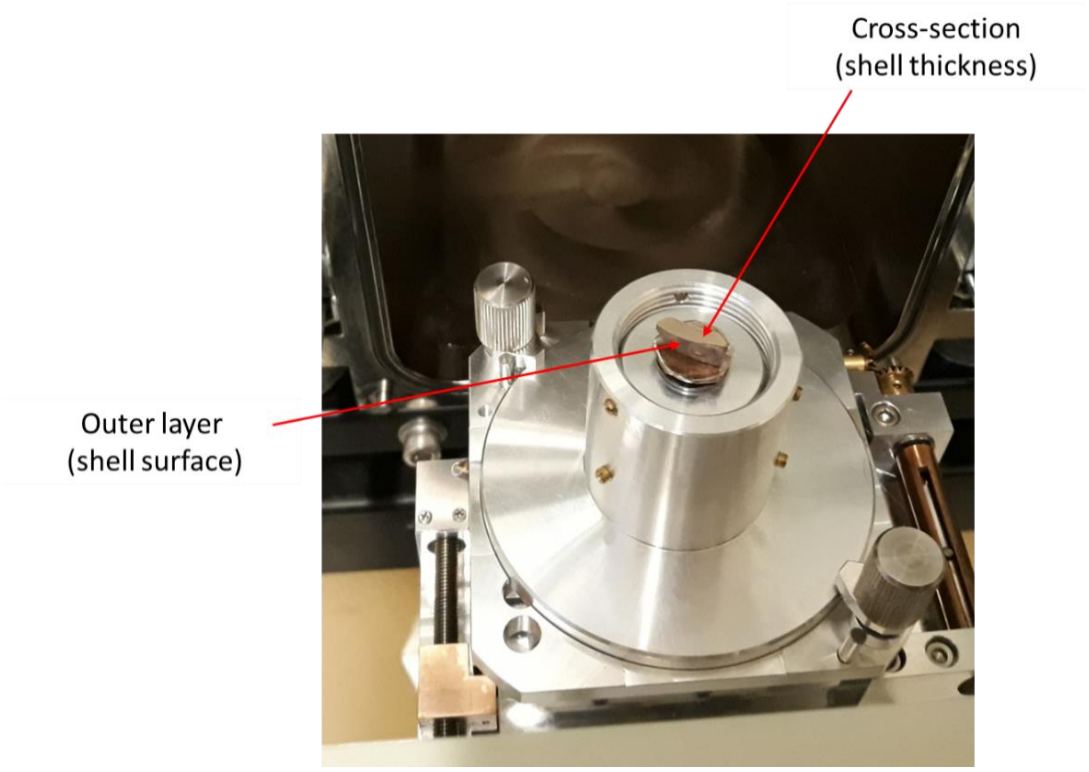

Figure 2.7 *Candlenut shell mounted onto SEM sample holder with shell's cross section faces up.*

Resin-embedding preparation for reflected light microscope, EDS-SEM, and FIB-SEM scans.

Candlenut shell and vanilla seed were embedded in epoxy resin in an aluminum pan and polymerized at room temperature for 1dThe hardened resin was then mechanically polished with silicon carbide grinding paper and colloidal alumina polishing suspension and resulted in a surface finish with ~50nm of surface roughness. The sample was coated with 6 nm of platinum-palladium in a sputter coater (Cressington 208HR sputter, Cressington Scientific Instrument, Watford, UK), to make the conductive thus reducing surface charging. Sample was observed using reflected light microscope Axio Scope A.1 (Zeiss, Oberkochen, Germany) in the dark field mode). The sample

was then mounted onto FIB-SEM sample holder using double-sided carbon tape and scanned in FIB-SEM instrument (FEI Helios 600 NanoLab, FEI company, Hillsboro, OR, USA) at operating voltage of 10 kV. For elemental distribution analysis, the sample was mounted onto SEM instrument sample holder using double-sided carbon tape and scanned in environmental SEM (FEI Quanta 600 FEG, FEI company, Hillsboro, OR, USA) at operating voltage of 15kV.

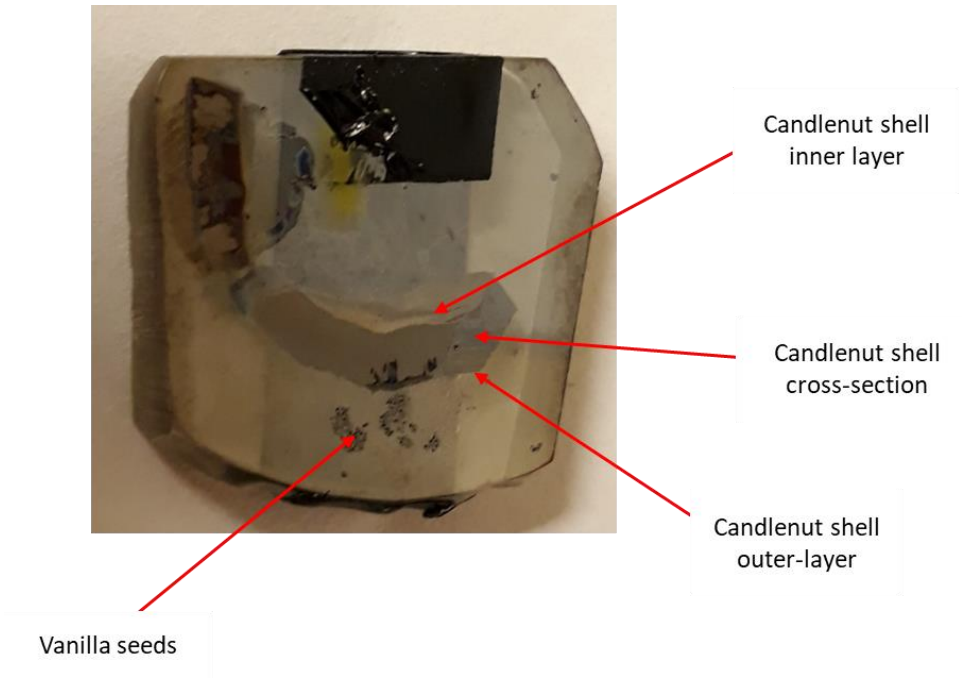

Figure 2.8 *Candlenut shell and vanilla seed embedded in resin. Position of vanilla seed, candlenut shell's outer layer, cross-section, and inner layer are indicated by red arrows.*

2.4 Result and Discussion

Vanilla seed's surface is covered by dark material known as *phytomelan* that start to accumulate in the outer and the lateral cell wall of the outermost layer of outer integument before sclerotization of outermost layer of outer integument.[26] The outermost layer of outer integument becomes seed coat, the only part of vanilla that contain C-lignin. Vanilla seed size is approximately

300μm in diameter (**Figure 2.9**). Morphology of cells that construct vanilla seed coat was studied using transmitted, reflected lights, and electron microscopes.

Figure 2.9 *Reflected light microscopy image of vanilla seed. The size of vanilla seeds is approximately 300μm.*

Cell dimension can be determined using measurement on tangential section or on macerated tissue.[27] Here, we used macerated tissue to determine cell size and type of vanilla seed by macerating in Franklin solution for 2h, 4h and 6h. Franklin solution is a mixed of concentrated glacial acetic acid and 30% hydrogen peroxide used to soften hard tissues.[28] After 2 hours, vanilla entire seed parts were still integrated and the black outer surface started to wear off. Transmitted light microscopy of unstained, 2h-macerated seeds show yellowish/brownish seeds **(Figure 2.10 left image**).

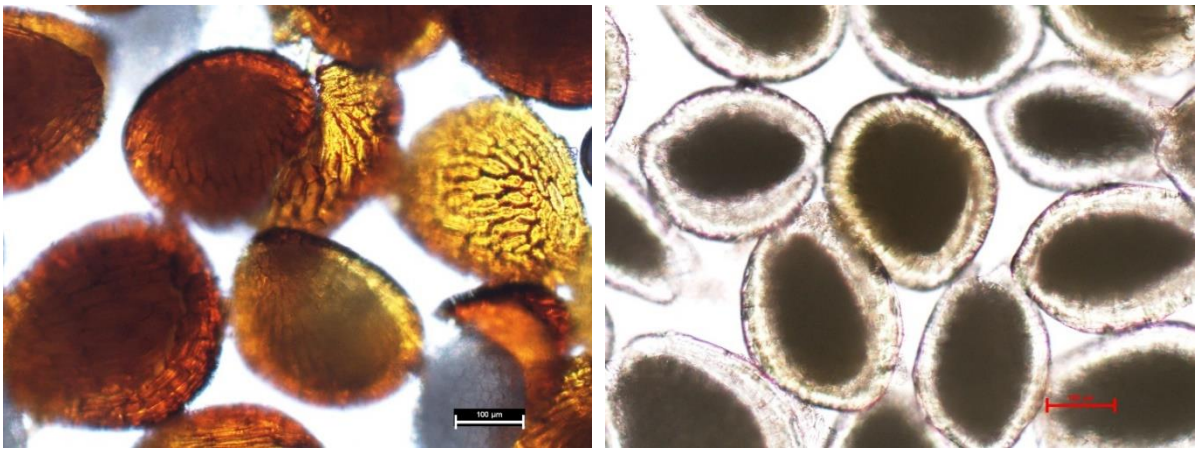

Figure 2.10 *Transmitted light microscope images of unstained, macerated vanilla seeds.* ***Left*** *– 2h macerated vanilla seeds;* ***Right*** *– 4h macerated vanilla seeds.*

After 4 hours, transmitted light microscope image of unstained vanilla seeds shows transparent outer layer and dark inner layer (**Figure 2.10 right image**). The transparent outer layer indicates that *phytomelan* has been removed from the seed's outer surface. Image of stained-macerated vanilla seeds (**Figure 2.11**) show seed coat's cells looks from outer surface. The cells seem to be ranging from 30-90 μm in length and 20-30 μm in width, with a lumen at the center of individual cell. The cells were still well-integrated on the outer surface. The appearance of the cell shape observed from the outer surface looks like the osteosclereids cells observed from the outer layer of *Pisum elatium*.[29] The image also shows the embryo that discharged from the seed coat. The outer surface of embryo is covered with similar cell shape to seed coat outer surface. Dark material accumulated on the outer surface of vanilla seeds was still observed, although most of the surface area has been turn into transparent.

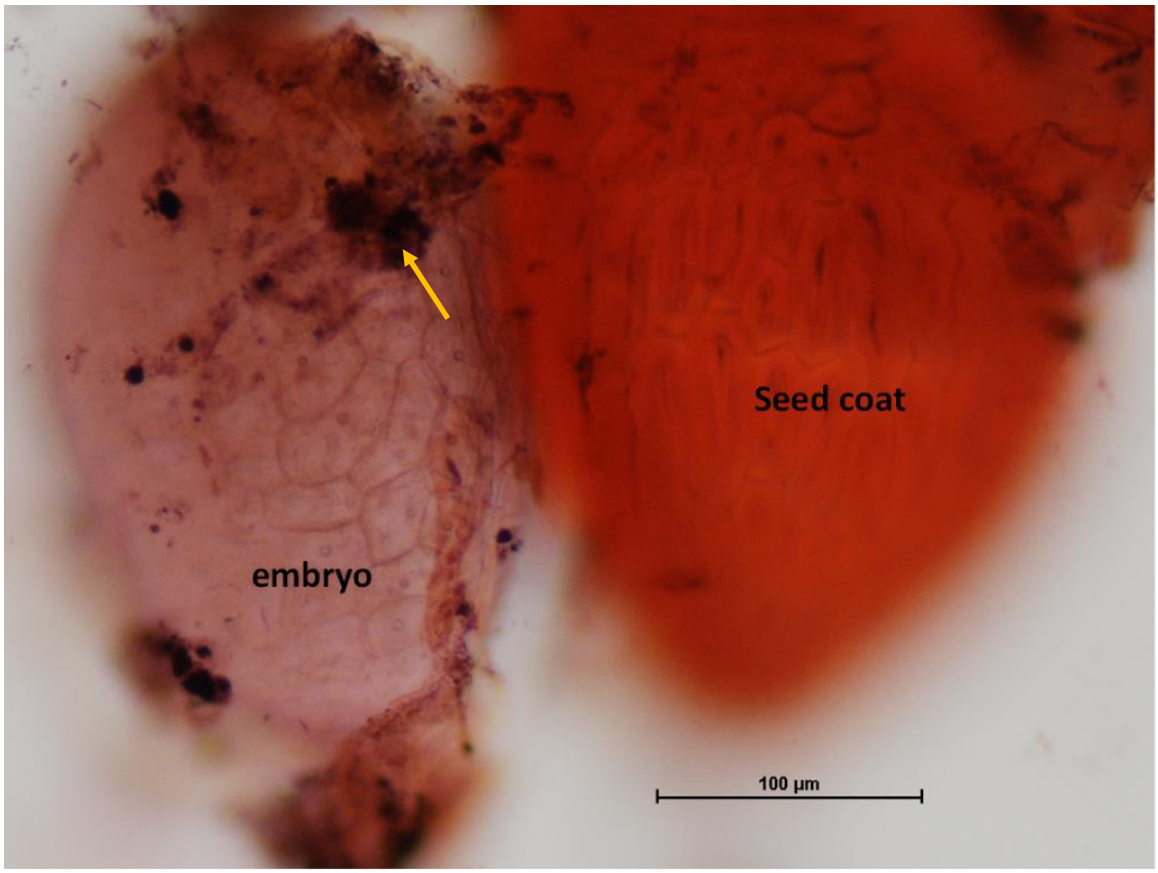

Figure 2.11 *Transmitted light microscopy image of vanilla seed after 4h maceration, stained with Safranin O and observed in transmitted light microscope. Outer cells are still connected one to another, but the some phytomelan (indicated by yellow arrow) still can be observed. Scale bars indicate 100µm.*

Vanilla seeds macerated for 6h show that some cells are separated from the unit. *Phytomelan* is still observed in some parts of the surface (**Figure 2.12, indicated by yellow arrow**). The borders of cells are also more obvious. The cells observed from the surface of 6h macerated vanilla seeds look like the elongated or stretched isodiametric cells. The 6h-macerated seed shows that most cells located in the medial are longer than those close to the pole and cell has lumen.

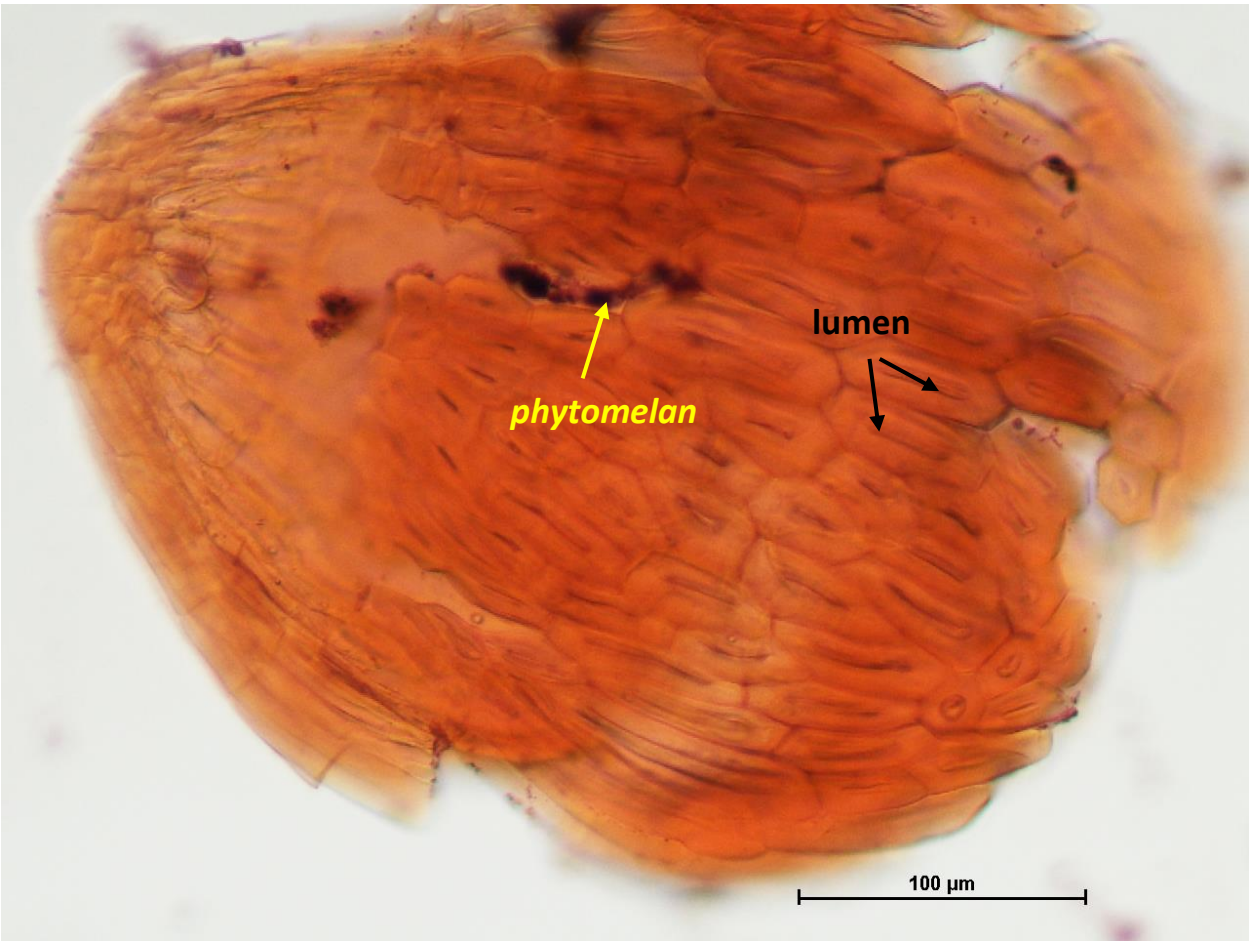

Figure 2.12 *Transmitted light microscopy image of vanilla seed after 6h maceration, stained with Safranin O. Some seed coat cells have been detached from the outer seed surface and some phytomelan (as indicated by yellow arrow) is still observed on the surface.*

To identify the cell type of vanilla seed coat, the 4h-macerated tissues were scanned using scanning electron microscopy. The tissue macerated for 4h is preferred than the 2h or 6h ones, since by macerating for 4h, most of the *phytomelan* has been removed but the cells has not disintegrated yet. Images obtained from SEM scanning at different magnifications were shown on **Figure 2.13**.

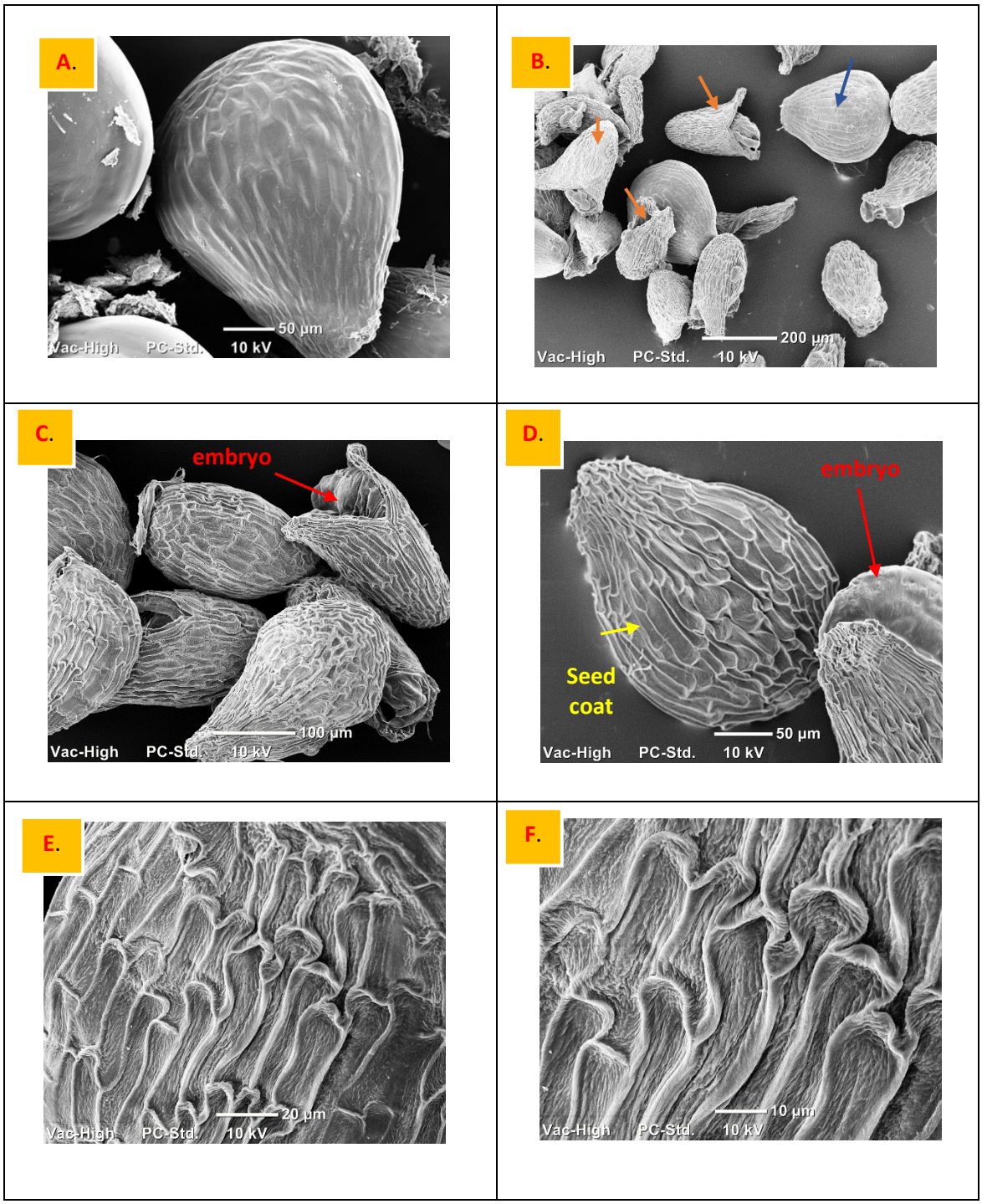

Figure 2.13 *SEM images of non-macerated vanilla seeds at 300X magnification* ***(A)****, and macerated vanilla seeds at different magnifications:110X* ***(B)****, 240X* ***(C)****, 340* ***(D)****, 900X* ***(E)****, and 1500X* ***(F)****. Image B shows some seeds have embryo popped out (****orange arrows****) and some seeds were intact (****blue arrows****). Images C and D show the embryo and seed coat of macerated vanilla seed. Images E and F show the surface of macerated vanilla seed coat.*

SEM images of 4h-macerated vanilla seeds show that after 4h maceration, some seeds have embryos popped out (**Figure 2.13 A and B**). The surface of vanilla seed is covered by elongated cells. The shape of individual cell is rectangular, with medial cell are highly elongated compared to cells in the poles (**Figure 2.13 C and D**). **Figure 2.13 E and F** are seed coat cells located in the middle. The seed coat cell wall shows undulated anticlinal curvature. According to Barthlott and co-workers, seed orchids usually have no endosperm, look like a balloon, with air-filled space between embryo and seed coat. Seed coats in orchids usually have tetragonal, hexagonal, or polygonal shape, with variation such as isodiametric, elongate in the longitudinal axis and rectangular, and cells are elongate but rounded at the ends.[30]

Elemental analysis using energy dispersive spectroscopy-scanning electron microscopy (EDS-SEM) was used to identify the chemical compositions and distribution in vanilla seed coats and candlenut shells. Vanilla seed shows the deposition of calcium in its entire seed part (**Figure 2.14**), and it is distributed almost equally among seed coat, area between seed coat and embryo, and embryo as shown on **Table 2.1**. Calcium deposition is common in higher plant's cell-wall,[31-33] and usually associated with regulation of certain plant metabolisms and responses to environmental stress.[34]

Table 2.1 Elemental composition of vanilla seed

Area	C (%)	O (%)	Al (%)	Ca (%)
Outer seed coat (11)	52.11	47.40	-	0.31
Embryo (12)	49.38	42.17	8.17	0.26
Inner seed coat (13)	37.00	42.58	20.06	0.35

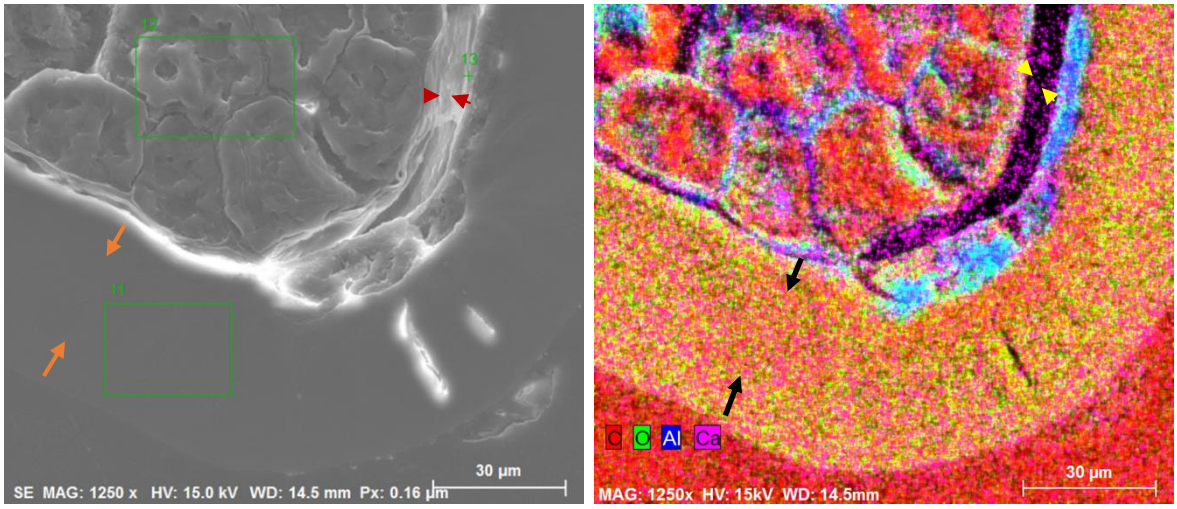

Figure 2.14 *EDS-SEM scan of vanilla seed coat (left) and elemental distribution in the inner layer of candlenut shell (right). Orange and black arrows indicate outer seed coat area in SEM and EDS images respectively; red and yellow arrows indicate inner seed coat area in SEM and EDS images respectively.*

Candlenut shell outer surface is rough, dark brown in color, and often covered by white yellowish flaky substances which easily removed by brushing or wiping with wet cloth (**Figure 2.16**). The globules candlenut sized approximately 3-3.5 cm in diameter, with part near *micropyle* (bottom) tapered. The thickness of the shell is ≈ 0.3 mm and part near *hilum* (top part of seed that attached to the stem) and *micropyle* are less thin (≈ 0.2 mm). Candlenut shell is denser than wood. From various sample collected, the density of candlenut shell ranges from **≈1.0 – 1.3 g/cm^3**, with

average density **1.14 ± 0.07 g/cm^3**.This value is comparable to macadamia nutshell (1.5 g/cm^3 fresh/wet, 1.27 g/cm^3 dry).[35] SEM image of the outer surface after flaky substance removal (**Figure 2.17**) show an arrangement that look like a honeycomb. It seems that the pattern is created by the end-tips of cells that occupy the cross-section area of the shell.

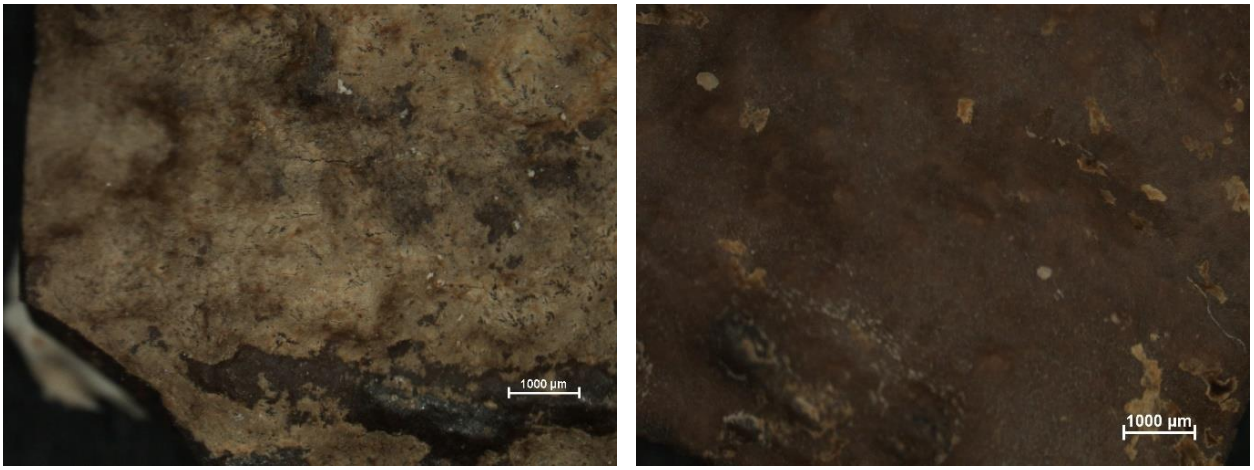

Figure 2.16 *Reflected light microscope images of candlenut shell outer surface:* ***Left****–White yellowish flaky substance is observed on the outer surface of candlenut shell;* ***Right****– candlenut shell outer surface after the removal of flaky substance.*

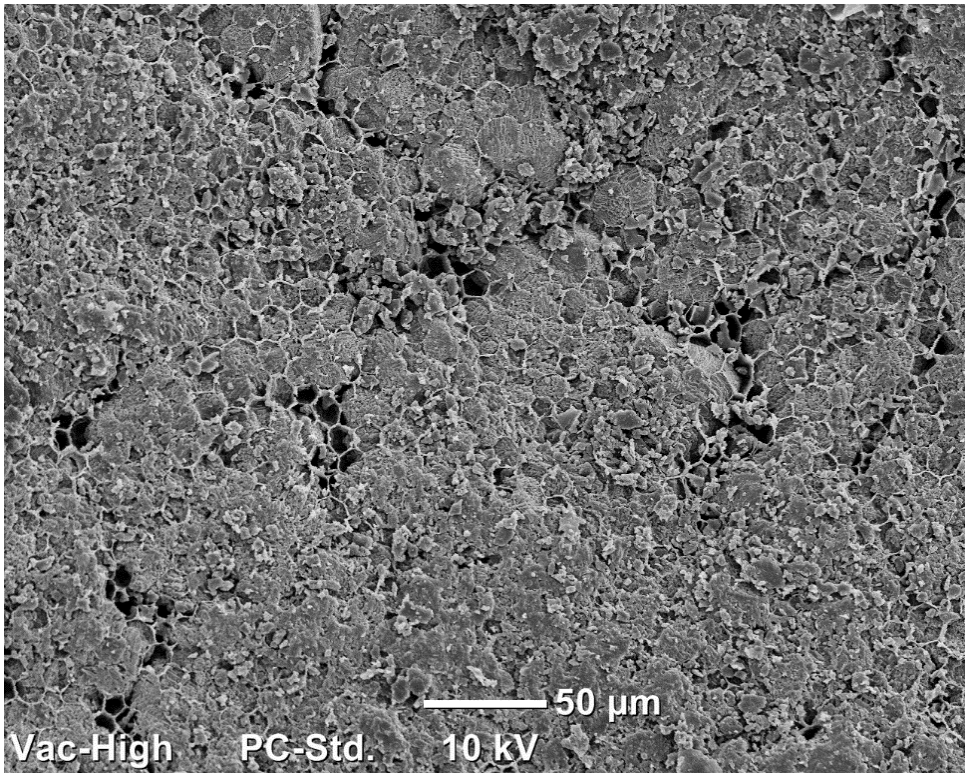

Figure 2.17 *SEM image of outer surface after flaky substance removal*

The cross-sectional area makes up the shell thickness (**Figure 2.18**). This area consists of homogenously elongated long tubular cells with needle-like bundles appearance, tightly adhered to each other's. Some parts of the cross-section seem to have darker color than the other part. The difference of color in the shell is perhaps an optical effect called 'light-line' (*linea lucida*)[36] but could also be a deposition of polyphenol in the form of tannin cell.[12] The cells seem to be sclerotized and reinforce the shell structure. SEM image taken on cross-section layer was shown in **Figure 2.19**. The needle-like bundles observed in the cross-section looks like a striated wall.

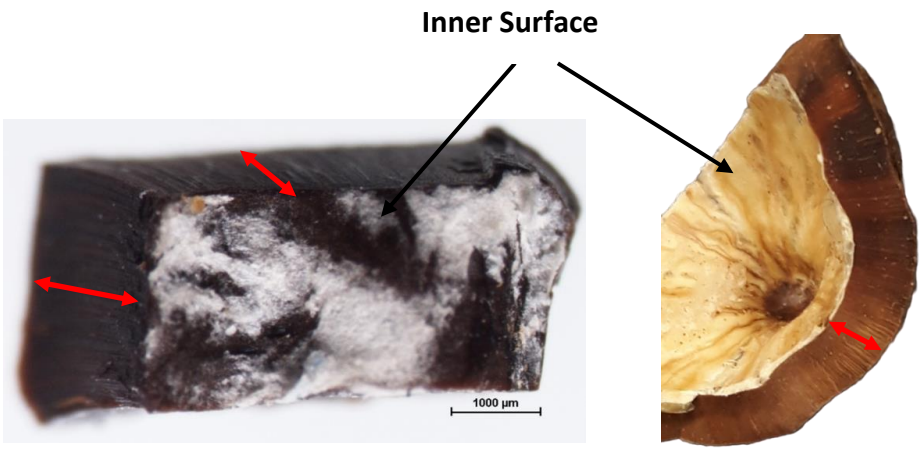

Figure 2.18 *Cross sectional area of candlenut shell (indicated by red arrows), which is also the thickness of the shell.*

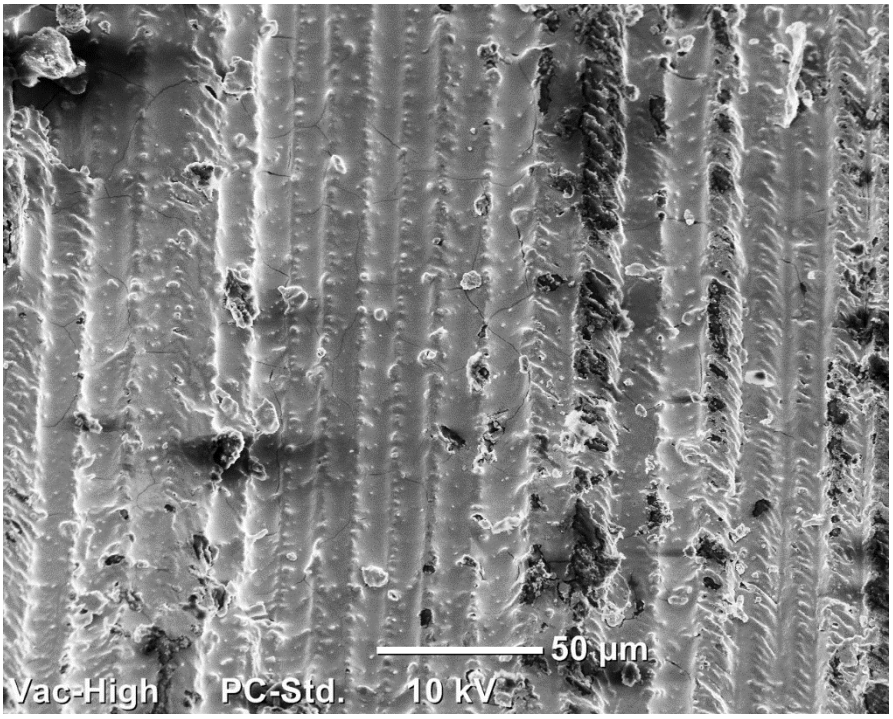

Figure 2.19 *SEM image of candlenut shell cross-section area*

The inner look of candlenut shell is a single hollow, with no interlocked packing as observed in black walnut (*Juglans nigra*) shell (**Figure 2.20**). The inner surface of candlenut shell is coated by thin, pale-colored layer (**Figure 2.21**). Candlenut shell has different colors that distinguish the

outer surface, the middle cross section, and the inner surface. The thin, pale colored thin layer of inner surface looks spongy and airy. This layer is attached to the woody-brown cross-section and can be removed by scratching with sharp object, such as cutter and knife.

Figure 2.20 *Candlenut inner surface compared to black walnut inner surface.*

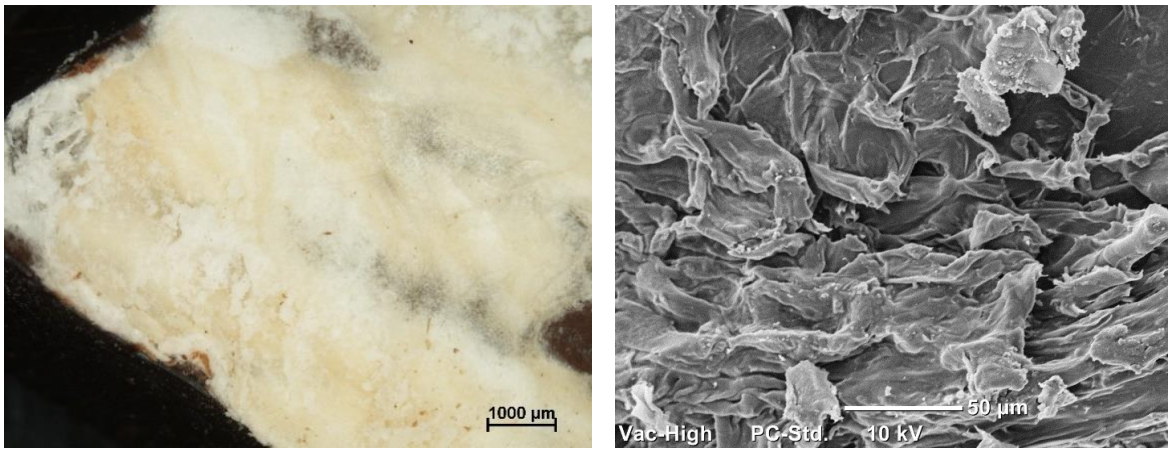

Figure 2.21 Left *– Reflected light microscope image of candlenut shell inner surface that covered by pale-colored and airy substance;* ***Right*** *– SEM image of candlenut shell inner surface.*

Maceration of candlenut shell in Franklin solution for 3 days result in white-transparent, soft shell. The upper surface and lower surface were disintegrated, but the cross-section part is still integrated. The integrated needle-like like was separated using dissecting needle, stained, and observed with reflected light (**Figure 2.22**) and transmitted light (**Figure 2.23**) microscopes. The

cells in nutshell's cross-section are long, tubular cells; they are known as macrosclereids-type sclereids, as observed in the seed coat of pea (*Pisum sativum*).[37, 38] The length of candlenut macroscelereids is 2481.54 ± 155.46 μm and the diameter is 3.16 ± 0.52 μm. Macrosclereids are also known as Malphigian cells, commonly found in hard legumes seeds and associated with seed coat permeability.[13]

Macroclereids are the only cell type isolated from maceration process. Macrosclereids are commonly found in legumes and form a thick, waterproof layer of seed coat.[39] SEM images taken on isolated macrosclereids (**Figure 2.24**) show how dense and homogenous the macrosclereids in candlenut shell are. The dense cellular arrangement provides reinforcement to the nutshell structure, making the nutshells hard to crack**.** SEM images (**Figure 2.24 a, c and d**) show the end tips of the sclereids, but it is not sure if these are the end-tips of the outer surface or the inner surface of the candlenut shell.

Figure 2.22 *Reflected light microscope image of macerated candlenut shell.*

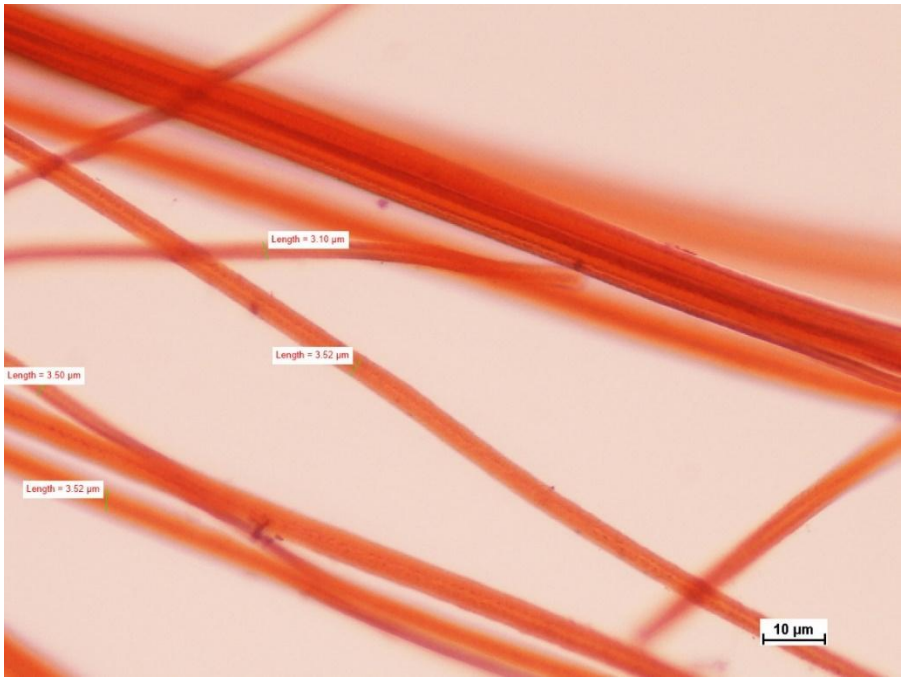

Figure 2.23 *Transmitted light light microscope image of macerated candlenut shell.*

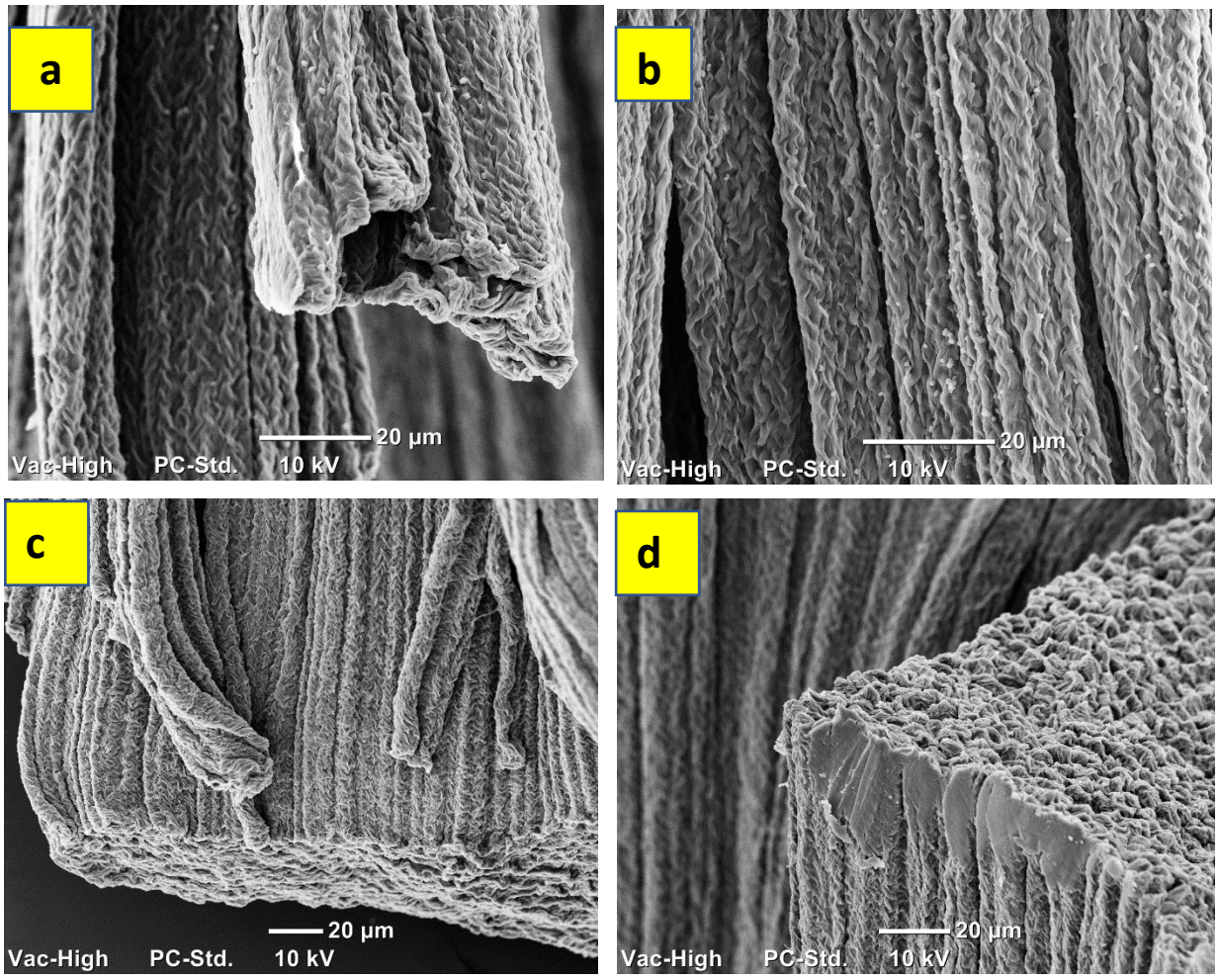

Figure 2.24 *SEM images of isolated macrosclereids at different magnification: (a). 1100X (b). 1300X (c). 700X (d). 540X. Macrosclereids lined up densely and adhered one to another. Images a, c and d show the end-tip of macrosclereids, image b show the middle region of macrosclereids.*

Deposition of G and C-lignin in *Cleome hassleriana* was reported to occur independently, in which C-lignin deposited later than G-lignin. The synthesis of C-lignin is indicated by the downregulation of O-methyltransferase.[24] We used candlenut shell embedded on resin and using reflected light microscopy FIB, and EDS-SEM to check if there is separated layer that can indicate the deposition of G and C lignin in candlenut cross-section. Images are taken from the area that is close to the outer surface and those close to the inner surface.

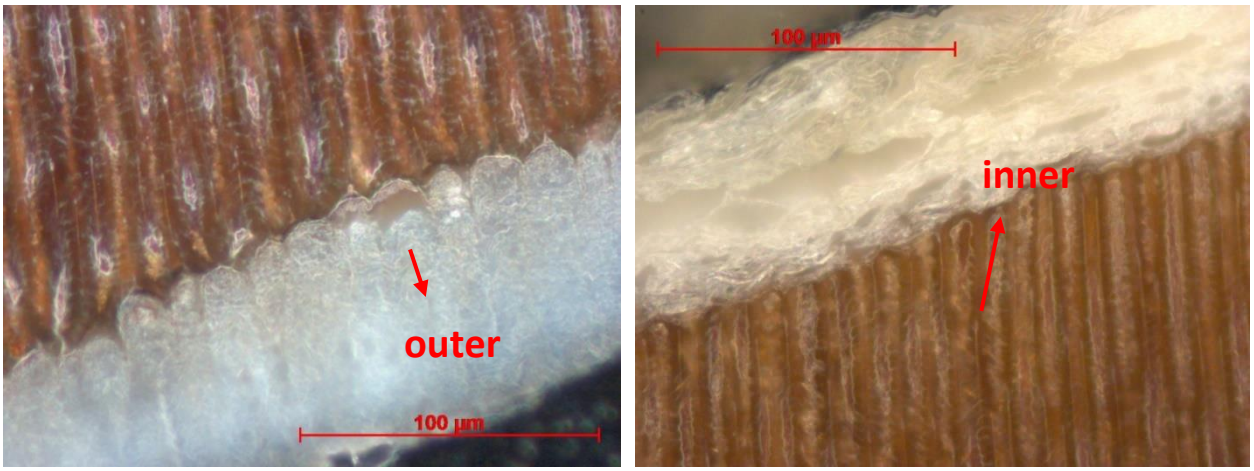

Figure 2.25 *Reflected light microscope images:* ***Left*** *– outer surface of candlenut (direction indicated by red arrow) and macrosclereids end-tip that occupy area near the outer surface area.* ***Right*** *– Inner surface of candlenut (direction indicated by red arrow) and macrosclereids end-tip that occupy area near the inner surface area.*

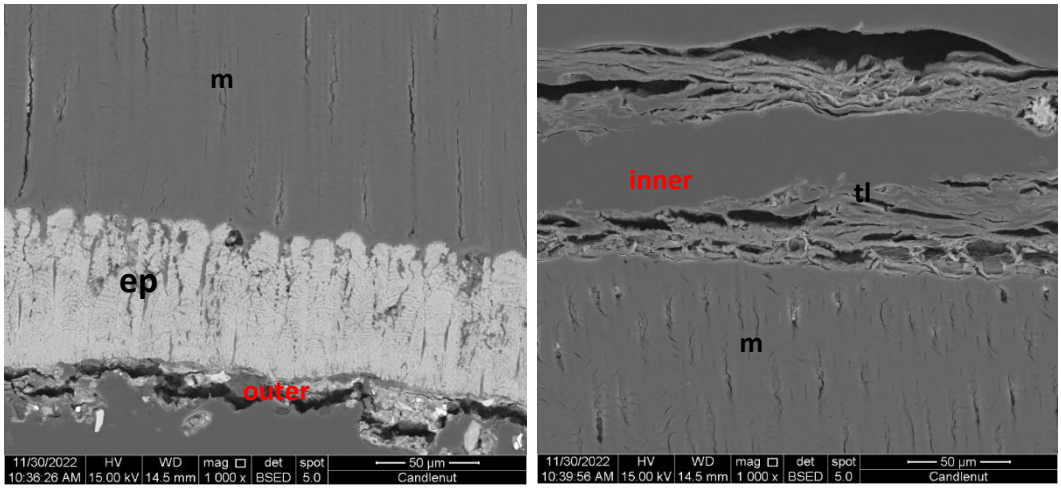

Figure 2.26 *FIB-SEM image* ***Left*** *– Outer surface of candlenut shell: epidermis layer (****ep****) and macrosclereids layer (m);* ***Right*** *– Inner surface of candlenut: thin layer around the seed (****tl****) and macrosclereids layer (****m****).*

Figure 2.25 shows macrosclereids's end-tips that close to the outer surface of the shell (**left**) and end-tip that close to the inner surface of the shell (**right**) observed with reflected light microscope. Macrosclereids looks like perforated tubes, covered by whitish layers in the outer and inner surfaces. FIB-SEM image (**Figure 2.26 left**) show the epidermis layer (**ep**) as the outermost layer of the shell and covers macrosclereids (**m**). A thin layer (**tl**) covers the inner surface (**Figure 2.26 right**) and becomes the innermost layer that border macrosclereids (**m**) layer to the seed.

Elemental distribution analyzed using EDS-SEM for the area near the outer and inner surfaces were shown on **Figure 2.27** and **2.28** respectively. In the region near the outer surface (**Figure 2.27**), the calcium distribution is more abundant in the epidermis (**ep**) layer area than in macrosclereids layer (**m**) (**Table 2.2**). The area near the inner surface (**Figure 2.28**) shows calcium deposition as chunk in the thin layer (**tl**) region instead of evenly distributed as shown in epidermis. No significant calcium deposition in the macrosclereids (**m**) layer (**Table 2.3**). The deposition of calcium in candlenut shell's epidermis and thin layer probably has no correlation to the occurrence of both G and C-lignin in candlenut shell despite calcium being known to regulate certain biological functions and reinforce mechanical properties.[32-34, 40] Calcium deficiency in plant has been reported to result in reduction in wood increment, vessel size and fiber length, and reduction in carbonyl and methoxy group from S-lignin.[41] However, it is interesting to know that in vanilla seeds, calcium is present in the entire seeds part including the sclerotic seed coat (**Figure 2.14**), while it seems to be absent in candlenut shell's macrosclereids layer (**Figure 2.27 and 2.28**).

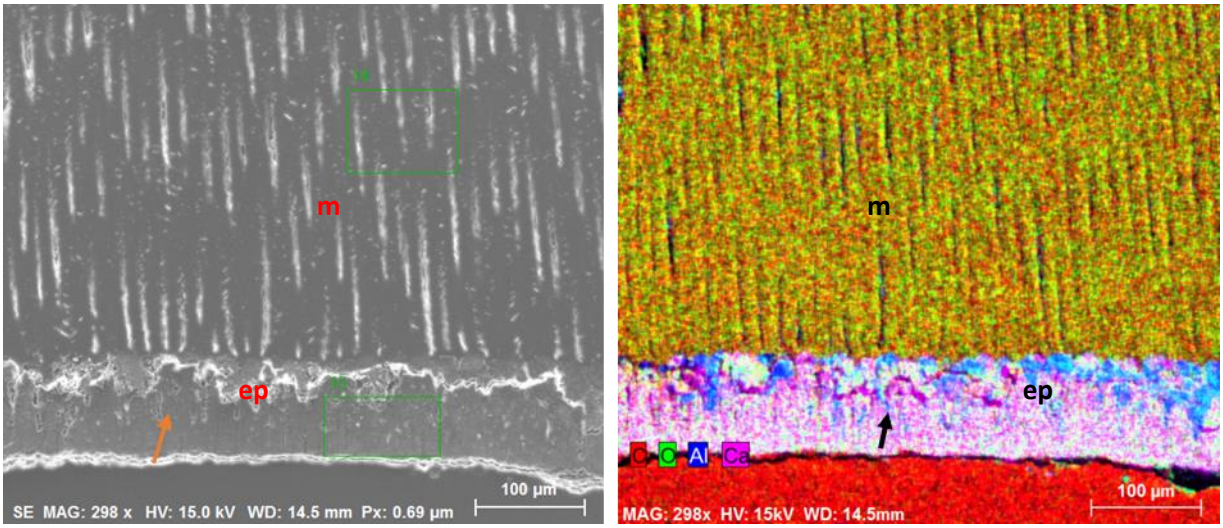

Figure 2.27 *EDX scan of candlenut shell,* ***Left*** *– epidermis (****ep****)outermost layer of the shell and macrosclereids (****m****) region;* ***Right*** *– elemental distribution in epidermis (ep) and macrosclereids. Orange and black arrows indicate direction from outer surface of the shell in SEM and EDS images respectively.*

Table 2.2 Elemental candlenut shell cross section from the outer layer.

Area	C (%)	O (%)	Al (%)	Ca (%)
Shell cross section near outer layer surface area (14)	65.76	34.07	0.04	0.13
Outer layer surface area (15)	29.10	55.74	0.74	11.88

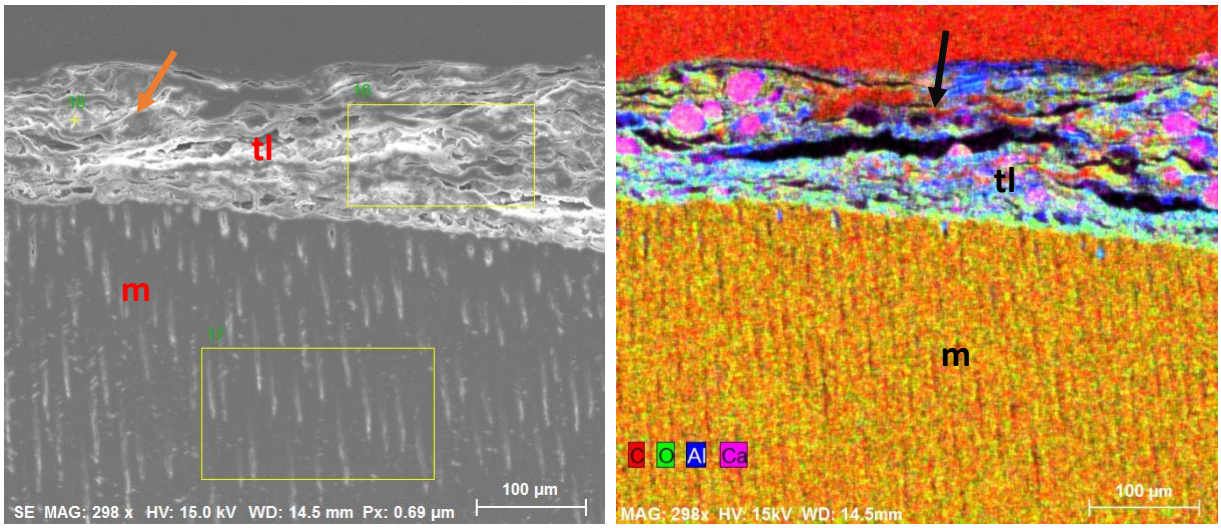

Figure 2.28 *EDX scan of candlenut shell,* ***Left*** *– thin layer (**tl**)innermost layer of the shell and macrosclereids (**m**) region;* ***Right*** *– elemental distribution in thin layer (**tl**) and macrosclereids (**m**). Orange and black arrows indicate direction from inner surface of the shell in SEM and EDS images respectively.*

Table 2.3 Elemental candlenut shell cross section from the inner layer

Area	C (%)	O (%)	Al (%)	Ca (%)
Inner layer surface area (16)	56.01	40.06	2.78	1.04
Shell cross section near inner layer surface area (17)	66.34	33.61	-	0.05
Inner layer with Ca-deposition (18)	24.03	45.87	-	30.10

Based on the images collected from reflected light microscopy on resin-embedded and intact candlenut shell and FIB-SEM scan on resin-embedded candlenut shell, the cell structure of the cross-sectional region that construct candlenut shell thickness can be mapped as shown in the **Figure 2.29**. The structure of candlenut shell from outer surface to inner surface is epidermis layer, macrosclereids layer, and thin layer that surrounds the seed. Macrosclereids are dominating the

shell thickness region, as it sized ~ 2000-3000 µm, almost equally to the shell thickness, and left perhaps 20-30 µm for each epidermis and the thin layer.

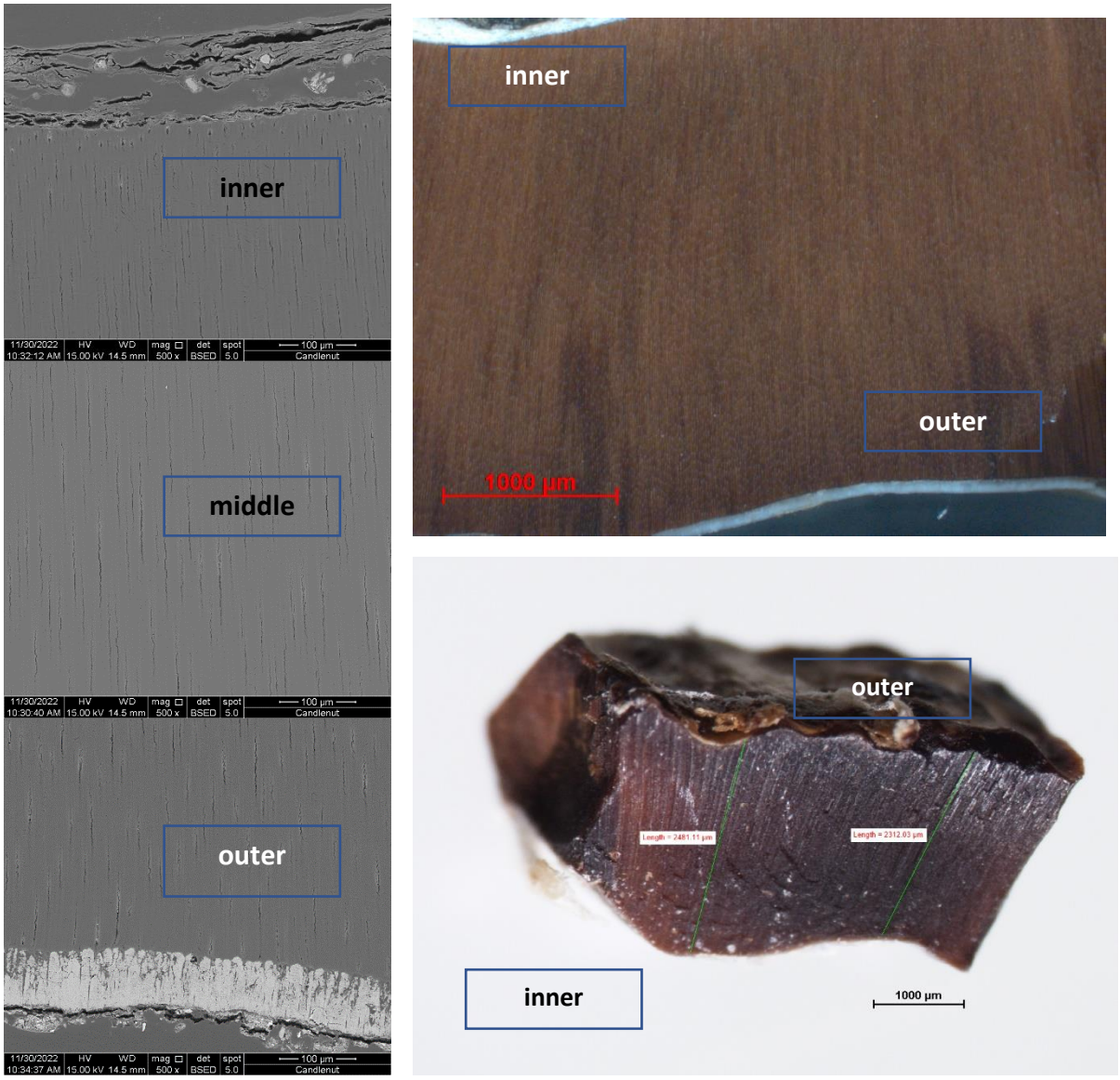

Figure 2.29 Left *– FIB-SEM images of resin-embedded candlenut shell taken separately from the outer, middle and inner regions;* ***Right*** *–* ***Upper****: reflected light microscope image of resin-embedded shell;* ***Right*** *–* ***Lower****; reflected light microscope image of cross-sectional region of intact candlenut shell.*

2.5 Conclusion

Vanilla seed coat and candlenut shell are both hardening tissues that protect the embryo. Vanilla seed coat and candlenut shell have different sclereids that construct their seed coat/nutshell. Vanilla seed coat has osteosclereids type sclereid that cover the entire outer surface of the seed. The size of individual cells is ranging from 30 to 90 μm in length and 20-30 μm in width. Meanwhile, candlenut shellis constructed by epidermis, macrosclereids and thin layer that surrounds the seeds. Candlenut shell macrosclereids are composed of long and thin cells that stretches along the shell thickness, with ratio of its diameter to length is about 1:800. Although both vanilla seed coat and candlenut shell are highly sclerotized, the two tissues exhibit different behavior towards calcium deposition. The vanilla seed coat that has C-lignin shows calcium deposition in its sclereid while candlenut macrosclereids that have both G/S-lignin do not favor calcium deposition.

2.6 References

1. Bonacorsi, N. K.; Gensel, P. G.; Hueber, F. M.; Wellman, C. H.; Leslie, A. B., A novel reproductive strategy in an Early Devonian plant. *Curr Biol* **2020,** *30* (9), R388-R389.

2. Bareke, T., Biology of seed development and germination physiology. *Advances in Plants & Agriculture Research* **2018,** *8* (4).

3. Holsinger, K. E., Reproductive Systems and Evolution in Vascular Plants. *PNAS* **2000,** *97* (13), 7037–7042.

4. DiMichele, W. A.; Davis, J. I.; Olmstead, R. G., Origins of Heterospory and the Seed Habit: The Role of Heterochrony. *Taxon* **1989,** *38* (1), 1-11.

5. Verhage, L., Secrets of the seed: uncovering the real identity of the endosperm-surrounding cuticle. *Plant J* **2020,** *104* (3), 565-566.

6. Linkies, A.; Graeber, K.; Knight, C.; Leubner-Metzger, G., The evolution of seeds. *New Phytol* **2010,** *186* (4), 817-831.

7. Huss, J. C.; Gierlinger, N., Functional packaging of seeds. *The New Phytologist* **2021,** *230* (6), 2154.

8. Schweingruber, F. H.; Börner, A., Cellular composition of the plant body. In *The Plant Stem: A Microscopic Aspect*, Schweingruber, F. H.; Börner, A., Eds. Springer International Publishing: Cham, 2018; pp 11-28.

9. Terashima, N.; Fukushima, K., Heterogeneity in formation of lignin XI: An autoradiographic study of the heterogeneous formation and structure of pine lignin. *Wood Sci. Technol.* **1988,** *22*, 259-270.

10. Mottiar, Y.; Vanholme, R.; Boerjan, W.; Ralph, J.; Mansfield, S. D., Designer lignins: harnessing the plasticity of lignification. *Curr Opin Biotechnol* **2016,** *37*, 190-200.

11. Voxeur, A.; Wang, Y.; Sibout, R., Lignification: different mechanisms for a versatile polymer. *Curr Opin Plant Biol* **2015,** *23*, 83-90.

12. Boesewinkel, F. D.; Bouman, F., The Seed: Structure. In *Embryology of Angiosperms*, Johri, B. M., Ed. Springer Berlin Heidelberg: Berlin, Heidelberg, 1984; pp 567-610.

13. Boesewinkel, F. D. a. B., F., The Seed: Structure and Function. In *Seed development and germination*, Kigel, J.; Galili, G., Eds. CRC press: New York, 1995; Vol. 41, pp 1-21.

14. Scutt, C. P.; Vinauger-Douard, M.; Fourquin, C.; Finet, C.; Dumas, C., An evolutionary perspective on the regulation of carpel development. *J Exp Bot* **2006,** *57* (10), 2143-52.

15. Lorts, C. M.; Briggeman, T.; Sang, T., Evolution of Fruit Types and Seed Dispersal: A Phylogenetic and Ecological Snapshot. *J Syst Evol.* **2008,** *46* (3), 396-404.

16. Dardick, C.; Callahan, A. M., Evolution of the fruit endocarp: molecular mechanisms underlying adaptations in seed protection and dispersal strategies. *Front Plant Sci* **2014,** *5*, 284.

17. Dejardin, A.; Laurans, F.; Arnaud, D.; Breton, C.; Pilate, G.; Leple, J. C., Wood formation in Angiosperms. *C R Biol* **2010,** *333* (4), 325-34.

18. Li, P.; Wang, H.; Liu, P.; Li, Y.; Liu, K.; An, X.; Zhang, Z.; Zhao, S., The role of JrLACs in the lignification of walnut endocarp. *BMC Plant Biol* **2021,** *21* (1), 511.

19. Landucci, L.; Smith, R. A.; Liu, S.; Karlen, S. D.; Ralph, J., Eudicot Nutshells: Cell-Wall Composition and Biofuel Feedstock Potential. *Energy & Fuels* **2020,** *34* (12), 16274-16283.

20. Preston, C. M.; Sayer, B. G., What's in a Nutshell: An Investigation of Structure by Carbon-13 Cross-Polarization Magic-Angle Spinning Nuclear Magnetic Resonance Spectroscopy. *J. Agric. Food Chem.* **1992,** *40*, 206-210.

21. Antreich, S. J.; Xiao, N.; Huss, J. C.; Gierlinger, N., A belt for the cell: cellulosic wall thickenings and their role in morphogenesis of the 3D puzzle cells in walnut shells. *J Exp Bot* **2021,** *72* (13), 4744-4756.

22. Antreich, S. J.; Xiao, N.; Huss, J. C.; Horbelt, N.; Eder, M.; Weinkamer, R.; Gierlinger, N., The Puzzle of the Walnut Shell: A Novel Cell Type with Interlocked Packing. *Adv Sci (Weinh)* **2019,** *6* (16), 1900644.

23. Chen, F.; Tobimatsu, Y.; Havkin-Frenkel, D.; Dixon, R. A.; Ralph, J., A polymer of caffeyl alcohol in plant seeds. *Proc Natl Acad Sci U S A* **2012,** *109* (5), 1772-7.

24. Tobimatsu, Y.; Chen, F.; Nakashima, J.; Escamilla-Trevino, L. L.; Jackson, L.; Dixon, R. A.; Ralph, J., Coexistence but independent biosynthesis of catechyl and guaiacyl/syringyl lignin polymers in seed coats. *Plant Cell* **2013,** *25* (7), 2587-600.

25. Li, Y., Shuai, L., Kim, H., Motogamwala, A. H., Mobley, J. K., Yue, F., Tobimatsu, Y., Havkin-Frenkel, D., Chen, F., Dixon, R. A., Luterbacher, J. S., Dumesic, J., Ralph, J., An "ideal lignin" facilitates full biomass utilization. *Sci. Adv.* **2018,** *4*, 1-10.

26. Nishimura, G.; Yukawa, T., Dark Material Accumulation and Sclerotization During Seed Coat Formation in Vanilla planifolia Jacks. ex Andrews (Orchidaceae). *Bull. Natl. Mus. Nat. Sci., Ser. B* **2010,** *36* (2), 33-37.

27. Kitin, P.; Funada, R.; Sano, Y.; Beeckman, H.; Ohtani, J., Variations in the Lengths of Fusiform Cambial Cells and Vessel Elem in Kalopanax *Annals of Botany* **1999,** *84*, 621-632.

28. Ribeiro, R. C.; Oliveira, D. M. T., Small and hard seeds: a practical and inexpensive method to improve embedding techniques for light microscopy. *Acta Botanica Brasilica* **2014,** *28* (4), 624-630.

29. Werker, E.; Marbach, I.; Mayer, A. M., Relation Between the Anatomy of the Testa, Water Permeability and the Presence of Phenolics in the Genus Pisum. *Ann. Bot.* **1979,** *43*, 765-771.

30. Barthlott, J., Große-Veldmann, B., and Korotkova, B., Orchid seed diversity: A scanning electron microscopy survey. Turland, N. J., Ed. Botanic Garden and Botanical Museum Berlin-Dahlem: Berlin, 2014.

31. Ilarslan, H.; Palmer, R. G.; Horner, H. T., Calcium Oxalate Crystals in Developing Soybean Seeds. *Scanning Microsc.* **1999,** *13* (2-3), 321-339.

32. Arnott, H. J.; Webb, M. A., Twin Crystals of Calcium Oxalate in the Seed Coat of the Kidney. *Protoplasma* **1983,** *114*, 23-34.

33. Arzate-Vazquez, I.; Mendez-Mendez, J. V.; Nicolas-Bermúdez, J.; Chanona-Perez, J. J.; Domínguez-Fernandez, N.; Velez-Rivera, N., Effect of calcium oxalate crystals on the micromechanical properties of sclerenchyma tissue from the pecan nutshell (Carya illinoinensis). *Plant Physiol. Biochem.* **2022,** *170*, 249-254.

34. Kauss, H., Some Aspects of Calcium-Dependent Regulation in Plant Metabolism. *Ann. Rev. Plant Physiol.* **1987,** *38*, 47-72.

35. Jennings, J.; Macmillan, N., A tough nut to crack. *Journal of materials science* **1986,** *21* (5), 1517-1524.

36. Smykal, P.; Vernoud, V.; Blair, M. W.; Soukup, A.; Thompson, R. D., The role of the testa during development and in establishment of dormancy of the legume seed. *Front Plant Sci* **2014,** *5*, 351.

37. Harris, W. M., On the Development of Macrosclereids in Seed Coats of Pisum sativum L. *Amer. J. Bot.* **1983,** *70* (10), 1528-1535.

38. Crang, R.; Lyons-Sobaski, S.; Wise, R., Fruit, Seeds, and Seedlings: The Seed Coat Surrounds the Embryo and Storage Tissues. In *Plant Anatomy: A Concept-Based Approach to the Structure of Seed Plants*, Springer: 2018; pp 667-669.

39. Crang, R.; Lyons-Sobaski, S.; Wise, R., Fruits, Seeds, and Seedlings. In *Plant Anatomy: A Concept-Based Approach to the Structure of Seed Plants*, Crang, R.; Lyons-Sobaski, S.; Wise, R., Eds. Springer International Publishing: Cham, 2018; pp 649-678.

40. Borchert, R., Functional Anatomy of the Calcium-Excreting System. *Bot. Gaz.* **1984,** *145* (4), 474-482.

41. Lautner, S.; Fromm, J., Calcium-dependent physiological processes in trees. *Plant Biol (Stuttg)* **2010,** *12* (2), 268-74.

Chapter 3.

The *in-situ* Glass Transition of Catechyl Lignin in Vanilla (*Vanilla Planifolia*) Seed Coat and Candlenut shell (*Aleurites moluccana*) Nutshell

Attribution

In this Chapter all work was conducted by E. Ristanti, with the exception of the data shown in Figure 3.21 solid-sanded candlenut and 80 mesh-plots were conducted by Mitchell Patrowicz, a 2019 NSF, REU student.

3.1. Abstract

Catechyl lignin, or C-lignin, is a linear homopolymer of caffeyl alcohol with benzodioxane intermonomer linkages that differ from conventional guaiacyl (G)/syringyl (S)-lignin. C-lignin is found in some angiosperm seed coats and nutshells as the only lignin type, such as in vanilla (*Vanilla planifolia*) seed coat; whereas in candlenut (*Aleurites mollucana*) shell C-lignin is accompanied by G-lignin. This unusual lignin merits a study in the perspective of cell-wall structure/property relationship. Using a torsional rheometer, dynamic mechanical analysis (DMA) was conducted to measure the glass transition temperature (Tg) in vanilla seed coat and candlenut shell. Analysis was conducted in solvent-submersion mode; ethylene glycol (EG) and N-methyl pyrrolidone (NMP) were used as plasticizers. Compressive-torsion in low amplitude oscillation rheology method was applied to accommodate tissues' shape and size. T_g measurement in vanilla seed coat shows an onset of transition at ~120°C for both specimens saturated in EG and NMP, suggesting that the T_g was around 160°C. We expected that candlenut would show lower T_g than vanilla seed coat as the effect of G-lignin, or it would show two separate transitions, but we found that candlenut showed variations of transition behavior within different specimen forms (solid or

particulate). The intact candlenut shells showed transition onset that similar vanilla seed coat. With such highly regular structure, C-lignin might be expected to exhibit high crystallinity. However, XRD diffractograms of vanilla seed coat and candlenut shell indicate that C-lignin is amorphous.

3.2. Introduction

Lignins are complex phenylpropanoid polymers that stiffen and strengthen plant secondary cell walls; they are derived from oxidative polymerization of principally three monolignols, p-coumaryl, coniferyl, and synapyl alcohol, that give rise within the lignin polymer of hydroxyphenyl (H), guaiacyl (G), and syringyl (S) units respectively.[1, 2] Lignins are amorphous and optically inactive heteropolymers.[3] In vascular plants, lignin is distributed in tracheids, vessels, and fibrous tissue.[4, 5] Lignin deposition in the vascular plant cell walls is the result of evolutionary process[6, 7], to survive in terrestrial environment by providing sturdiness into cell wall[3], water conduction[8], and protection against pathogens[9].

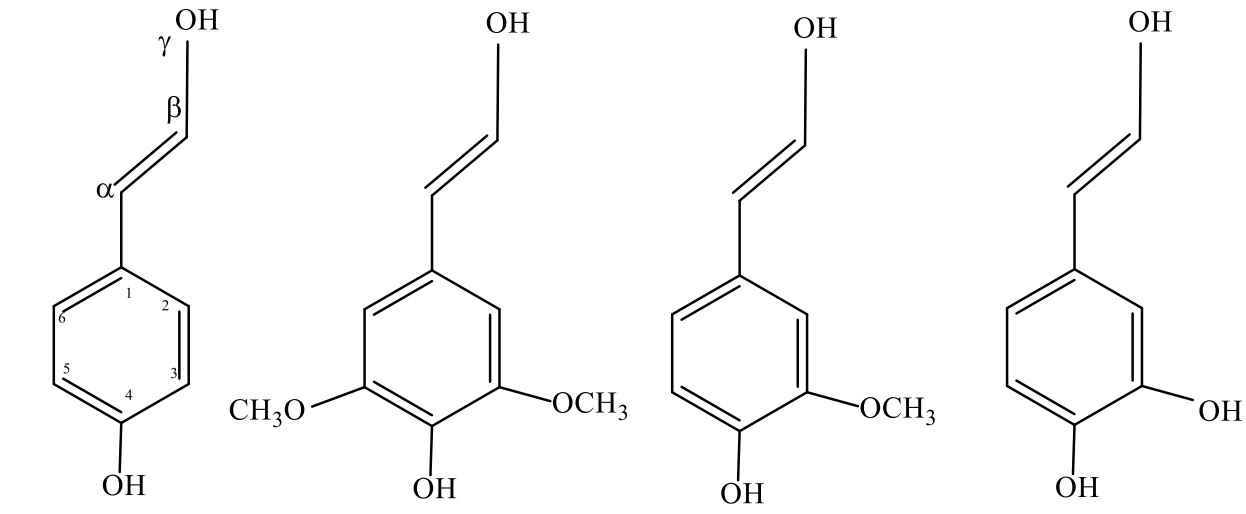

p-coumaryl alcohol synaphyl alcohol coniferyl alcohol caffeyl alcohol

Figure 3.1 *The most common lignin monomers and caffeyl alcohol*

In 2012, an unexpected novel lignin that derived solely from caffeyl alcohol was discovered in the seed coat of vanilla orchid (*Vanilla planifolia*).[10] Unlike conventional lignins that are heteropolymeric and connected mostly by alkyl-aryl ether linkages[11], catechyl-lignin (C-lignin) is a linear homopolymer of caffeyl alcohol connected exclusively by benzodioxane linkages (**Figure 3.2**). Compared to S/G/H-lignin, C-lignin is unusually resistant to acidolysis and thermal degradation, as discussed later.[12]

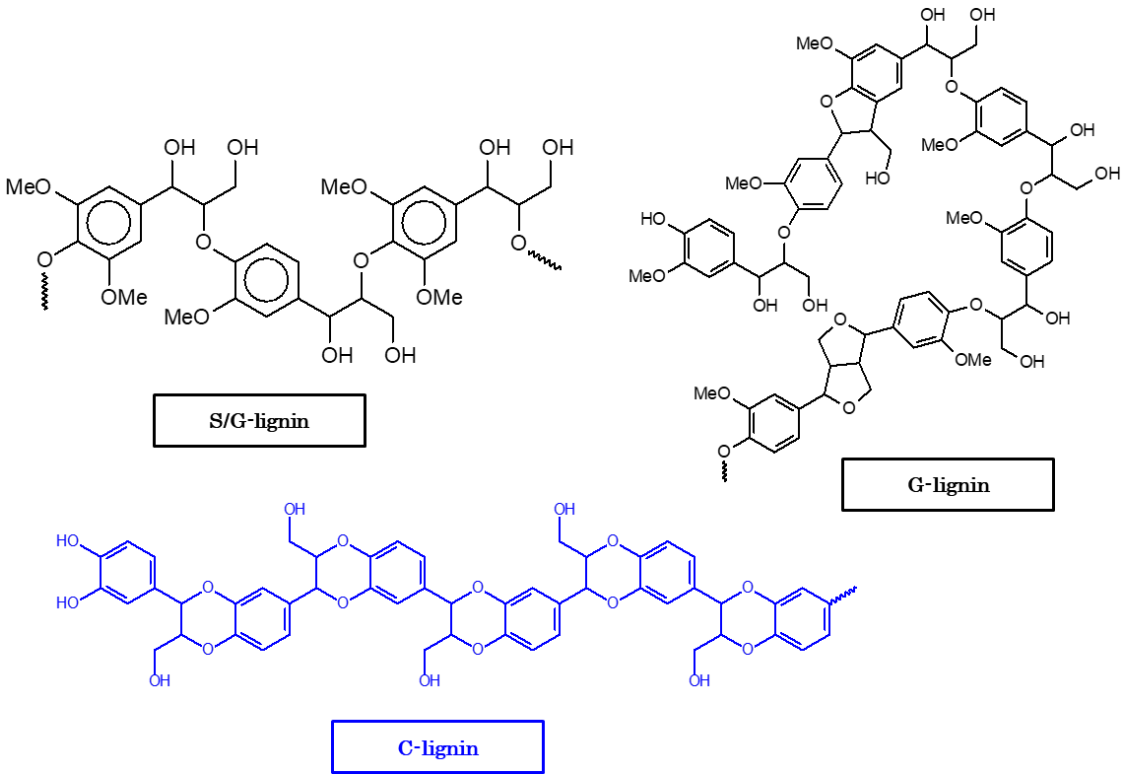

Figure 3.2 *Structure of S/G, G, and C-lignin*

Vanilla planifolia is one of the members of 110 different species in *Vanilla* genus.[13] The existence of C-lignin in *Vanilla* genus is not common. Among *Vanilla* genus, other than in *V. planifolia* seed coat, the seed coats of *Vanilla pompona* and *Vanilla tahitensis* were also reported to exhibit C-lignin.[10] However, C-lignin was not found in other plant parts (pods, stem, leaves) of

V. planifolia and its close relative, other members of order Asparagales, such as Moth orchids, Asparagus, and Agave.[10]

Later in 2013, C-lignin was found in some other plants, in these cases accompanied by G/S lignin. Some oil producing plants which are commonly used as biodiesel feedstocks from Euphorbiaceae family: candlenut (*Aleurites moluccana*), castor (*Ricinus communis*), tung tree (*Vernicia fordii*), and jatropha (*Jatropha curcas*), exhibit both C-lignin and G/S-lignin in their seed coats or nutshells.[14] C-lignin formation is associated with the downregulation of the CCoAOMT andCOMT enzymes responsible for converting hydroxyl groups to methoxy groups, hence stopping G/S lignin formation.[14] Seed coats are developed from ovular tissue and carry genetic characters of the mother plants.[15, 16] Plant-seed coats are constructed from different cell sizes and type; they develop highly lignified secondary cell walls and are relatively hydrophobic.[17, 18] Lignification in plant-seed coats and nutshells results in exceptional mechanical strengths despite their thin walls, making them hard to crack.[19]

Figure 3.3 *Image of bulk vanilla seeds.*

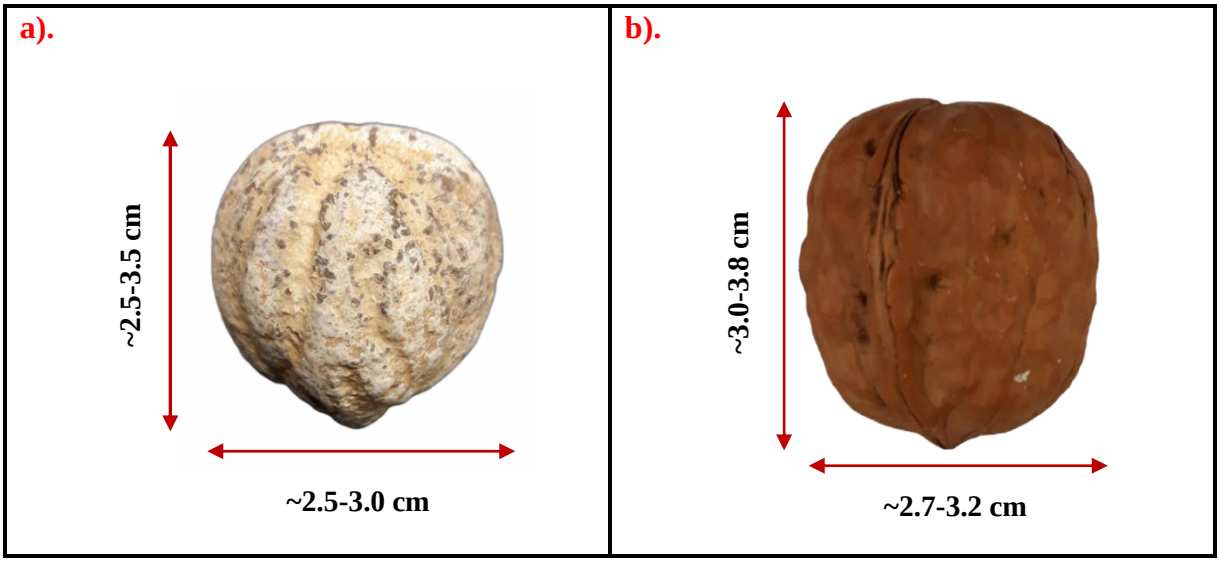

Figure 3.4 *Comparison of* ***(a).*** *candlenut to* ***(b)*** *walnut seed. Candlenut is slightly smaller than walnut. Both candlenut and walnut seed coats have uneven surface, but candlenut surface is sometimes covered with white, flaky-waxy substances.*

Vanilla seed coats and candlenut shells differs in many ways. Vanilla has many tiny seeds that lie in the "white" inner region of the vanilla pod.[13] These seeds are covered by black, seed coat (**Figure 3.3**) that hardened as they are matured .[20] Candlenuts, on the other hand, are sized slightly smaller than walnut (**Figure 3.4**). Candlenut seed is covered by brown-rough shell resembles to walnut of its irregularity and roughness. The shell's outer surface is sometimes, covered with white flaky-waxy substance that fall off easily. Candlenut size is approximately 3 cm in diameter of round-shaped globule with slightly tapered at the bottom.[21]

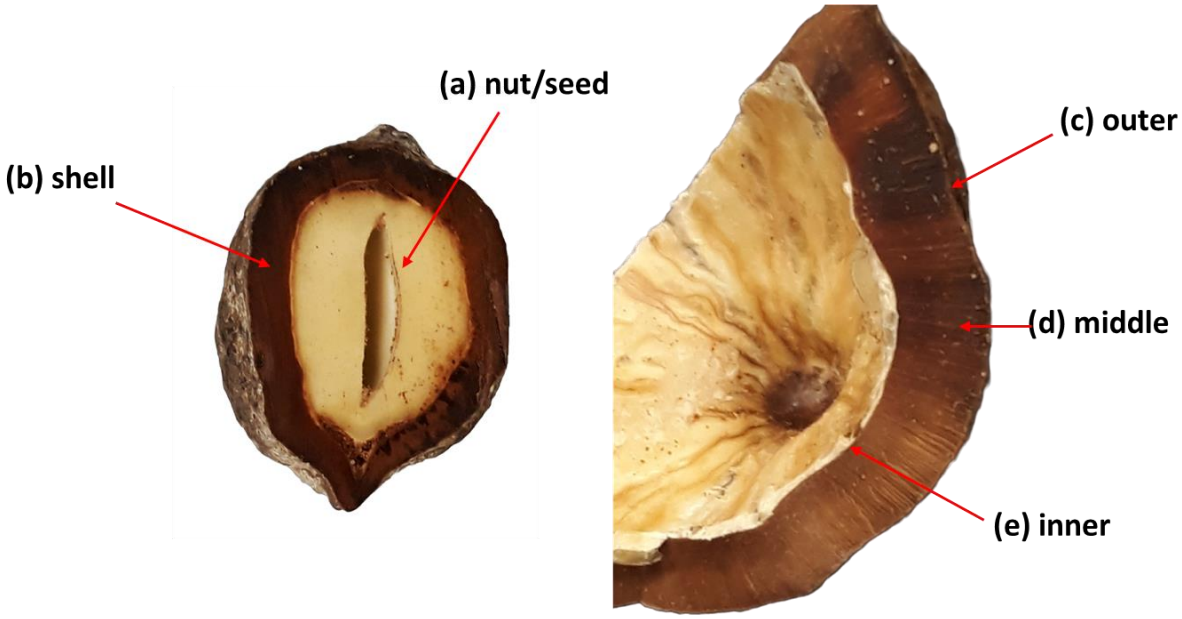

Figure 3.5 *Candlenut seed structure (a). nut/seed; (b). shell; (c). outer layer; (d). middle layer; and (e). inner layer.*

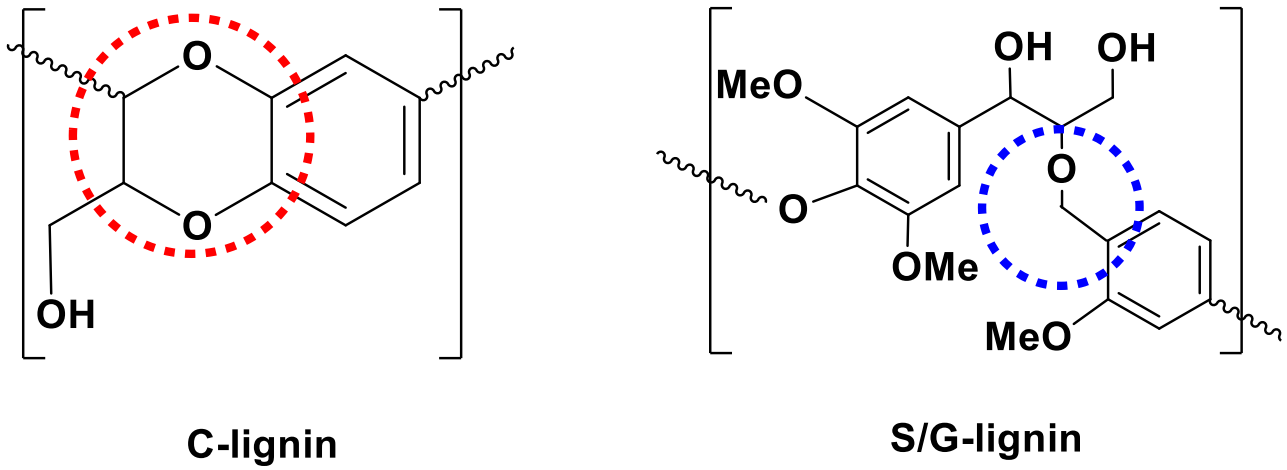

Figure 3.6 *Comparison of benzodioxane structure in C-lignin to the common β-alkyl ether linkage in an S/G lignin. Dotted circles highlight differencesin rotational freedom, much less in C-lignin.*

The ability of some seed coats/nutshell in angiosperms to synthesize a new type of lignin is another level of lignin evolution. However, the role of C-lignin related to the function of the seed coat is unclear while it exhibits different behaviors to the regular G/S/H-lignin. Regular G-lignin is subject to acidolysis (β-O-4 cleavage) that leads to repolymerization (crosslinking).[22] The benzodioxane linkages in C-lignin (**Figure 3.6**). is unusually stable against acid-catalyzed cleavage compared to G/S lignin.[12] In term of chain flexibility, the β-alkyl ether linkage in conventional lignin allows some rotation freedom, while the benzodioxane restricts that rotation and thereby stiffening the chain.

The entirely new and unusual lignin holds merit for cell-wall structure/property study in vanilla seed coat and candlenut shell. The methods used here were measurement of glass transition temperature (T_g) using dynamic mechanical analysis (DMA), determination of C-lignin crystallinity using x-ray diffraction (XRD), and reflective light microscopy for morphological observation of seed coat and nutshell. Elemental analysis, thermogravimetric analysis and compression testing were used as supporting tools to the XRD, microscopy, and DMA methods. Due to the benzodioxane linkages, C-lignin is less flexible than G/S/H-lignin and therefore Tg measured in tissues with catechyl lignin is expected to be higher than those in tissues with G/S/H-lignin. The regular, homopolymeric-structure of C-lignin is also expected to show high crystallinity pattern in XRD scan.

3.3. Experimental

3.3.1. Materials

Vanilla seeds were obtained from Prof. Fang Chen (University of North Texas). Candlenut was obtained from three sources: Prof. Fang Chen (University of North Texas), purchased from Hawaiian Art Shop (Hawaii), and from local plantation in Bukittinggi, West Sumatra, Indonesia.

Sandpaper: 80 and 220 grits (3M). Solvents: Ethanol 190 Proof (Decon Lab), n-hexane, ethylene glycol, N-methyl-2pyrrolidone (Fischer Chemical), 1,2,4-trichloro benzene (Sigma-Aldrich), acetone (Millipore-Sigma), nonionic surfactant Triton X-100 (Promega), L.R. White Resin (Electron Microscopy Science), silicon carbide grinding paper 8" P1200 grits (Ted Pella), colloidal alumina suspension (MSE supplies), and DI water.

3.3.2. Methods

Vanilla Seed Coat Purification

Figure 3.7 presents the vanilla seed coat purification steps.Vanilla seeds (≈ 5g) were first cleansed by washing with n-hexane (3x, 20ml), followed by washing with ethanol (3x, 20ml), and air-dried overnight. Seeds were subjected to rotary-knife milling (1-minute pulse, 10-minutes break for a total milling time 5 minutes) (A11 Basic Mill, beater blade A11.3; IKA-Werke, Staufen, Germany). Milled-seeds (≈ 0.1g) were added to a mixture of 1,2,4-tricholoro benzene (TCB, 15ml) : n-hexane (HXN, 5ml) (3:1, v/v), then centrifuged (5000 rpm, 15 minutes; Eppendorf 5804, Hamburg, Germany); the denser seed coats spun down to the tube bottom (**Figure 3.7**), and the floating seed embryos were removed by decantation. Seed-coat pellet was washed with acetone (3x, 20ml) and air dried. Purification continued by immersing seed coat in a mixture of water (15mL):ethanol (3:1, v/v) and 2 drops of Triton-X surfactant. The mixture was centrifuged (5000 rpm, 15 minutes). Floating impurities were decanted, and seed-coat pellet was washed with water (3x, 30ml) and air-dried overnight before preparation for solvent-submersion DMA.

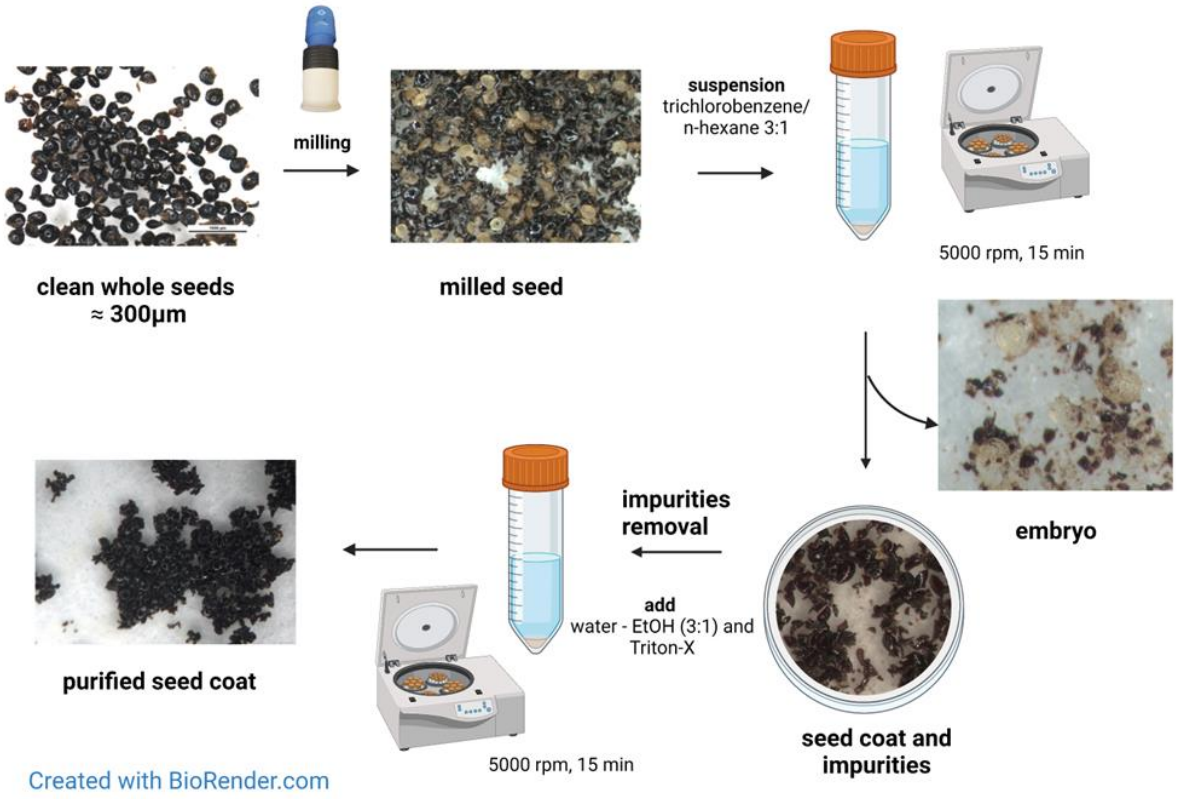

Figure 3.7 *Visual outline of vanilla seed-coat purification steps.*

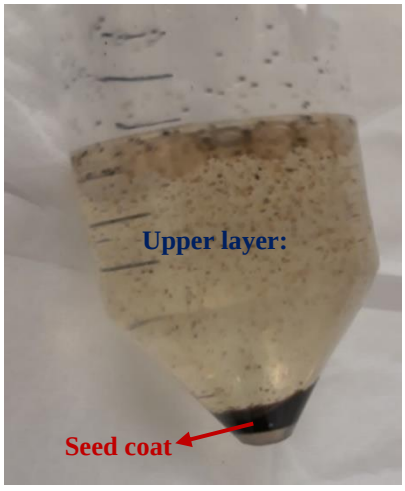

Figure 3.8 *Separation embryo and seed coat in 1, 2, 4-trichlorobenzene:n-hexane mixture after centrifugation.*

DMA Specimens Preparation

Candlenut shells were separated from nuts by hammer crushing, and the resulting shell fragments were converted into two specimen types, solid and disk-like, or milled and particulate. Solid disk-like specimens (≈8mm dia., original shell thickness ≈3.5-4.5 mm) were manually cut with a scissor, where the specimen-thickness dimension was parallel to the shell thickness). Two types of solid disk-like specimens were prepared: "solid-whole" where the natural inner and outer surfaces were preserved, and "solid-sanded" where ≈ 2mm of both the natural inner and outer surfaces was removed by manual sanding (grit size = 80). Particulate specimens were prepared by milling (Wiley mill GE 5XBG00B D, 1725 RPM;Thomas Scientific, Swadesboro, NJ, USA) to pass 80 mesh and 100 mesh screens. 200 mesh particulate specimen was obtained by hand sanding (grit size=220) inner layer of candlenut shell. Each specimen then saturated in ethylene glycol and N-methyl pyrrolidone. Submerged specimens were vacuumed at 30 mbar for 15 minutes and keep at atmospheric pressure ambient (**Figure 3.9**).

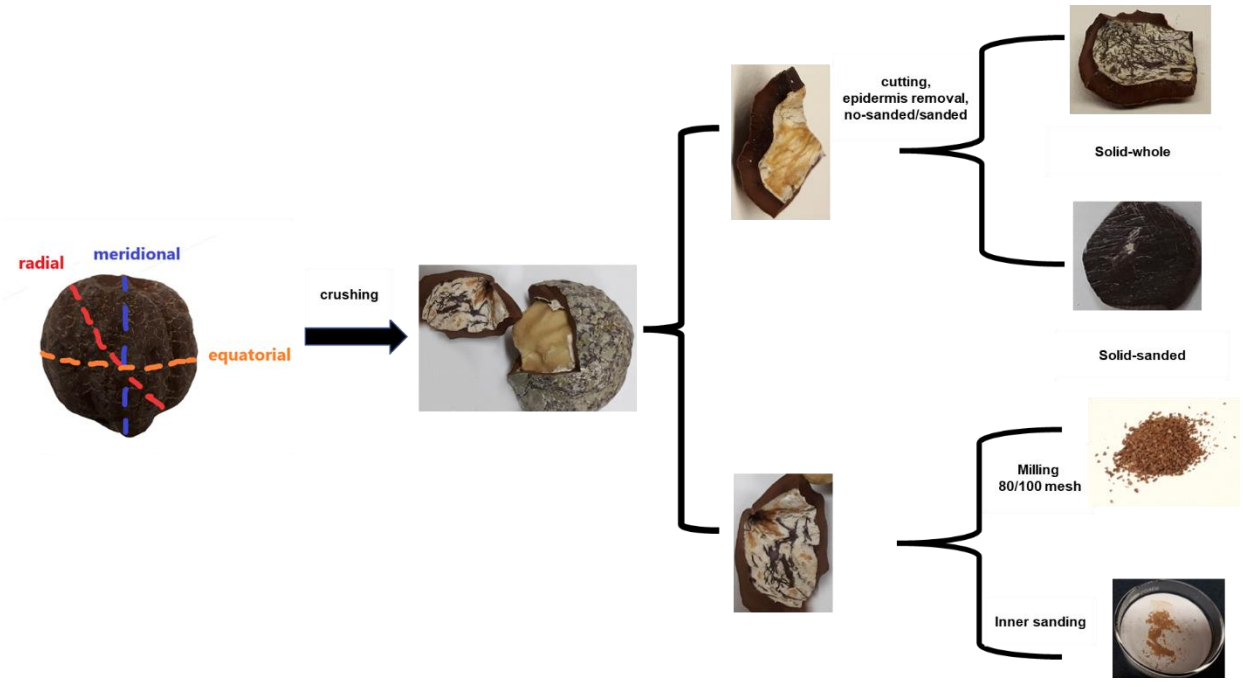

Figure 3.9 *Visual outline of candlenut shell specimen type and their preparation.*

Thermoravimetric Analysis (TGA)

Oxidative TGA analysis was conducted in Q500 (TA Instruments, New Castle, DE, USA). Approximately 4-6 mg sample (vanilla seed coat, 80 and 100 mesh-ground candlenut shell and 80 mesh-ground Southern Yellow pine) used for each analysis. Analysis was performed at 30-1000^{o}C, with heating rate 50^{o}C/min, using hi-resolution mode at resolution = 1, and sensitivity = 4 in air environment.

X-ray Diffraction (XRD)

Approximately 0.30-0.50 g of candlenut shell ground (80 mesh-ground) and purified vanilla seed coats were mounted onto XRD instrument's PMMA ring sample holder (specimen well Ø = 40 mm, sample holder ring Ø = 51.5 mm, height = 8.5 mm) and scanned on a D8 ADVANCE diffractometer (Bruker Corp., Billerica, MA, USA) equipped with a seal tube Cu-Kα source. Scans were collected from 2θ = 10 to 50^{o} with step size 0.04°; time per step 96 s, goniometer radius 305.0 mm, wavelength anode Cu-Kα1 1.54060Å; Cu-Kα2 1.54039Å; Cu-Kβ 1.39222Å, X-ray generator 40 kV, 40 mA, primary soller slit (Divergence: 1 mm, Antiscatter: 5 mm). % Crystallinity was calculated using XRD deconvolution method as performed by Park and co-workers (2010).[23] Diffractograms were deconvoluted in OriginLab 2019b software to separate amorphous and crystalline contribution. Peaks were fitted using Gaussian assumption to the best fit that corresponds to coefficient correlation, R^2 greater than 0.90. % Crystallinity (or crystallinity index, CI) was calculated as the ratio of all crystalline peak to the total area.[23]

Elemental analysis

Elemental analysis was provided by the Analytical Chemistry Research Laboratory (Pharmacology/Toxicology) at the Virginia-Maryland College of Veterinary Medicine on the

Virginia Tech Blacksburg campus; using inductively coupled plasma with mass spectroscopy ICP-MS 7900 (Agilent, Santa Clara, CA, USA). Approximately 200 mg of sample (vanilla seed coat and 100-mesh particulate nutshell) were microwave digested (Multiwave GO microwave digestion system; Anton Paar GmbH, Graz, Austria) in 10 mL of a mix of nitric acid and hydrogen peroxide. The samples digested clear and were taken to a final volume of 50 mL with 18.2 MΩ.cm deionized water prior to being again diluted in 2% nitric acid for ICP-MS analysis.

Sample Saturation Status using Compression Testing

Simple compression testing was used to check the candlenut shell-saturation status. Candlenut shell disks were obtained by hand-sawing whole seeds approximately 0.5 mm-up and 0.5 mm-down from seed equatorial position, then removing the seed kernel, resulting in a ring. The ring was then cut into 8-9 equal parts and thus resulted in ≈10 mm x 8 mm disks with nutshell's original thickness, and compression was applied parallel to the thickness direction. The disk specimen was mounted between compression platens of 2kN load cell of compression test instrument (5944 Single Column Universal Testing System; Instron corp., Norwood, MA., US) with nutshell inner-side up and set the test speed to 0.2 mm/min. Displacement and balance were set into 0 before starting the measurement. Data was recorded as load (kN) vs displacement (mm) and measurement was set to stop after reaching max load (specimen breaks). Stress is determined in kN/m^2 unit and calculated as load in kN divided by area in m^2. Strain is determined as displacement (mm) divided by initial length (mm) and therefore it is unitless. Young's modulus is determined as the slope of stress vs strain plot in the initial linear region before the upturn. Strength is determined as maximum load (kN) divided by specimens' area. The maximum load of candlenut specimens with ≈11x8.5mm surface areas were between 500 to 1600N.

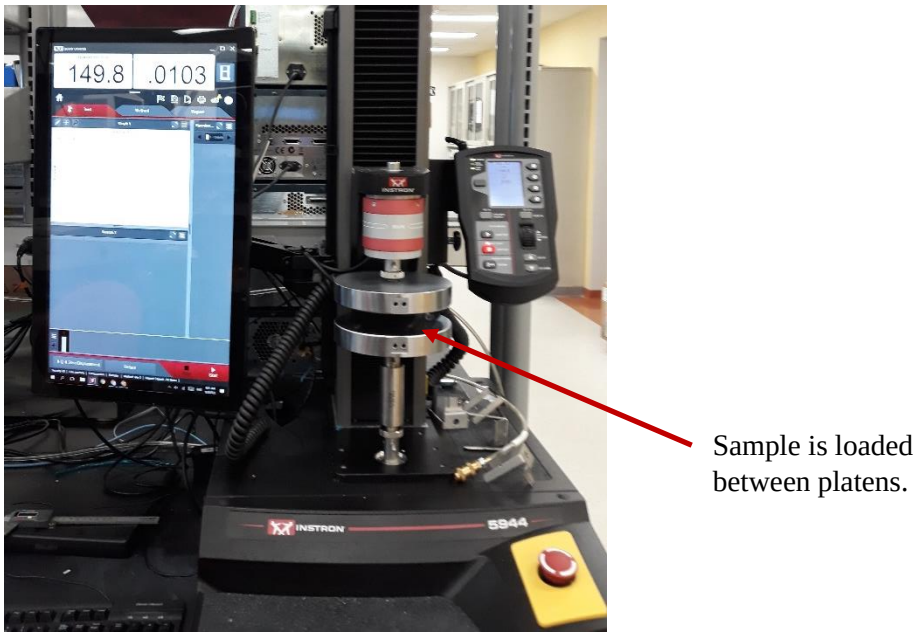

Figure 3.7 *Universal testing instrument with 2 kN load cell capacity*

Microscopy

Reflective-light microscopy was used to determine vanilla seed size and viewed candlenut cross section. Approximately 100-200 mg seed was put onto a petri dish lined with filter paper and observed with reflective light microscope Nikon SMZ 745 (Nikon Instrument Inc., Tokyo, Japan). Seed size was defined as the distance from tapered end to the bulging end and measured using image analysis software (NIS Elements Software ver. BR 4.11). Candlenut cross section is defined as the distance from the outer shell's surface to the inner shell's surface. A piece of candlenut shell (≈0.5 mm x 4 mm) was observed on a reflective light microscope (Nikon SMZ 745; Nikon Instrument Inc., Tokyo, Japan) with cross section area faced up. To measure seed coat thickness, cleaned seeds were embedded in polyhydroxy-aromatic acrylic resin (LR White resin) in an aluminum weighing pan then cured at room temperature for 1 day. The hardened resin was then

mechanically polished with silicon carbide grinding paper and colloidal alumina polishing suspension and resulted in a surface finish with ≈50nm of surface roughness. Sample was observed using reflective light microscope Axio Scope A.1 (Zeiss, Oberkochen, Germany) in the dark field mode. Vanilla seed coat purity changing during seed coat purification were also observed using reflective light microscope Nikon SMZ 745 (Nikon Instrument Inc., Tokyo, Japan).

DMA measurement

Torsional Rheometer Set Up

Compressive-torsion DMA measurement were all performed in AR2000 DMA instrument (TA Instrument, New Castle, DE, USA). All tests were performed in an environmental test chamber (ETC) under nitrogen gas and temperature controlled with active cooling (liquid nitrogen purging). Compressive clamping was achieved at 20N static normal force, with normal force tolerance 0.1N. Gap change limit was controlled to be 2,000 μm up and 2,000 μm down. Measurement was performed within the linear viscoelastic response (LVR) of solvent-plasticized specimens. Submerged specimens were vacuumed at 30 mbar for 15 minutes and let at atmospheric pressure and ambient temperature, where saturation times were varied from 1-4 days.

LVR Determination

LVR was determined using stress sweep experiments at extreme high and low temperatures (20N normal force; 1 Hz; high-temperature = 122°C; low-temperature = 23°C; stress range = 2 to 12 kPa). Dynamic stress/strain plots were fitted to a line (**Figure 3.8 and 3.9**). The LVR limit was defined as the stress beyond which the correlation coefficient (R^2 for the least square fit) was less than 0.9999. Maximum stress limit for both extreme temperatures at R^2 = 0.9999 were 6500 Pa and thus stress used for DMA measurement was set at 6kPa.

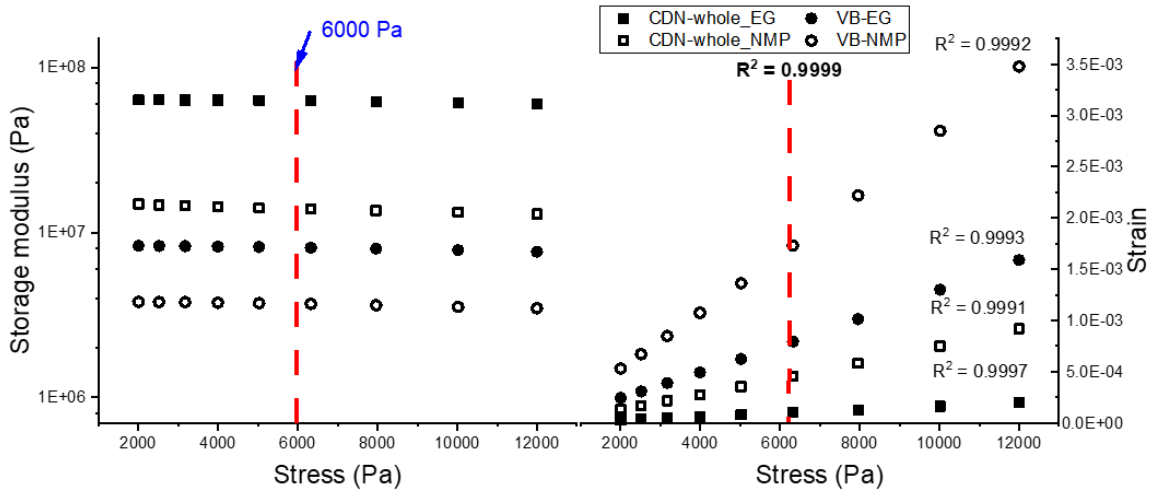

Figure 3.8 *LVR data showing storage modulus vs stress, and stress vs strain at 122°C for candlenut shell-solid whole specimen and vanilla seed coat. Red-dotted lines indicates the LVR used in this study.*

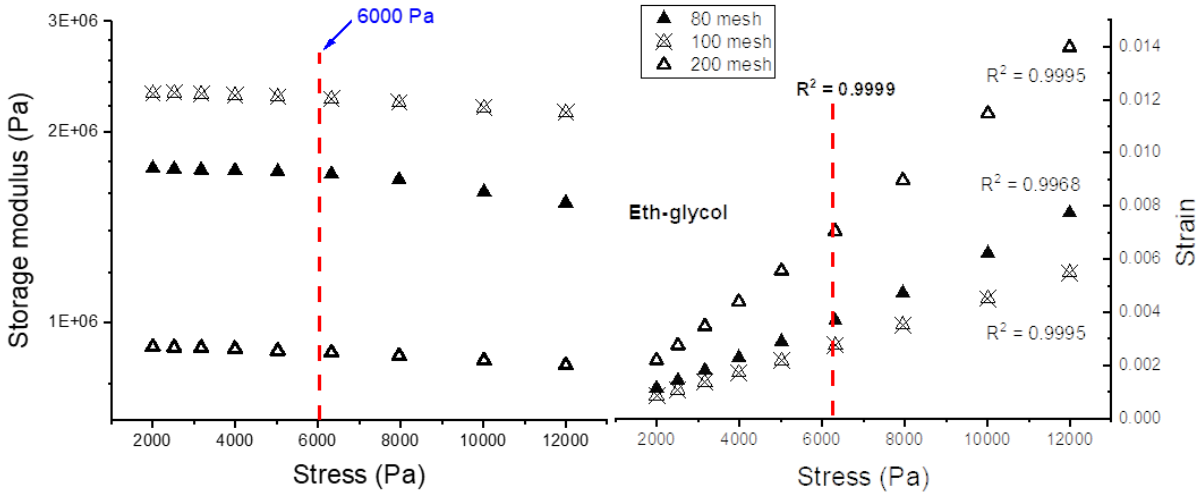

Figure 3.9 *LVR data showing storage modulus vs stress, and stress vs strain at 122°C for candlenut shell-80,100 and 200 mesh saturated in ethylene glycol. Red-dotted lines indicate the LVR used in this study.*

Temperature Ramp

Solvent-saturated pecimens were mounted onto instrument sample holder and clamped between 8-mm parallel plates. Sample holder was filled with solvent. Specimens were subjected to heating/cooling treatments. Specimens were heated to 122℃ (2 ℃/min) and equilibrated for 3 minutes, then cooled to 120 ℃ (1℃/min) and equilibrated for 2 minutes. Specimens were ramped down to minus 23℃ (2℃/min).

3.3. Result and Discussion

This research aims to study C-lignin material structure/property relationship by measuring *in situ* Tg and crystallinity. Vanilla seed coat is exclusively consisted of C-lignin. To obtain pure seed coat, it should be separated from the embryo and other seed components. Candlenut has both G and C-lignin that deposited in the nutshell, but it is not known if G and C-lignins in candlenut shell are deposited in different time/place. Tobimatsu and co-workers[14] showed that in *Cleome hassleriana* C-lignin is deposited at a separate time/place with G/S-lignin, indicated by two distinguished layers observed in the transverse seed section. This means, measurement of T_g in tissue that exhibits both C and G/S lignin like candlenut, could possibly show several transition behaviors that represent C-lignin's transition, G/S-lignin's transition and or a new transition affected by both C and G/S-lignin.

In their natural forms, seed coats and nutshells do not lend themselves to traditional bending- or tensile-mode DMA. DMA testing in seed coats or nutshells is challenging due to specimens' size and shape. Moreover, there is no knowledge on how the DMA response of tissues with C-lignin will be. Here, we used wood as a reference on conducting DMA test and expected data. In

wood, viscoelasticity is determined by its component's behavior, the semi-crystalline cellulose, the amorphous components (hemicellulose and lignin), water, and interaction among them.[24, 25]

Viscoelastic properties of amorphous components such as lignin and hemicellulose are sensitive to diluents and heat. Studying viscoelastic behavior by isolating components of lignocellulosic materials was found to be problematic, since lignin is altered during isolation.[26] Consequently, measuring viscoelastic properties in biomass tissue is preferred.[27-29] *In situ* measurement of lignocellulose Tg is better done in DMA instrument as this instrument is more sensitive compared to calorimetry[30] For studying C-lignin properties in the context of cell-wall structure/properties relationships, the seed coat and nutshell need specimen preparation and adjustment to fit DMA's .

Observation and determination of vanilla seeds size using reflective light microscope show that vanilla seeds are sized ≈300 μm (**Figure 3.10**). Observation on resin-embedded sample using light microscope in dark field-mode indicated that the area where seed coat and embryo located are differed in color (**Figure 3.10**); the embryo occupies area with bright color, while the seed coat occupies the dark area surrounding embryo. Thus, seed coat thickness was measured from the border of the bright and dark area to the outer surface, which is 36.6 μm (±3.0: n=30). Candlenut shell is a hard, woody-like material. Observation of candlenut shell on cross section area using reflective light microscopy shows that the thickness is approximately ≈3.0-3.55mm (**Figure 3.11 Left**). The thickness of candlenut shell is distributed unevenly, with the part near the hilum, where it attached to the branch, is thicker than the part near micropyle, the small opening at the bottom part of mature seed (**Figure 3.11 Right**). To perform DMA measurement and crystallinity study, vanilla seed coat was separated from embryo and candlenut shell was processed into disk and particulate (**Table 3.1**) according to the previously described in specimens' preparation method.

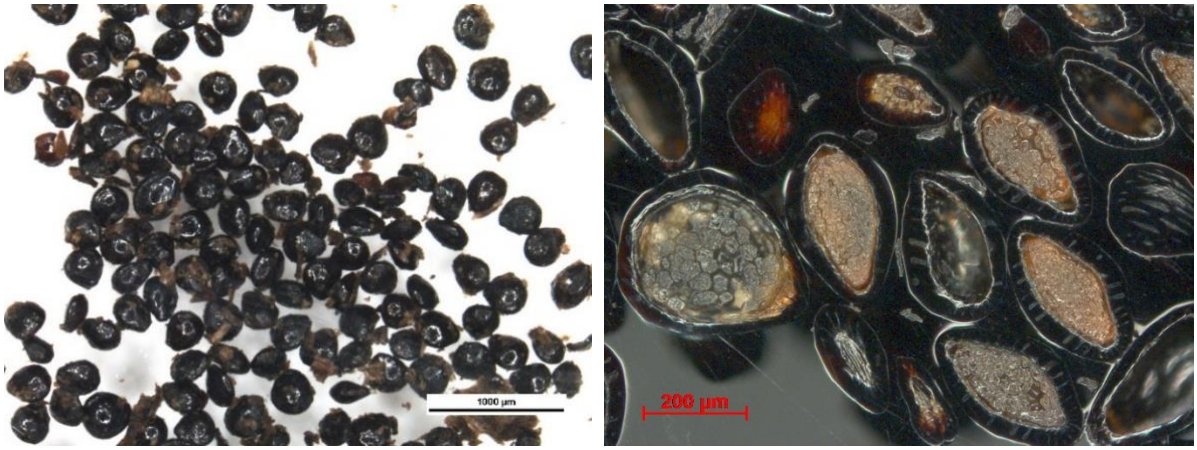

Figure 3.10 *Vanilla seed sized ~300µm (left), while seed coat thickness ranges ~40-50 µm (right)*

Figure 3.11 Left *– Candlenut cross section. Macroslereids stretch along the cross section of candlenut shell making their lengths are equal to the shell thickness.* ***Right*** *– Candlenut shell is thicker in the area near hilum, and thinner in the area near micropyle.*

Table 3.1 *Candlenut shell specimen variations*

Specimen Type	Particle Size	Preparation Method	Image
Solid whole	~ 8 mm diameter	cutting	
Solid sanded	~ 8 mm diameter	Cutting and sanding both sides	
Powder	~ 80 mesh (177 μm)	Milling, whole shell	
Powder	~ 100 mesh (149 μm)	Milling, whole shell	
Powder	~ 200 mesh (73 μm)	Hand-sanding, inner layer	

Oxidative TGA was used to observe purity of seed coat during purification process starting from milled vanilla seed that still has embryo mixed with seed coat to water:EtOH purified seed coat (**Figure 3.12**). Vanilla seed coat is highly sclerotic[31], while the embryo is mostly protein[32] which will decompose at lower temperatures than sclerotic seed coat. Due to the embryo removal, the TGA curve of TCB:HXN and water:EtOH purified seed coat can be distinguished from the cleaned-milled seed. The TGA cannot not show the difference decomposition pattern between seed coat from TCB-HXN step to seed coat from water-EtOH step, which may lead to question if the water-EtOH purification step is necessary. But embryo is rich in protein which commonly has

polar backbone, and therefore water-EtOH purification is useful to remove remnants embryo, which can be observed by microscope; seed coat is cleaner after water-EtOH purification step.

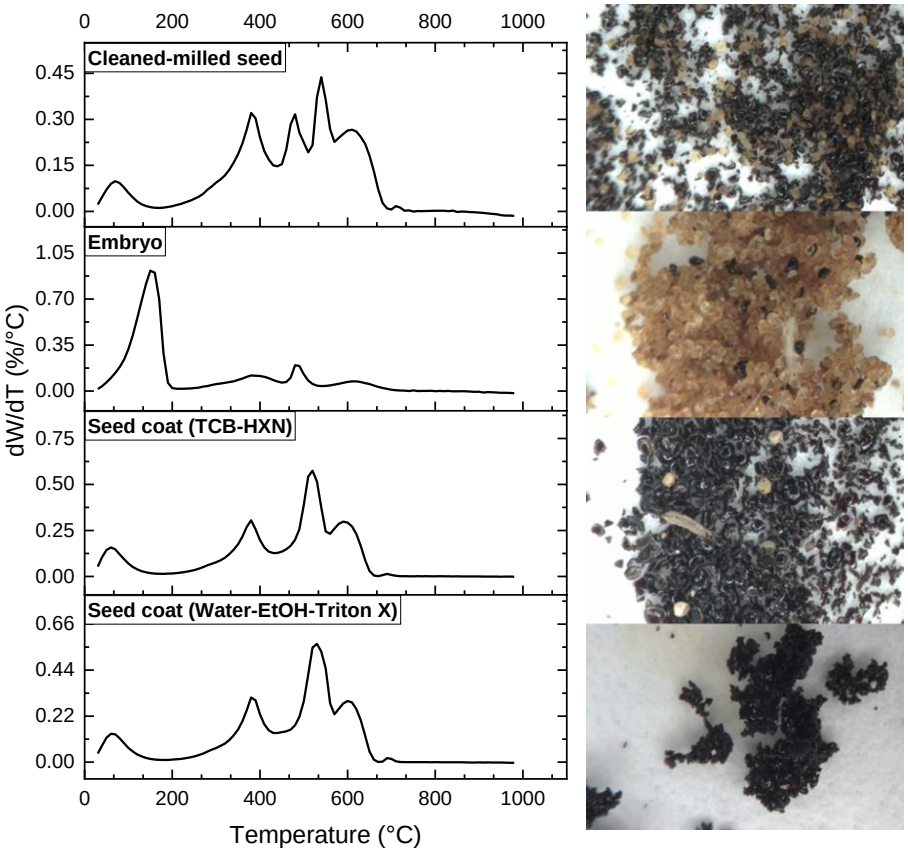

Figure 3.12 Left *– Changes in mass during vanilla seed coat purification.* ***Left*** *– example of derivative-weight loss TGA curves for progressive stage of seed-coat cleaning (Different scale was used for each step for best viewing TGA curve).* ***Right*** *– corresponding specimen images.*

Southern yellow pine ground into 80 mesh was used to compare lignin decomposition in conventional G-lignin tissue to tissues with C-lignin (**Figure 3.13**). Wood tissue shows two major decomposition stages. The first stage is the sharp and high-intensity peak at 400-450°C and the second stage is the short and broad peak at 500-650°C. The sharp peak in pine is cellulose peak, and the high intensity indicates high cellulose content in pine wood tissue. The broad peak at 500-

650°C is associated with lignin decomposition, which is in pine tissue, it refers to G-lignin. In vanilla seed coat, the first stage's peak is much lower in temperature and intensity compared to wood, with no shoulder observed. Candlenut shell first stage's peak shows a broader peak with shoulder, but the intensity is also lower than pine. The low intensity peaks at the first stage for vanilla seed coat and candlenut shell are associated with low cellulose content in both tissues. At the second stage, both vanilla seed coat and candlenut shell show higher intensity peaks than wood. Vanilla seed coat shows a shoulder beyond ≈550°C, while candlenut shell shows shoulder at ≈450°C. The peaks at the second stage are associated with lignin decomposition. Considering the peak at high temperatures for both vanilla seed coat and candlenut shell are higher in intensity than peaks at low temperatures, it indicates that seed coat and nutshell have high lignin than cellulose content. This may be affecting the crystallinity of seed coat and nutshell, which will be discussed later.

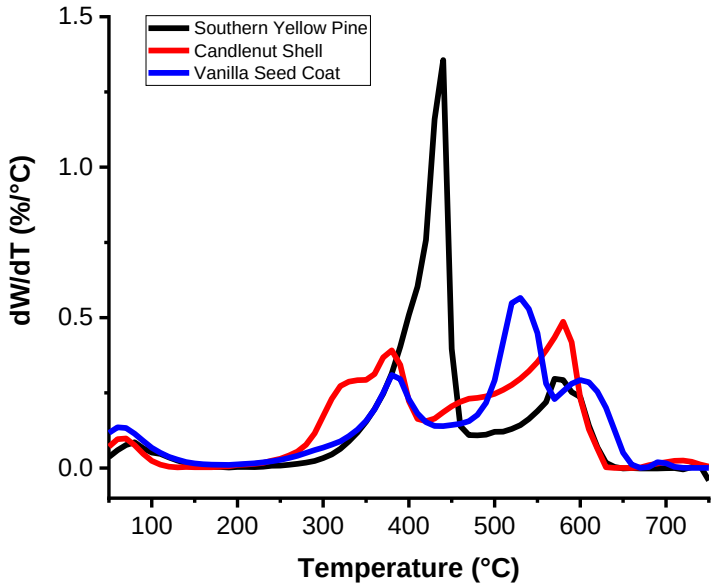

Figure 3.13 *Derivative- weight loss TGA curves of Southern pine compared to vanilla seed coat and candlenut shell*

Crystallinity of vanilla seed coats and candlenut shells

XRD is a powerful method to determine crystallinity and crystallite size. In the native cell wall, XRD is useful to characterize cellulose's unit lattice parameters and crystallinity.[33] Conventional lignin, due to its complex-branched structure, is amorphous. XRD scan in conventional lignin is not beneficial since the amorphous lignin does not have regular repeating arrangement and results in diffused peak. With the regularity of linear homopolymer structure, C-lignin could perhaps be expected to exhibit crystallinity. XRD can be used to check whether C-lignin contributes to crystallinity by comparing XRD diffractograms of tissue with C and G/C lignin to tissue with conventional lignin.

XRD powder diffraction was used to scan exclusively C-lignin tissue-vanilla seed coat and G/C-lignin tissue candlenut shell. Southern Yellow Pine which has G-lignin, is used to observe the difference of XRD patterns between seed coat/nutshell with normal wood. The diffractogram of Southern Yellow Pine should indicate a native cellulose pattern, cellulose I allomorph, which is characterized by the strongest peak at ~22.5°(2θ) or Bragg angle of 11.3°(θ) using CuK_{α} assigned to crystallographic plane (002) from planes that include the microfibril axis. Another important crystallographic plane for cellulose is (040) occurs at Bragg angle of 17.2°(θ).[34] Native cellulose is also characterized by crystallographic planes (101) and $(10\bar{1})$ at $2\theta = \sim 15\text{-}16°$. [35-37]

Figure **3.14 a, b, and c** show examples of XRD diffractogram of Southern Yellow Pine, vanilla seed coat, and candlenut shell respectively. Diffractogram of Southern Yellow Pine is the typical XRD pattern of cellulose I allomorph found in higher plants.[38-41] Southern Yellow Pine diffractogram shows a well-defined peak separation between peaks show at 15°(2θ) and 25°(2θ) and small peak at 35°(2θ). Diffractogram of experimental measurements of vanilla seed coat and candlenut show amorphous material patterns that indicated by broad, irregular, and not well-

resolved diffraction patterns, broaden from 12-30° (2θ). Candlenut shell shows small peak observed at 30°(2θ) in addition to the peaks that similar to both Southern Yellow Pine and vanilla seed coat.

Crystalline materials patterns in XRD scans can be distinguished from amorphous materials sharp and well-defined edges peaks. Peaks deconvolution method was used obtain the crystalline model and % crystallinity of vanilla seed coat, candlenut shell, and Southern Yellow Pine powder. The experimental data was subtracted with amorphous background using "Peak Analyzer" mode in OriginLab software. Crystalline peak was then fitted using "Multiple Peak Analyzer" to separate broad peaks. The Gaussian method was selected to deconvolute peaks. The detailed progress of deconvolution steps is shown in supplemental data 1.

Result of deconvolution peaks of each sample are shown in **Figure 3.14d**. After deconvolution, Southern Yellow Pine shows four crystallographic planes, which identified as peak at 15.1°(2θ) assigned to ($1\bar{1}0$) crystallographic plane; peak at 16.8° (2θ) assigned to (110) crystallographic plane; peak at 22.4° assigned to crystallographic plane (200); and peak at 34.8° assigned to crystallographic plane (004). Coefficient correlation (R^2) at this deconvolution is 0.986. This result is qualitatively comparable to diffractogram of Norway spruce.[40] % Crystallinity is calculated from the ratio of total crystalline peaks obtained from the deconvolution to the total crystalline peaks area of background subtracted XRD scan. Details of calculations are available in the supplemental section. The calculated % crystallinity of Southern Yellow Pine (**Table 3.2**) is 68.6%, which is higher compared to the crystallinity of various softwood species determined using ^{13}C-NMR by Newman and Hemmingson (1990)[42], which varied from 54 to 62%. The high value of % crystallinity in Southern Yellow Pine is probably due to the pine particle size and amorphous background selection.

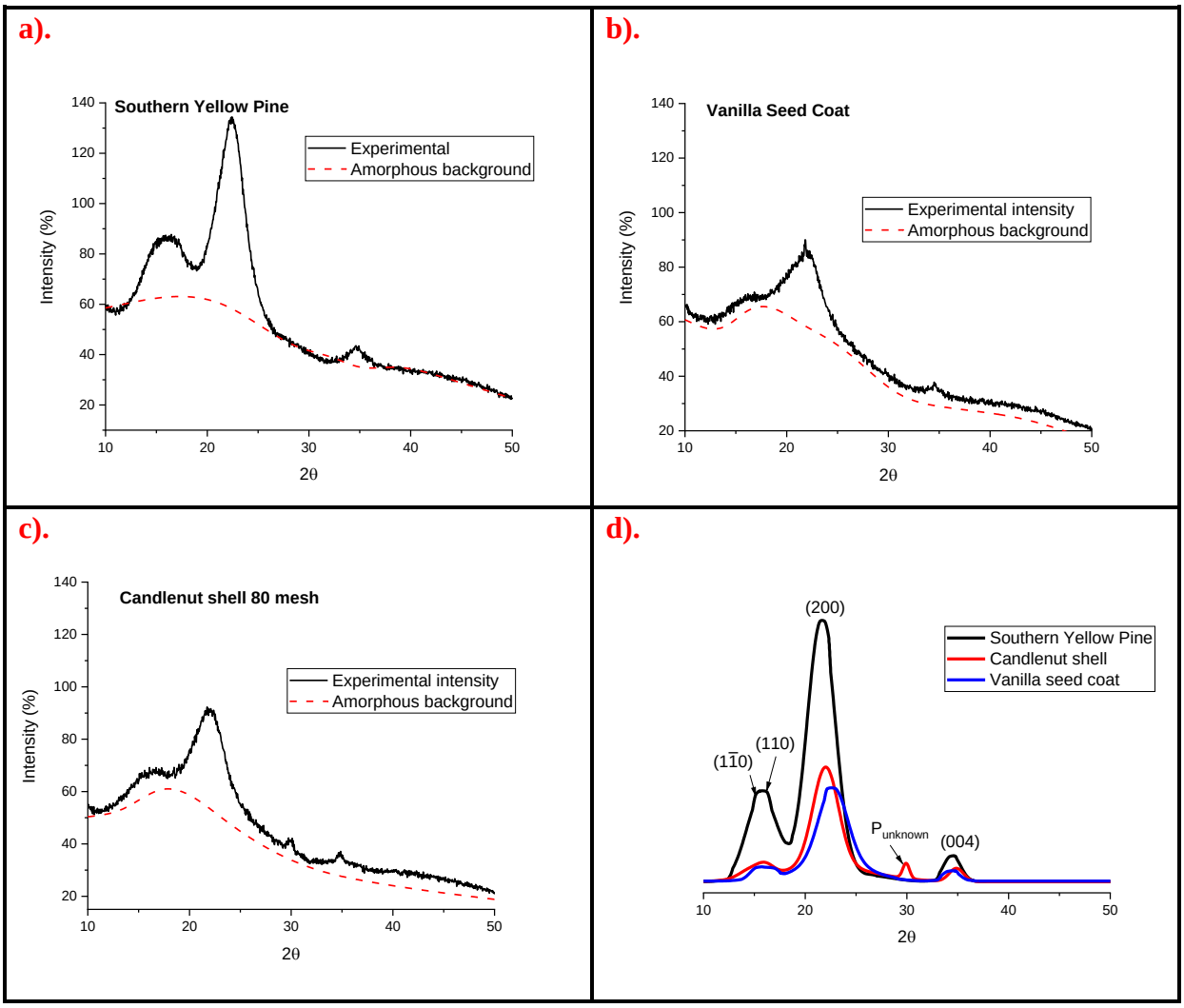

Figure 3.14 Example of XRD diffractogram of Southern Yellow Pine(a), vanilla seed coat (b), and candlenut shell (c) and crystalline model obtained from peak deconvolution method for the three samples.

Comparison of crystallographic planes and % crystallinity for vanilla seed coat ($R^2 = 0.97$) and candlenut shell ($R^2 = 0.986$) to Southern Yellow Pine after peak deconvolution are summarized on **Table 3.2**. Overall fitting indicates that vanilla seed coat has similar XRD pattern to Southern Yellow Pine, but the intensity is much lower, which is an indication that vanilla seed coat has similar cellulose type to Southern Yellow Pine, but the amount of cellulose is low. Chen and Dixon

(2019) reported that the crystallinity of cellulose in vanilla seed coat 16%.[43] Candlenut shows crystallographic plane at 30.3° that is not shown in either Southern Yellow Pine or vanilla seed coat. But this single peak itself cannot be claimed as C-lignin crystalline peak, as vanilla seed coat which has entirely C-lignin did not show this peak. This peak is also not correlated to any metal oxides, as both vanilla seed coat and candlenut shell have almost similar elemental compositions (elemental composition is shown in supplemental data 2). Crystalline cellulose content in candlenut was reported approximately 21%[14], higher than reported in vanilla seed coat.[43] Our finding shows that candlenut shell's crystallinity is 36%, higher than what we calculated in vanilla seed coat (29%). Cellulose microfibril in candlenut shell probably has different arrangement which led to the occurrence peak at 30.3°. Cellulose microfibril arrangement/orientation can be different within plant parts, which associated to the cell types and tissues.[44, 45]

Table 3.2 *Observed crystallographic plane after peak deconvolution at degree (2θ), calculated % crystallinity, and % amorphous calculated using peak deconvolution method.*

Sample	Crystallographic plane observed at °(2θ)					% Crystallinity	% Amorphous
	$(1\bar{1}0)$	(110)	(200)	$P_{unknown}$	(004)		
Seed coat	15.1	15.8	22.0	-	34.5	29.1	70.9
Nutshell	15.2	16.6	22.7	30.3	35.8	35.8	64.2
Pine	15.0	16.5	22.4	-	34.8	68.6	31.4

The low crystallinity observed in vanilla seed coat and candlenut shell seem to correlate with the low crystalline cellulose content compared to lignin in both tissues. According to Chen and Dixon, the ratio of crystalline cellulose to lignin in vanilla seed coat is almost 1:5.[43] Candlenut also has low crystalline cellulose content which ratio between crystalline cellulose to lignin is about 1:3.[14] In cellulose, ratio to lignin in softwood is approximately 4:3[46], with crystalline

cellulose accounted for 65% of the cellulose content, which result in higher intensity of diffractograms compared to vanilla seed coat and candlenut shell. Diffractograms of vanilla seed coat and candlenut shell do not show any peaks other than those correlated with crystalline cellulose peaks as observed in Southern Yellow Pine, and therefore there is no indication that tissues with C-lignin is crystalline, or possession of C-lignin contributes to increase crystallinity.

DMA sample preparation – Saturation Checking

Rheological study in biomass required plasticization and solvent-submersion mode measurements to operate at non-damaging temperatures.[47] Ethylene glycol and N-methyl-2-pyrrolidone are common plasticizers used to plasticized wood for DMA measurement.[48] Seed coat and nutshell are hydrophobic and exhibit an incredibly high strength and toughness. For example, to crack a macadamia, it needs a force range ~2000-4000 N.[18] Therefore, before running DMA measurement on vanilla seed coat and candlenut shell specimens need to be fully saturated with plasticizers. Plasticizers will reduce the strength and stiffness of the materials and thus the T_g will be lower. However, how long seed coat and nutshell need to be saturated was not known. Consequently, simple compression testing was performed on candlenut shell to test saturation in ethylene glycol. Specimen's stiffness and strength are assumed to decrease with saturation time and there is no change when it reaches full saturated condition.

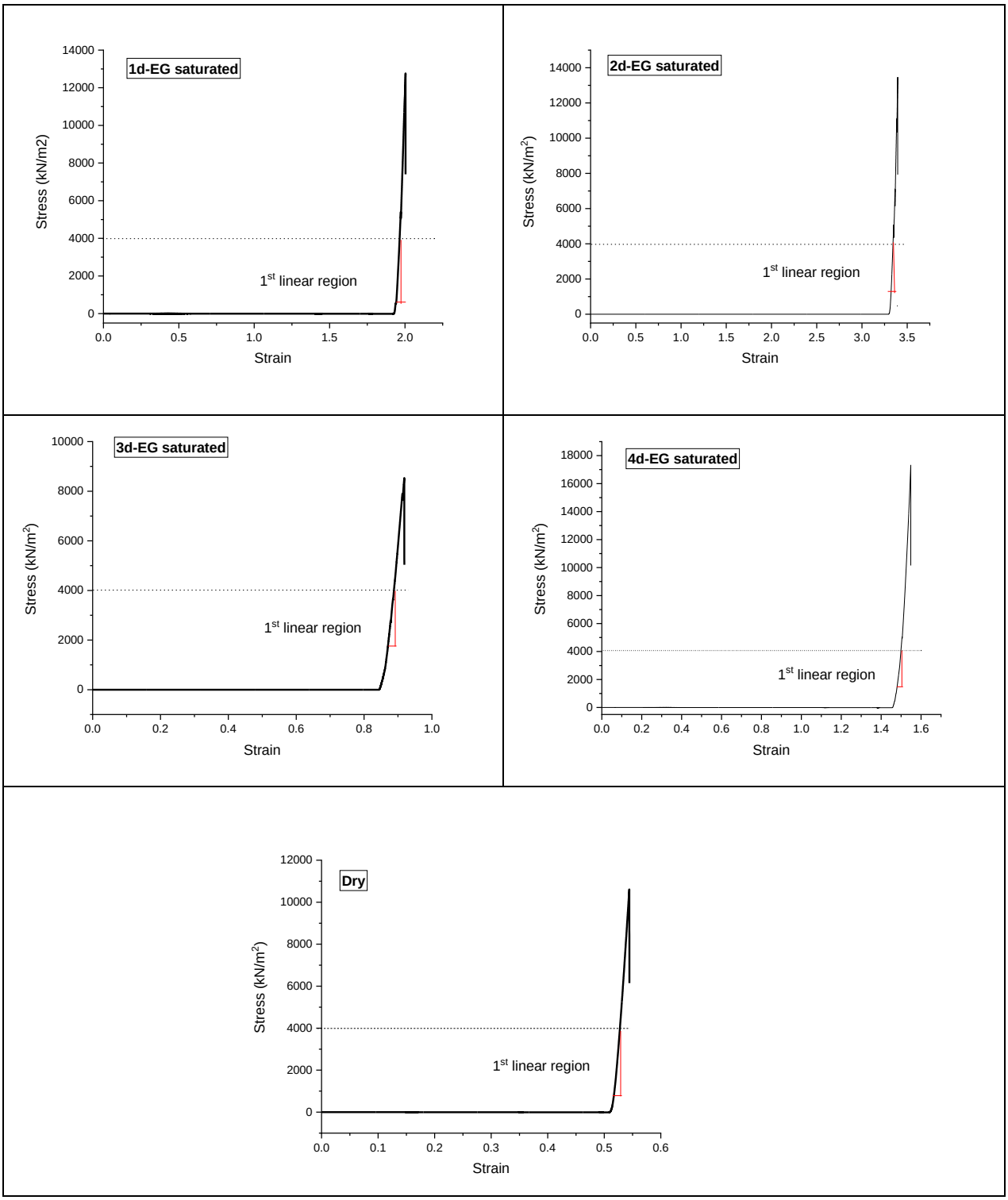

Figure 3.15 *Example of stress-strain plot of dry and 1-4 days ethylene glycol- saturated candlenut shell specimen measured using universal testing instrument in compression mode.*

Compression test mode was selected instead of tensile test mode to collect stress-strain data for calculating strength and stiffness of candlenut shell due to nutshell shape. Nutshell has curvature, make it difficult to obtain long-enough flat surface to be cut into dog-bone shape to perform tensile test. Compression test enables small specimens gripped between two platens and collects stress-strain data.

Stress-strain plot of dry and 1-4 days ethylene glycol-saturated candlenut shell are shown in **Figure 3.15**. Stress value is determined as load (kN) per specimen surface area (m^2) and strain is determined as displacement divided by initial sample length. Slope of stress-strain is used to determine Young's moduli. Stress-strain plots have several linear regions. Here, we selected linear region, starting from the initial increment to stress value of 4,000 kN/m^2 or marked on the plot as 1^{st} linear region to determine Young's moduli. Later, normalized stress-strain plots are used to better visualize selected linear region (**Figure 3.16**).

The values of maximum stress over specimen's area were plotted against saturation treatment and known as strength value over saturation treatment (strength plot) (**Figure 3.17, left image**). Young's moduli values were plotted against saturation duration is called as Young's moduli plot (**Figure 3.17, right image)**. Overall, specimens' strengths do not show a logical correlation to the saturation as strength in plasticized specimens is higher than in dry specimens. But Young's moduli show logical correlation to the saturation duration.

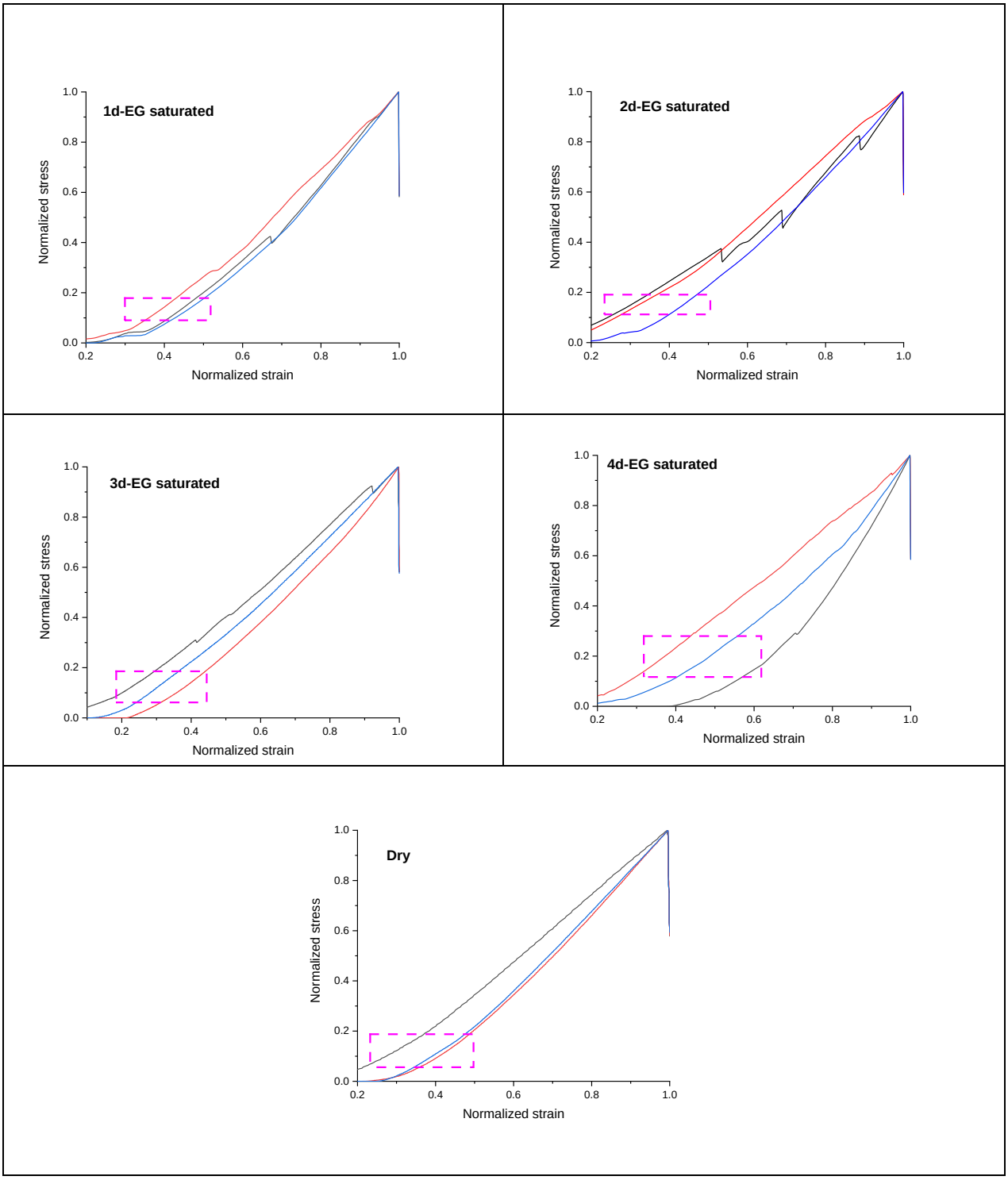

Figure 3.16 *Young's modulus values were determined as the slope of normalized stress-strain plot at the linear region. Magenta dashed boxes show selected linear region for each specimen used to determine Young's modulus value.*

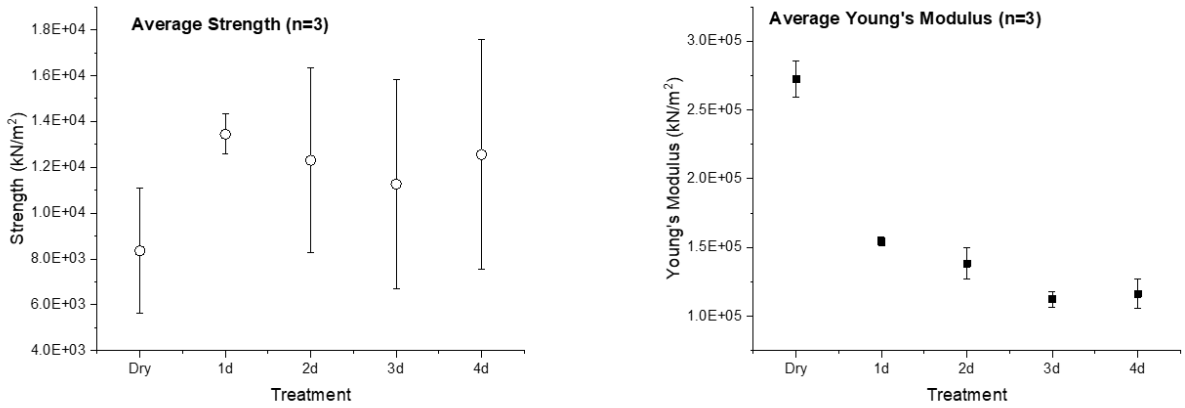

Figure 3.17 Left *– average strength plot vs saturation treatment (dry and 1-4 days saturation);* ***Right*** *– average Young's modulus plot vs saturation treatment (dry and 1-4 days saturation).*

We used Young's moduli to determine the minimum saturation period. Young's modulus values are decreasing as saturation duration is longer, but after 3-days, the Young's modulus remains stable. Therefore, it was determined that 3 days of specimen saturations were required; consequently, all specimens (seed coat, nuts shell and wood disk) DMA scans shown hereafter met this standard saturation.

C-lignin T_g

Glass transition is the transition glassy state to viscous, rubbery state; measured as dynamic stiffness, or storage modulus. Glass transition of lignocellulose material is indicated by thermomechanical softening transition associated with lignin.[27] Several studies on *In situ* wood thermomechanical properties have been done using DMA.[26-28, 47, 49] Measurement of T_g in lignocellulose requires plasticization, solvent-submersion measurement mode, and measurement within LVR. The T_g of wood is observed as lignin softening which depends on the moisture;

expressed as the temperature at maximum tan δ (ratio of loss to the storage). Different organic plasticizers: ethylene glycol, glycerol, N,N-dimethylformamide (DMF) and N-methyl-2-pyrrolidone (NMP) show different lignin relaxation in wood, with DMF and NMP are known to be the stronger plasticizer in wood than alcohols.[48]

DMA measurement was performed in compressive-torsion, solvent-submersion mode in a torsional rheometer (**Figure 3.18**). Vanilla seed coats and candlenut shells are not conventionally in shape and size for typical DMA. Torsional rheometer allows specimen gripping to occur by compression of specimens between parallel-plates, and low-amplitude torsional oscillation. T_g in wood is observed as softening, in which wood plasticized in water exhibit glass transition between 80-100°C, depends on measurement frequency.[50] T_g in wood is also affected by lignin monomer composition.[24, 51]

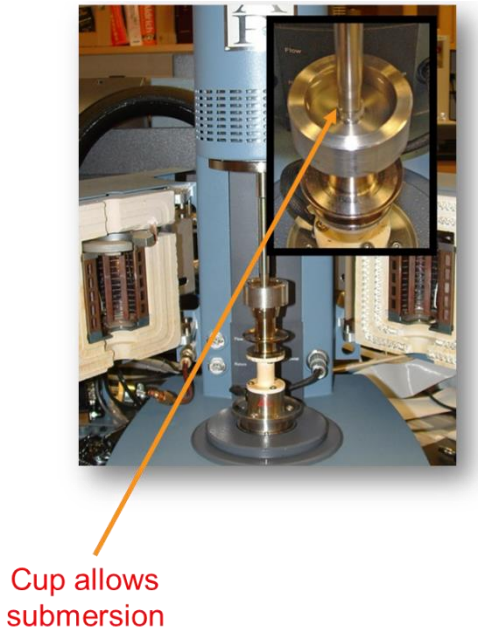

Figure 3.18 *DMA Instrument modification to accommodate solvent-submersion technique*.

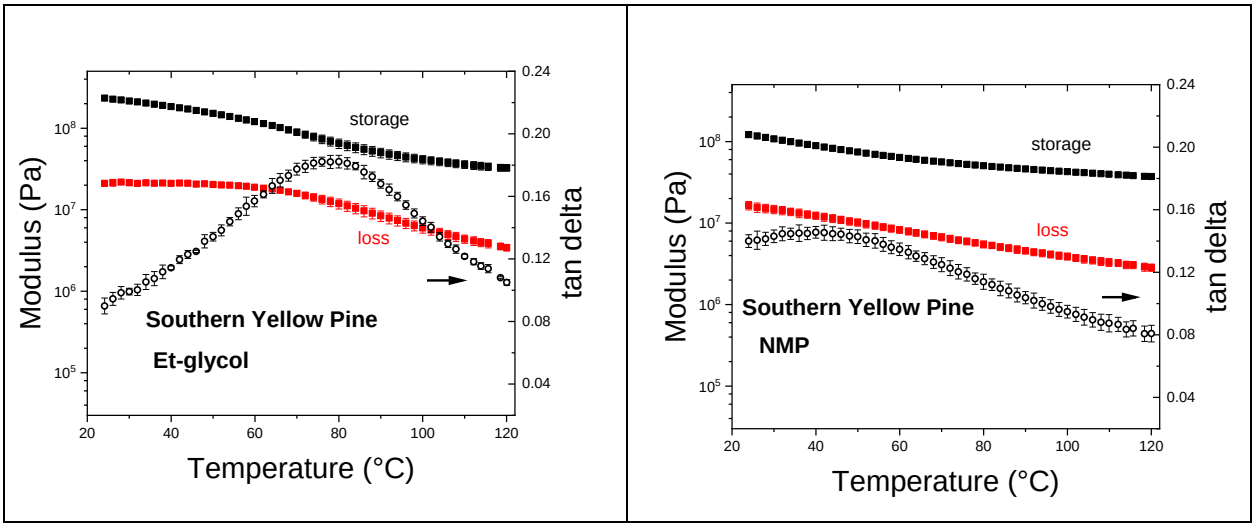

Figure 3.19 *DMA scans of storage-loss modulus and tan δ for ethylene glycol and N-methyl-2-pyrrolidone plasticized Southern Yellow Pine 3 mm-disk subjected to 1st cooling. Error bars represent ±1; n=3.*

In organic plasticizer such as ethylene glycol and NMP, transition behaviors of Southern Yellow pine are observed as broad spectra of tan delta with peak at 80°C in ethylene glycol. DMA scans of Southern Yellow Pine are shown in **Figure 3.19**. In NMP, the tan delta spectra are even broader with peak at ~43°C. vanilla seed coat and candlenut shells might be expected to exhibit softening pattern as in wood, but T_g are expected to be higher than what observed in wood due to the C-lignin linear-benzodioxane linked homopolymer structure that impedes rotation. Furthermore, it is interesting to look at the effect of C-lignin co-existence with G-lignin in candlenut shells to the T_g compared to wood tissue.

Comparison of DMA results of vanilla seed coat and candlenut shell-solid whole specimens saturated in ethylene glycol and NMP subjected to 1st cooling are shown on **Figure 3.20**. Vanilla seed coat specimens saturated in both plasticizers exhibit onset transition temperature at 120°C.

This onset is evidence that C-lignin has a high T_g that could be as high as 160°C or 180°C. The result also suggests that NMP is a stronger plasticizer than ethylene glycol indicated by higher tan δ value. Interestingly, candlenut shell's solid whole specimens exhibit similar onset transition to the seed coat, considering that this tissue has G and C-lignins in the cell-wall. In addition, the effect of plasticizers in candlenut shell is opposite to those in vanilla seed coat; ethylene glycol plasticized shell shows higher tan δ maximum than the N-methyl-2-pyrrolidone one. Candlenut also exhibits higher storage modulus than vanilla, even though the absolute values of moduli are questionable, moduli values of candlenut shells plasticized in both plasticizers are higher than in the corresponding vanilla seed coats.

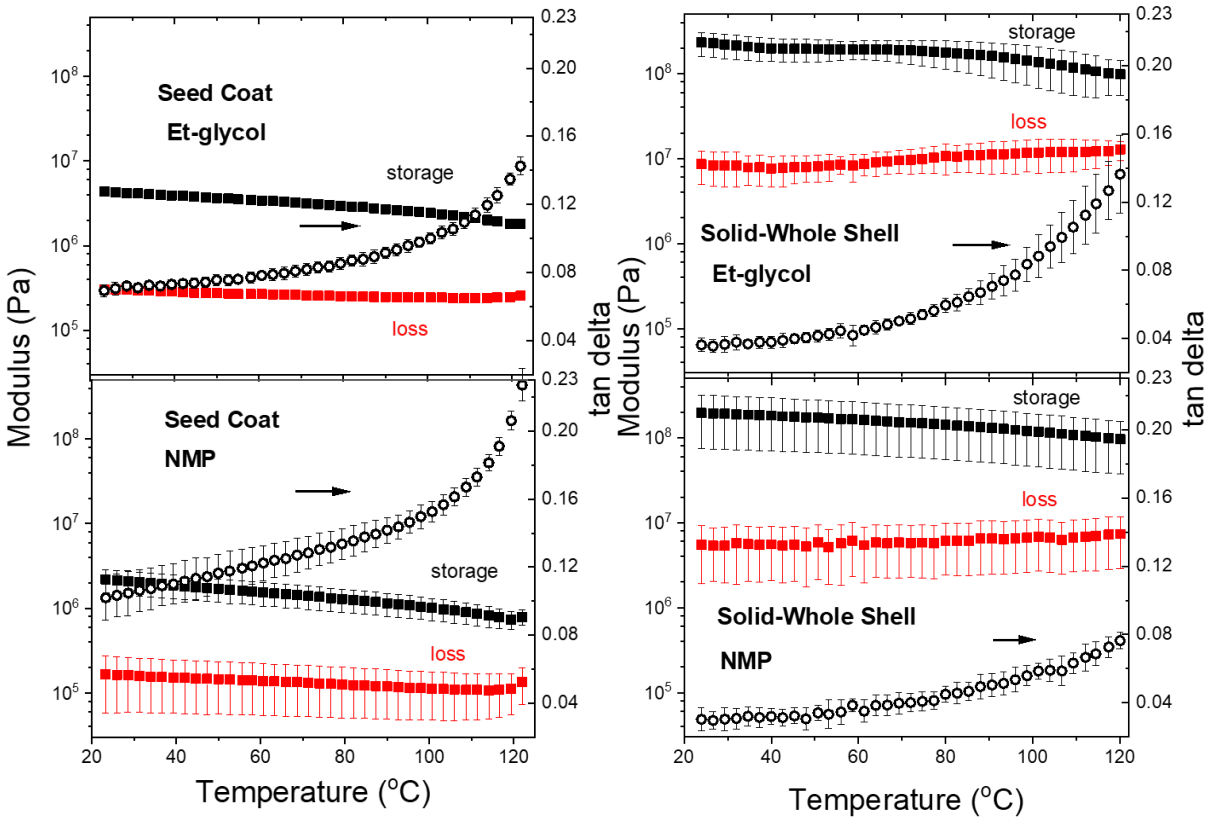

Figure 3.20 *DMA scans of modulus and tan δ curves for ethylene glycol and NMP plasticized vanilla seed coat and solid-whole candlenut shell subjected to 1st cooling. Error bars represent ±1 standard deviation; n=3.*

Tobimatsu and co-workers[14] mentioned the deposition of C-lignin perhaps occurs later than G-lignin due to the downregulation of O-methyltransferase. If so, the abundance of C-lignin is perhaps more in the inner layer than the outer layer. To see if there is an effect of G/C-lignin to the T_g, candlenut shells varied in shape and particle size. Comparison of transitions observed in solid-sanded, 80-and 100-specimens saturated in ethylene glycol are shown on **Figure 3.21**. The storage and loss moduli decreased as particle size is smaller, but the value of storage and loss moduli are not reliable due to the nature of the particulate specimens. However, the damping coefficient (tan δ) – ratio of loss to storage moduli, is unitless and not affected by fluctuating storage and loss moduli values. The three-different specimens shape/size show similar onset transition at ~60-70°C and thus it seems that the peak or partial peak of tan δ is at 120°C, or probably at 130°C at the highest.

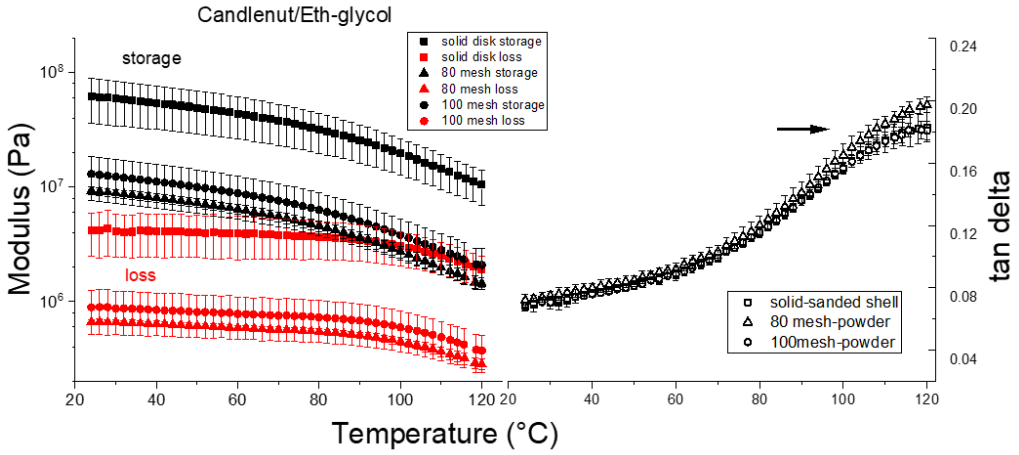

Figure 3.21*DMA scans of storage-loss modulus (**left**) and tan δ (**right**) curves for ethylene glycol saturated solid-sanded, 80-and 100- mesh powder candlenut shell subjected to 1st cooling. Error bars represent ±1 standard deviation; n=3.*

DMA scans of solid-sanded, 80-and 100-mesh specimens saturated in NMP are shown in **Figure 3.22**. These specimens show variation in the onset transitions. Powder specimens seem to

have reached maximum tan δ around 100°C, while solid-sanded specimen shows similar onset at ≈120°C, similar to that saturated in ethylene glycol. Loss modulus in powder specimens saturated NMP at temperature around 100°C also decreases compared to those in ethylene glycol that might indicates the occurrence of lignin softening. Nevertheless, removing and reducing particle size affect transition behavior that result in lowering the T_g.

The different transitions behavior in candlenut shell that observed with the change in specimen shape/size apparently imply a correlation between cell arrangement and T_g, but how far the effect of cell arrangement to the T_g is not known. The whole-shell specimens still have cells in the original shape, size and order/arrangement, while sanded and powder specimen have some amount of lignin removed and cell shape/size/ arrangement altered.

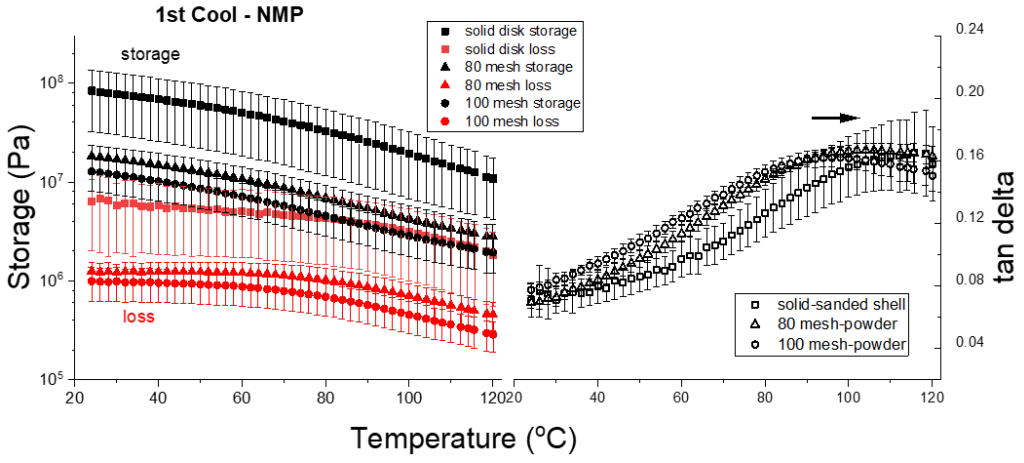

Figure 3.22 *DMA scans of storage-loss modulus (**left**) and tan δ (**right**) curves for NMP-saturated solid-sanded, 80-and 100-mesh powder candlenut shells subjected to 1st cooling. Error bars represent ±1; n=3.*

Tobimatsu and coworkers[14] reported that microscopy observation of *Cleome hassleriana* resulted in distinguished layers of G and C-lignins, suggesting that C-lignin is deposited later than G-lignin and C-lignin is predominantly the inner layer of cleome seed coat. With the assumption that inner layer has more C-lignin than outer layer, the inner layer of candlenut shell was collected by sanding. DMA scans of 200-mesh powder specimens are shown in **Figure 3.23**.

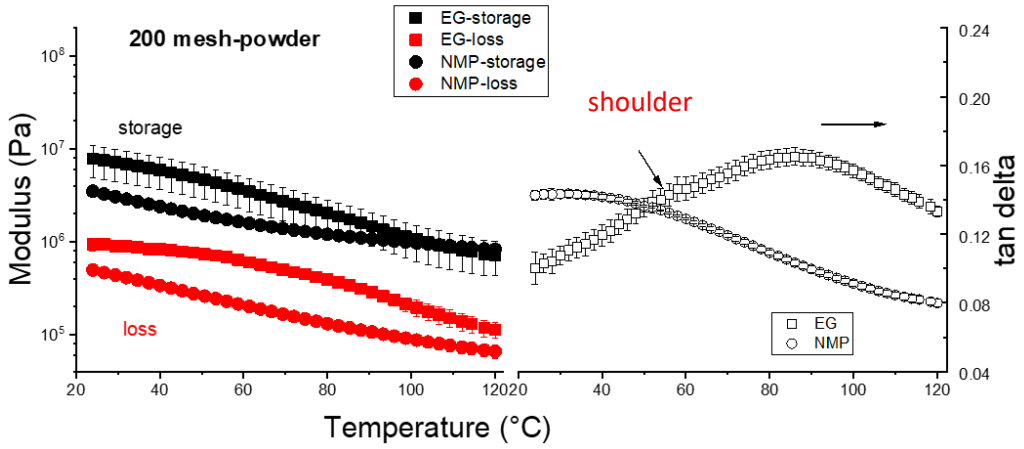

Figure 3.23 *DMA scans of storage-loss modulus (**left**) and tan δ (**right**) curves for EG and NMP-saturated 200-mesh powder candlenut shells subjected to 1st cooling. Error bars represent ±1; n=3. Note: shoulder peak observed in EG-saturated specimens.*

The 200-mesh powder specimens show surprising DMA results that similar wood transition in both plasticizers. Specimens saturated in ethylene glycol show a broad transition with maximum tan δ at ~90°C or approximately 10° higher than pine tissue. The DMA curve also show a small shoulder at ~60°. Specimens saturated in N-methyl-2-pyrrolidone show an even broader transition with maximum tan δ with no indication of second transition. These transitions are similar to pine, but the T_g value observed in specimen saturated in ethylene glycol is about 5-10°C higher than pine, while the T_g value of specimen saturated in NMP is about 10°C lower than pine.

Value of T_gs observed in the candlenut shell at different specimen shape and size are summarized on **Table 3.3**. Specimen shape and size are factors that affect the T_g in candlenut shell which has both G/C-lignins in addition to the plasticizers effect. The transition behavior of specimens with particle size of 200-mesh obtained from sanding the inner layer of candlenut shells are found to be very surprising since we expect that transition from this layer will look like vanilla seed coat due to the presence of C-lignin. The T_gs of candlenut 200 mesh specimen in both plasticizers drop significantly. Meanwhile, the transition behavior of solid-whole specimen, which the entire cells are in their original arrangement and dimensions, similar to vanilla seed coat. All samples were saturated for at least 3 days, therefore, the variation of T_{g-} is not caused by saturation problem. The decrease of T_gs as particle size decreases is probably due to more flexible polymer chain movements as particles are smaller. Therefore, sanding candlenut shells into 200 mesh probably has eliminated the stiff benzodioxane-linkage effect.

Table 3.3 *T_g Candlenut shell specimen variations compared to pine powder.*

Specimen form	**T_g (°C)**	
	EG	**NMP**
SYP Powder 80 mesh	79.9 ± 0.4	43.5 ± 0.9
Solid whole	Onset 120	Onset 120
Solid sanded	120.0 ± 0.1	116.0 ± 0.0
Powder 80 mesh	119.1 ± 0.9	105.2 ± 0.7
Powder 100 mesh	118.1 ± 1.1	96.9 ± 0.7
Powder 200 mesh	87.3 ± 2.6	32.2 ± 0.0

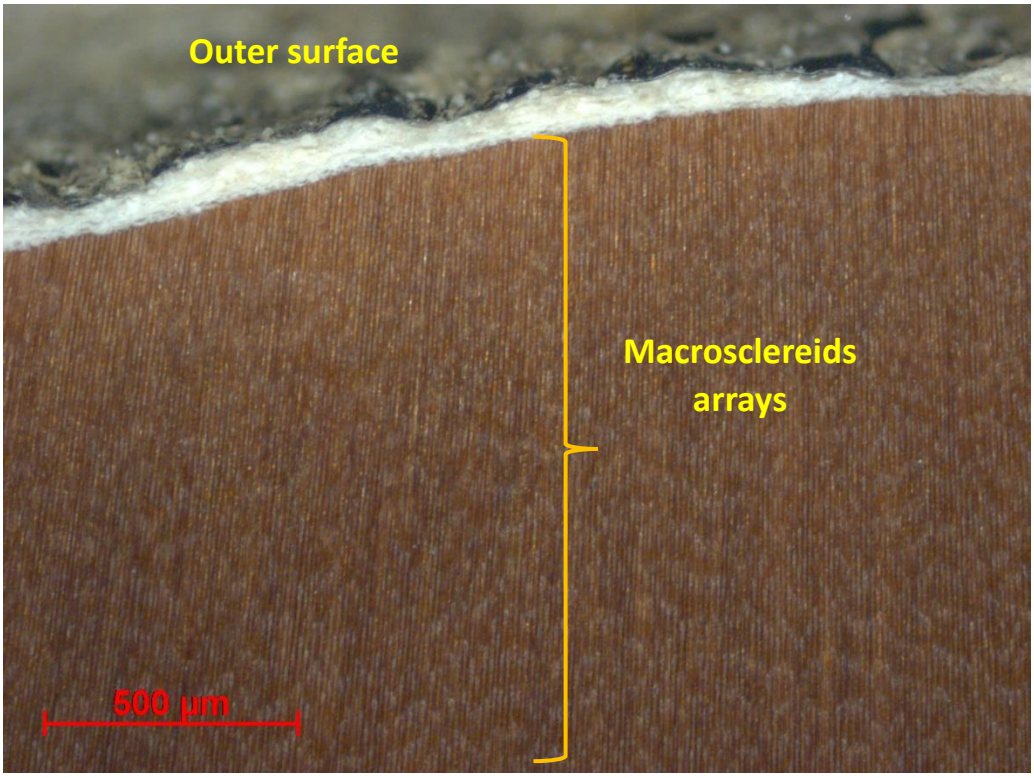

Figure 3.24 *Candlenut shell image taken with reflective light microscopy. Despite the variation on lignin composition in it, the candlenut shell has a homogenous cell type, macrosclereids, which lays along the cross section of the shell.*

What caused variations on T_g behavior in candlenut is probably associated with the cell type. Light microscopy image (**Figure 3.24**) shows that candlenut shells is occupied by a long-tubular cells. As seed coats and nutshell are highly sclerotic, this type of cell referred to macrosclereids, such as observed in legume seed coat, *Pisum sativum* L.[52] The long-size macrosclereids would have been damaged during the sample preparation, and the G/C-lignin layer that probably well defined in the intact shell would have been altered as the shells were sanded and milled. The XRD scans of seed coat and nutshell tissues show a similar pattern with Southern Yellow Pine powder

scan, suggesting no evidence that C-lignin is crystalline, despite its highly linear structure. Elemental analysis on seed coat and nut shells indicates that there is no specific element that could contribute to the crystallinity of both tissues (result is shown in supplemental data 2). Calcium and potassium are two most abundance element in vanilla seed coat and candlenut shell which are associated with biomineralizations in plant.[53] However, the amount is probably not significant enough to show as single, sharp peaks detected by XRD.

3.4. Conclusion

Crystallinity and T_g of plant tissues which exhibit C-lignin in their seed coat/nutshell are studied using XRD and DMA. Vanilla seed which has entirely C-lignin in its seed coat and candlenut which has both G/C-linin in its shell are used for studying C-lignin crystallinity and T_g. Southern Yellow Pine, which only has G-lignin, is used as reference. Vanilla seed coat requires separation process from the embryo. A two-steps purification are employed, step I: milling followed by density based-separation in a mixture of two organic solvents, tricholorobenze (TCB):n-hexane (HXN) ; step II: further purification using a mixture of water:ethanol and a drop of non-ionic surfactant. TGA is used to observe the purification progress, but TGA does not show the difference of purification degree between step I and step II. Microscopy observation helps to visualize the difference purification degree from step I and step II. Candlenut shell is prepared into disks(whole and sanded) and powder of different particle sizes (80, 100, and 200-mesh). XRD scans of vanilla seed coat and candlenut shell show a similar peaks pattern, but low in intensity compared Southern Yellow Pine, indicating that the crystalline contribution in seed coat and nutshell is cellulose, and due to low cellulose content, seed coat/nutshell diffractograms are low in intensity. This also suggest that C-lignin is not crystalline. DMA measurement is performed in a solvent-submersion compressive-torsion mode, with ethylene glycol and NMP as plasticizers. A

minimum of 3-days saturation is required to achieve a fully saturated sample. DMA measurement of vanilla seed coat indicates onset at ~120°C in both ethylene glycol, that suggest T_g in vanilla seed coat is as high as 160-180°C. Candlenut shell exhibit a variation of T_g. The intact shell exhibit T_g as in vanilla seed coat. Meanwhile, the 200-mesh powder exhibits broad transitions as observed in pine. Sanding candlenut shell into 200-mesh probably has eliminated stiff benzodioxane effect.

3.5. References

1. Freudenberg, K., Lignin: its constitution and formation from p-hydroxycinnamyl alcohols. *Science* **1965,** *148*, 595-600.

2. Higuchi, T., Biochemical Aspects of Lignification and Heartwood Formation. *bulletin of the Wood Research Institute Kyoto University* 1976, pp 180-199.

3. Barcelo, A. R., Lignification in Plant Cell Walls. *International Review of Cytology* **1997,** *176*, 87-132.

4. Singh, A.; Daniel, G.; Nilsson, T., Ultrastructure of S2 Layer in Relation to Lignin Distribution in Pinus radiata Tracheids. *J. Wood. Sci.* **2022,** *48*, 95-98.

5. Terashima, N.; He, L., Formation and Structure of Lignin in Monocotyledons IV. Deposition Process and Structural Diversity of the Lignin in the CellWall of Sugarcane and Rice Plant Studied by Ultraviolet Microscopic Spectroscopy. *Holzforschung* **1991,** *45* (3), 191-198.

6. Kenrick, P., Crane, P. R., The origin and early evolution of plants on land *Nature* **1997,** *384*, 33-39.

7. Novo-Uzal, E.; Pomar, F.; Gómez Ros, L. V.; Espiñeira, J. M.; Ros Barceló, A., Evolutionary history of lignins. *Advances in Botanical Research* **2012,** *61*, 309-350.

8. Raven, J. A., The Evolution of Vascular Land Plants in Relation to Supracellular Transport Processes. In *Advances in Botanical Research* Woolhouse, H. W., Ed. Academic Press Inc.: London, 1977; Vol. V, pp 153-219.

9. de Vries, S.; de Vries, J.; von Dahlen, J. K.; Gould, S. B.; Archibald, J. M.; Rose, L. E.; Slamovits, C. H., On plant defense signaling networks and early land plant evolution. *Commun Integr Biol* **2018,** *11* (3), 1-14.

10. Chen, F.; Tobimatsu, Y.; Havkin-Frenkel, D.; Dixon, R. A.; Ralph, J., A polymer of caffeyl alcohol in plant seeds. *Proc Natl Acad Sci U S A* **2012,** *109* (5), 1772-7.

11. Higuchi, T., Look back over the studies of lignin biochemistry. *Journal of Wood Science* **2006,** *52* (1), 2-8.

12. Li, Y., Shuai, L., Kim, H., Motogamwala, A. H., Mobley, J. K., Yue, F., Tobimatsu, Y., Havkin-Frenkel, D., Chen, F., Dixon, R. A., Luterbacher, J. S., Dumesic, J., Ralph, J., An "ideal lignin" facilitates full biomass utilization. *Sci. Adv.* **2018,** *4*, 1-10.

13. Cameron, K. M., Biology of Vanilla In *Handbook of Vanilla Science and Technology* Havkin-Frenkel, D.; Belanger, F., Eds. Blackwell Publishing, Ltd.: 2011; pp 241-254.

14. Tobimatsu, Y.; Chen, F.; Nakashima, J.; Escamilla-Trevino, L. L.; Jackson, L.; Dixon, R. A.; Ralph, J., Coexistence but independent biosynthesis of catechyl and guaiacyl/syringyl lignin polymers in seed coats. *Plant Cell* **2013,** *25* (7), 2587-600.

15. Boesewinkel, F. D. a. B., F., The Seed: Structure and Function. In *Seed development and germination*, Kigel, J.; Galili, G., Eds. CRC press: New York, 1995; Vol. 41, pp 1-21.

16. Debeaujon, I.; Lepiniec, L.; Pourcel, L.; Routaboul, J.-M., Seed Coat Development and Dormancy In *Seed Development, Dormancy and Germination*, Bradford, K.; Nonogaki, H., Eds. Wiley-Blackwell: 2007; Vol. 27, p 392p.

17. Boesewinkel, F. D.; Bouman, F., The Seed: Structure. In *Embryology of Angiosperms*, Johri, B. M., Ed. Springer Berlin Heidelberg: Berlin, Heidelberg, 1984; pp 567-610.

18. Schüler, P.; Speck, T.; Bührig-Polaczek, A.; Fleck, C., Structure-Function Relationships in Macadamia integrifolia Seed Coats – Fundamentals of the Hierarchical Microstructure. *PLOS ONE* **2014,** *9* (8), e102913.

19. Sano, N.; Rajjou, L.; North, H. M.; Debeaujon, I.; Marion-Poll, A.; Seo, M., Staying Alive: Molecular Aspects of Seed Longevity. *Plant Cell Physiol* **2016,** *57* (4), 660-74.

20. Yeh, C. H.; Chen, K. Y.; Lee, Y. I., Asymbiotic germination of Vanilla planifolia in relation to the timing of seed collection and seed pretreatments. *Bot Stud* **2021,** *62* (1), 6.

21. Susilowati, A.; Dalimunthe, A.; Rachmat, H. H.; Elviati, D.; Ginting, I. M.; Larengkeng, S. H. In *Morphology and germination of the candlenut seed (Aleurites moluccana) from Samosir Island-North Sumatra*, International Conference on Agriculture, Environment and Food Security, IOP Publishing: 2019.

22. Lundquist, A., Characterization in Solution: Chemical Degradation Methods-Acidolysis. In *Methods in lignin chemistry*, Lin, S. Y., Dence, C. W. (Eds.), Ed. Springer Verlag: 1992; pp 289-298.

23. Park, S.; Baker, J. O.; Himmel, M. E.; Parilla, P. A.; Johnson, D. K., Cellulose crystallinity index: measurement techniques and their impact on interpreting cellulase performance. *Biotechnol Biofuels* **2010,** *3* (10), 1-10.

24. Olsson, A.-M.; Salmen, L., The effect of lignin composition on the viscoelastic properties of wood. *Nordic Pulp and Paper Research Journal* **1997,** *12*, 140-144.

25. Brown, R. M., The Biosynthesis of Cellulose. *Journal of Macromolecular Science, Part A* **2006,** *33* (10), 1345-1373.

26. Kelley, S. S.; Rials, T. G.; Glasser, W. G., Relaxation Behavior of the Amorphous Components of Wood. *J. Mater. Sci.* **1987,** *22* (2), 617-624.

27. Sun, N.; Das, S.; Frazier, C. E., Dynamic mechanical analysis of dry wood: Linear viscoelastic response region and effects of minor moisture changes. *Holzforschung* **2007,** *61* (1), 28-33.

28. Chowdhury, S.; Fabiyi, J.; Frazier, C. E., Advancing the dynamic mechanical analysis of biomass: comparison of tensile-torsion and compressive-torsion wood DMA. *Holzforschung* **2010,** *64* (6).

29. Wan, G.; Frazier, T.; Jorgensen, J.; Zhao, B.; Frazier, C. E., Rheology of transgenic switchgrass reveals practical aspects of biomass processing. *Biotechnol Biofuels* **2018,** *11*, 57.

30. Menard, K. P., A practical introduction. *Dynamic Mechanical Analysis* **1999**.

31. Swamy, B. G. L., On The Life-History of Vanilla Planifolia. *Botanical Gazette* **1947,** *108* (3), 449-456.

32. Philip, V. J.; Nainar, S. A. Z., Structural Changes During the in vitro Germination of Vanilla planifolia (Orchidaceae). *Annals of Botany* **1988,** *61*, 139-145.

33. Rongpipi, S.; Ye, D.; Gomez, E. D.; Gomez, E. W., Progress and Opportunities in the Characterization of Cellulose - An Important Regulator of Cell Wall Growth and Mechanics. *Front Plant Sci* **2018,** *9*, 1894.

34. Cave, I. D., Theory of X-ray measurement of microfibril angle in wood Part 1. The condition for reflection X-ray diffraction by materials with fibre type symmetry. *Wood Sci. Technol.* **1997,** *31*, 143-152.

35. Frey-Wyssling, A., The Fine Structure of Cellulose Microfibrils. *Science* **1954,** *119* (3081), 80-82.

36. Prud'homme, R. E.; Noah, J., Determination of Fibril Angle Distribution in Wood Fibers: A Comparison Between the X-Ray Diffraction and the Polarized Microscope Methods *Wood and Fiber Science* **1975,** *6* (4), 282-289.

37. Garvey, C. J.; Parker, I. H.; Simon, G. P., On the Interpretation of X-Ray Diffraction Powder Patterns in Terms of the Nanostructure of Cellulose I Fibres. *Macromolecular Chemistry and Physics* **2005,** *206* (15), 1568-1575.

38. O'Sullivan, A. C., Cellulose: the structure slowly unravels. *Cellulose* **1997,** *4*, 173-207.

39. Atalla, R. H.; Vander Hart, D. L., Native Cellulose: A Composite of Two Distinct Crystalline Forms. *Series* **1984,** *223* (4633), 283-285.

40. Andersson, S.; Serimaa, R.; Paakkari, T.; Saranpää, P.; Pesonen, E., Crystallinity of wood and the size of cellulose crystallites in Norway spruce (Picea abies). *Journal of Wood Science* **2003,** *49* (6), 531-537.

41. Harris, D.; DeBolt, S., Relative Crystallinity of Plant Biomass: Studies on Assembly, Adaptation and Acclimation. *PLOS ONE* **2008,** *3* (8), e2897.

42. Newman, R. H.; Hemmingson, J. A., Determination of the Degree of Cellulose Crystallinity in Wood by Carbon-13 Nuclear Magnetic Resonance Spectroscopy. *Holzforschung* **1990,** *44* (5), 351-355.

43. Chen, F., Dixon, R., Vanilla planifolia-The Source of the Unexpected Discovery of a New Lignin. In *Handbook of Vanilla Science and Technology 2nd Edition*, Havkin-Frenkel, D., Belanger, F. C., Ed. John Wiley & Sons, Ltd.: 2019; pp 447-455.

44. Burgert, I.; Fratzl, P., Plants control the properties and actuation of their organs through the orientation of cellulose fibrils in their cell walls. *Integr Comp Biol* **2009,** *49* (1), 69-79.

45. Thomas, L. H.; Forsyth, V. T.; Sturcova, A.; Kennedy, C. J.; May, R. P.; Altaner, C. M.; Apperley, D. C.; Wess, T. J.; Jarvis, M. C., Structure of cellulose microfibrils in primary cell walls from collenchyma. *Plant Physiol* **2013,** *161* (1), 465-76.

46. Ramsden, M. J.; Blake, F. S. R., A kinetic study of the acetylation of cellulose, hemicellulose and lignin components in wood. *Wood Sci. Technol.* **1997,** *31*, 45-50.

47. Laborie, M.-P. G.; Salmén, L.; Frazier, C. E., Cooperativity analysis of the in situ lignin glass transition. *Holzforschung* **2004,** *58*, 129-133.

48. Chowdhury, S.; Frazier, C. E., Thermorheological complexity and fragility in plasticized lignocellulose. *Biomacromolecules* **2013,** *14* (4), 1166-1173.

49. Horvath, B.; Peralta, P.; Frazier, C.; Peszlen, I., Thermal Softening of Transgenic Aspen. *BioResources* **2011,** *6* (2), 2125-2134.

50. Salmén, L., Viscoelastic properties of in situ lignin under water-saturated conditions. *J. Mater. Sci.* **1984,** *19*, 3090-3096.

51. Olsson, A.-M.; Salmen, L., Viscoelasticity of In Situ Lignin as Affected by Structure: Softwood vs Hardwood. In *National Meeting of American Chemical Society*, Glasser, W. G.; Hatakeyama, H., Eds. American Chemical Society: Boston, MA, 1992; pp 133-143.

52. Harris, W. M., On the Development of Macrosclereids in Seed Coats of Pisum sativum L. *Amer. J. Bot.* **1983,** *70* (10), 1528-1535.

53. Cuéllar-Cruz, M.; Pérez, K. S.; Mendoza, M. E.; Moreno, A., Biocrystals in Plants: A Short Review on Biomineralization Processes and the Role of Phototropins into the Uptake of Calcium. *Crystals* **2020,** *10* (7).

Supplemental Data

1. Crystalline model of candlenut shell and vanilla seed coat compared to wood powder

Crystalline model of candlenut shell, vanilla seed coat, and wood powder were obtained by subtracting the experimental peak with background using peak analyzer mode in OriginLab 2019b software. Peak area of XRD scan after background subtraction was determined using peak analyzer menu. One peak was selected (in this case the highest intensity peak) as reference, so all areas above it would be covered.

a). Candlenut shell

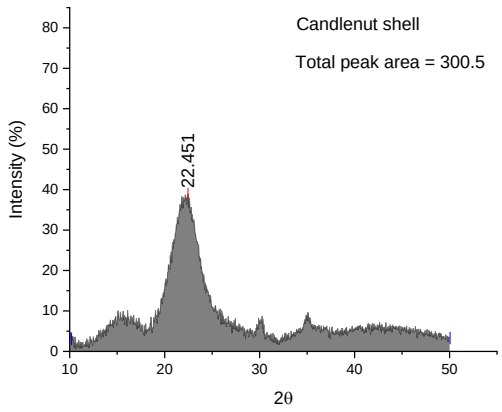

b). Vanilla seed coat

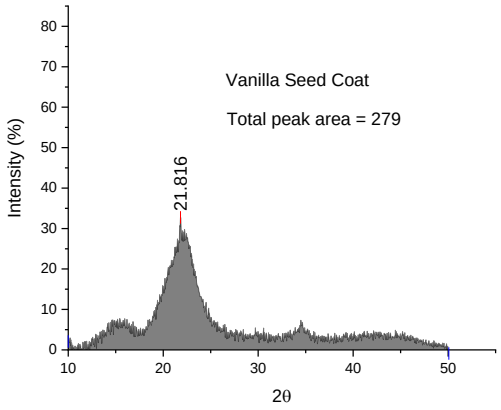

c). Southern Yellow Pine

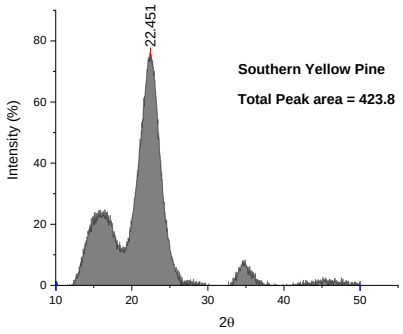

After background subtraction, the data was deconvoluted and fitted to obtain the crystalline model. Each peak area was calculated from the peak analyzer menu. % Crystallinity calculated as ratio of total crystalline peak area to total peak area. % Amorphous is calculated as (100% - % crystalline).

a). Candlenut shell

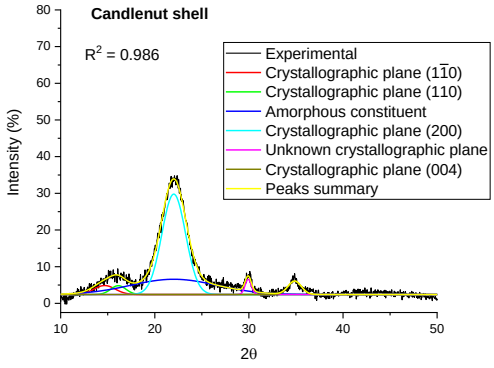

b). Vanilla seed coat

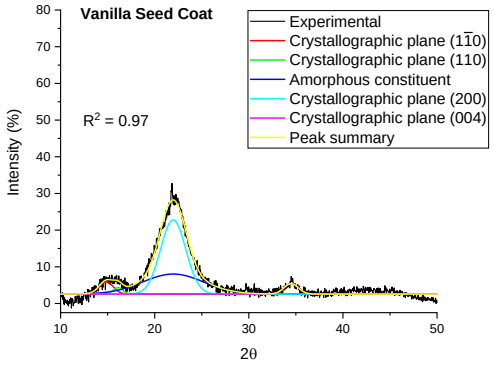

c). Southern Yellow Pine

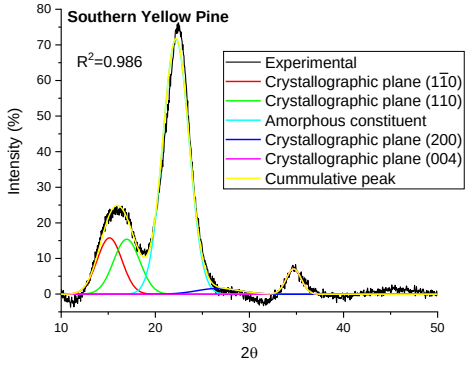

Sample	Peak Area							
	Plane (101)	**Plane (10$\bar{1}$)**	**Plane (002)**	**Unknown plane**	**Plane (040)**	**Total**	**% Crystallinity**	**% Amorphous**
Seed coat	6.0	2.1	67.6	0	5.4	279.0	29.1%	70.9%
Nutshell	6.9	4.8	86.1	3.4	6.4	300.5	35.8%	64.2%
Pine powder	48.9	27.6	194.2	0	19.9	423.8	68.6%	31.4%

2. Elemental Analysis

Element	Vanilla Seed Coat (µg/g, ppm)	Candlenut Shell (µg/g, ppm)
^{23}Na	267	93
^{24}Mg	712	938
^{27}Al	238	11
^{28}Si	309	45
^{31}P	134	18
^{39}K	3,101	724
^{44}Ca	882	1,137
^{52}Cr	1.8	0.6
^{55}Mn	64	11
^{56}Fe	684	129
^{60}Ni	2	6
^{63}Cu	31	6
^{66}Zn	44	ND
^{85}Rb	14	4
^{88}Sr	42	33
^{137}Ba	20	2

3. Temperature Control Problem

Temperature control problems were obtained at the initial scanning for both vanilla seed coat and candlenut specimen. Temperature control problem also occurs at the temperature ~50-60°C in vanilla seed coat.

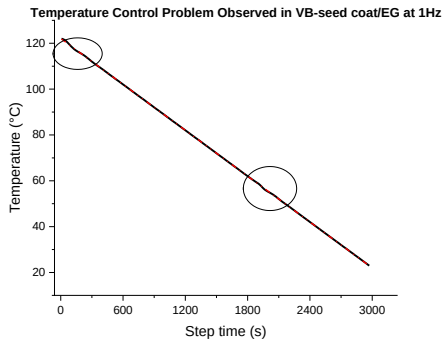

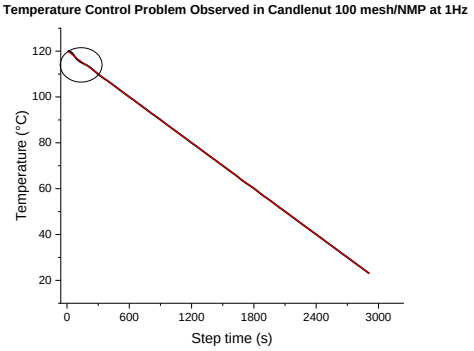

Chapter 4

Understanding Hydroxymethylated Resorcinol (HMR) Interactions with Lignin and Pectin from Loblolly Pine

(Short Study)

Attribution

In this Chapter all work was conducted by E. Ristanti, except for pectin isolation and pectin compositional analysis provided by Emilie Kohler and Dr. Bhawna Soni, respectively.

4.1 Abstract

Mechanism reaction between hyroxymethy resorcinol (HMR) with wood cell wall has not been well understood. This study observed the reaction between hydroxymethylated resorcinol resin with Loblolly pine crude milled wood lignin and pectin using heteronuclear single quantum coherence (HSQC)-nuclear magnetic resonance (NMR) and carbon-13 (^{13}C). Cured HMR and HMR cured at the presence of lignin and pectin were analyzed using HSQC and ^{13}C-NMR. HSQC spectra of cured HMR detected 4,4'-methylene bridge but did not show 2,4-methylene. HSQC spectra of HMR cured with Loblolly lignin showed both methylene bridges, but for HMR cured with pectin, only 4,4'-methylene was shown. Carbonyl groups at 191 and 194 ppm that originated from lignin's benzaldehyde and β-aryl ether units were missing in the cured HMR-lignin ^{13}C-NMR spectra. However, ^{13}C-NMR for cured HMR-lignin did not show formation of any new bond. ^{13}C-NMR spectra of cured HMR-pectin did not show any new bonds, while signals from esterified and non-esterified galacturonic acid and galactose residues were missing. HSQC spectra of cured HMR-pectin indicated that signal from esterified and non-esterified galacturonic and galactose

residues became weaker. The weakened HSQC signals of both lignin and pectin in the cured HMR-lignin and HMR-pectin in the absence of new bond signal indicate that the interaction between HMR and lignin/pectin perhaps occur via permeation.

4.2 Introduction

In 90s era, epoxy adhesive with greater resistance to delamination was on demand for more advanced use in transportation and architecture. This has led the discovery of a coupling agent known as hydroxymethylated resorcinol (HMR) by Forest Products Laboratory (FPL).[1] HMR is mono-, di, and tri-hydroxymethylated resorcinol synthesized by reacting formaldehyde with resorcinol in 1.54 mole ratio at a mild alkaline condition at room temperature for more than 4 hours but cannot go beyond 8 hours.[2] The structure of HMR is shown in **Figure 4.1**.

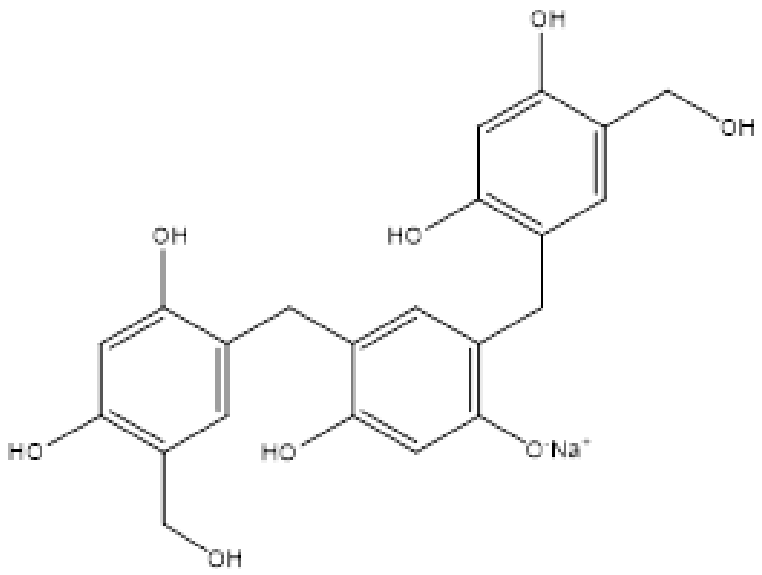

Figure 4.1 *Hydroxymethylated resorcinol structure*

General reaction of hydroxymethylated resorcinol is shown in **Figure 4.2**. Quantitative analysis on basic-catalyzed resorcinol-formadehyde (RF) resin has been studied by Werstler

(1986) using carbon-13 (^{13}C)-NMR and was able to identify hemiformal and methylol-related peaks.[3] Werstler did not specify sequence of chemical groups occurs during reaction. Later, Christiansen (2000) studied step-by-step formation of chemical groups during reaction of resorcinol-formaldehyde under mild alkaline conditions in HMR synthesis using ^{13}C-NMR.[4]

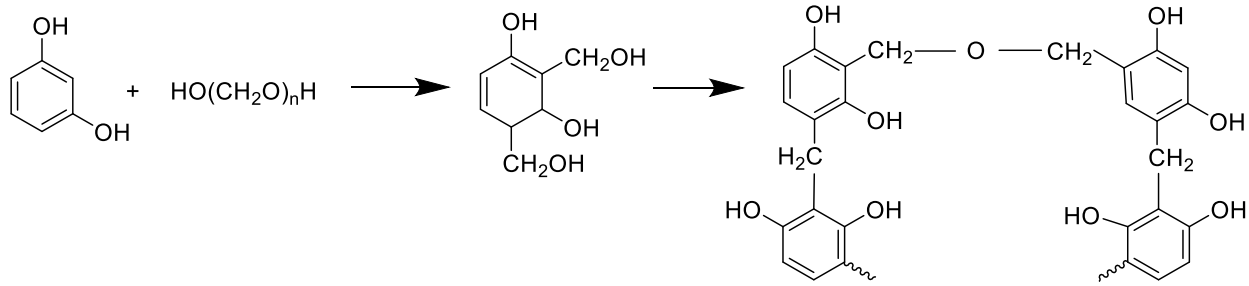

Figure 4.2 *General formation reaction of HMR from resorcinol and formaldehyde.*

HMR primer enhances the performance of epoxy-bonded wood lamellas. Application of HMR has known to improved bond strength in different type of wood.[5-7] Mechanism of HMR interaction with wood cell wall is not well understood, but some theories presume that the interaction occurs through interfacial adhesion, lumen filling, or cell wall permeation.[8-10] Nevertheless, none of these theories are proven yet.

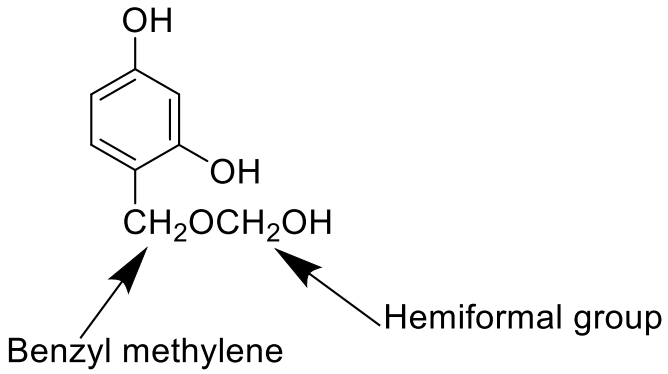

Figure 4.3 *Chemical compounds formed during reaction between resorcinol and formaldehyde are methylene and hemiformal.*

In 2017, Yelle[11] conducting experiments on heteronuclear nuclear single quantum coherence (HSQC)-NMR and ^{13}C-NMR analysis of hydroxymethylated resorcinol (HMR) cured in the presence of crude milled-wood lignin from *Acer saccharum* to find evidence if lignin and O-acetyl-(4-O-methylglucurono) xylan from wood will react with HMR through the formation of primary bonds. Yelle (2017)[11] used Novolak solution prepare the HMR resin and the cured resin HSQC spectra showed two methylene bridges' signals, 4,4'-methylene and 2,4-methylene, while the cured HMR-lignin HSQC spectra only showed 4,4'-methylene. Yelle (2017)[11] claimed that the presence of lignin and O-acetyl-(4-O-methylglucuronoxylan) avoid crosslinking to occur at 2-position. However, we found that Yelle made stoichiometry error in Novolak preparation, which lead to less amount of formaldehyde in the HMR resin.

Milled wood lignin is the most effective way to isolate lignin for studying chemical structure and reactivity of native lignin.[12, 13] Crude milled wood lignin (cMWL) is prepared based on Bjorkman method which use ball-milling.[14] Softwood lignin is predominated by guaiacyl (G) unit. Syringyl (S) unit content in softwood is very low.[15] Phenylcoumaran (β-5) accounts for 9-12% of total phenylpropanoid units in softwood. Dibenzodioxocin is also an important constituent in softwood, which the abundance is about 6%.[16, 17] NMR assignments of milled wood lignin isolated from Loblolly pine analyzed using ^{13}C-NMR is shown in **Table 4.2**.[18]

Table 4.2 ^{13}C-NMR chemical shift range of MWL loblolly pine (adapted from Huang,F. *et al*., 2011 and Holtman, K. M. et al., 2006)[19, 20]

chemical shift range (ppm)	assignment
198	C=O in 3-hydroxy-1-(4-hydroxy-3-methoxy-phenyl)propan-1-one
194	C=O in β-aryl ether with α-carbonyl
191	C=O in benzaldehyde
181	C=O in spirodienone
178.0 – 167.5	Unconjugated – COOH
167.5 – 162.5	Conjugated – COOH
154.0 –140.0	C3, C4 aromatic ether, or hydroxyl
140.0 – 127.0	C1, aromatic C – C bond
127.0 – 123.0	C5 in non-etherified, aromatic C – C bond
123.0 – 117.0	C6, aromatic C – H bond
117.0 – 114.0	C5, aromatic C – H bond
114.0 – 106.0	C2, aromatic C – H bond
90.0 – 78.0	Aliphatic C – O bond, C*β* in *β*-O-4, C*α* in *β-5* and *β-β*
79.0 – 67.0	Aliphatic C – O bond, C*α* in *β*-O-4
65.0 – 61.5	Aliphatic COR
61.5 – 57.5	Aliphatic C – O bond, C*γ* in *β*-O-4
57.5 – 54.0	Methoxyl –OCH_3
54.0 – 52.0	C*β* in *β-β* and C*β* in *β-5*

Pectin is a very complex biomacromolecules. The structure of pectin is a set of covalently linked polysaccharides, that can be constituted of 17 different monosaccharides.[21] Pectin composed of a (1→4)-linked *α-D*-galacturonan backbone, with region containing alternating units of →4)-*α-D*-Gal*A* (1→ and →2)-*α-L*-Rha-*p* (1→.[22] Galacturonic acid makes up 70% of pectin composition and it presents in all pectic polysaccharides.[23] In mature wood, pectin presents at a small amount as water insoluble calcium pectate or in combination with cellulose. Hydrolysis of pectic results in arabinose, galactose and D-galacturonic acid. Pectin may interfere lignin determination due to the formation of formaldehyde from the dehydration of uronic acid.[24]

4.2 Experimental

4.2.1 Materials

Loblolly pine tree (*Pinus taeda*) were harvested from Virginia Tech's Reynolds Homestead Forest Resources Research Center in Critz, Virginia. Each about 40 years old; the trees were grown in a natural setting with no silvicultural treatments. The trees were processed into lumber and air-dried. Chemicals: resorcinol (ACS reagents ≥ 99%, formaldehyde solution 37%, hydrochloric acid (HCl) in anhydrous methanol for GC derivatization, hexamethyldisilazane (HMDS), chlorotrimethylsilane (TMCS) (Sigma-Aldrich), HPLC-grade water, pyridine, (Fisher Scientific). NMR solvents: methyl sulfoxide (DMSO)-d6 99.9% atom D, deuterium oxide (D_2O) (Thermo Scientific).

4.2.2. Methods

Loblolly Crude Milled Wood Lignin Isolation

Loblolly powder was obtained by milling wood chips using (Wiley mill GE 5XBG00B D, 1725 RPM;Thomas Scientific, Swadesboro, NJ, USA) and passed into a 0.5 mm screen. Extractive was removed by Soxhlet extraction in water for 12 h followed by extraction in ethanol for 12 h, then air-dried and stored in vacuumed desiccator for at least 24 hours. Lignin samples were isolated following milled wood lignin procedure. Approximately 5 grams of wood powder was loaded into a 250 mL milling jar and 50 pieces of 10 mm Ø ZrO_2 balls. Milling was performed at 600 rpm in 30-minute segments (Retsch PM 100, Haan, Germany), followed by 10-minute non-milling segments to minimize excessive heating. Total milling time (sum of 30-minute segments) was 6 hours. The resulting fine wood flour was subjected to room temperature 96% dioxane/water extraction preceded by nitrogen purging for 5 minutes, then stirred using magnetic stirrer for 48

hours. The resulting mixture was then centrifuged at 600 rpm for 15 minutes and the supernatant evaporated using a rotary evaporator at 27°C. The remaining concentrate was rinsed with water at least three times, then dissolved with ~30 mL of HPLC water and transferred into plastic container for freeze-drying. The milled-wood lignin was kept in a vial bottle in a desiccator.

Loblolly Pectin Isolation

Loblolly pectin was isolated using acid extraction method which was modified from Gnanasambandam and Proctor (1998). [25] Extractive free loblolly powder was extracted with 0.1 N HCl (1:20) at 90°C for 60 minutes in a round bottom flask, then cooled to room temperature and filtered through brass sieve No. 325 (45 μm). Filtered liquid was transferred into 500 mL Nalgene centrifuge bottle then centrifuged (Beckman Coulter Avanti J-25 centrifuge) at 10,000 rpm and 15°C for 20 minutes to remove the remaining wood powder. The supernatant was collected dispersed in equal volumes of isopropanol and adjusted the pH to 3.5 and allowed to settle for 24 h. The precipitate was collected, centrifuged at 10,000 rpm and 15°C for 20 minutes. This was repeated two more time with isopropanol and finally with 70% isopropanol. The sediment was dispersed in a small amount of deionized water, deep-freeze at -80°C and freeze-dried.

Gas Chromatography (GC) Measurement

As much as 10 mg of loblolly pectin was transferred into a pressure tube with 2 mL 2M HCl in anhydrous methanol. The pressure tubes were conditioned in an oil bath at 100°C for 5 hours. The tubes were then removed from oil bath and allowed to cool to room temperature. Once cooled, 150μL of pyridine were added and mixed thoroughly, and 4 mL methanol with an internal standard sorbitol at 0.1 mg/ml. the solutions were filtered and 1 mL of solution was evaporated in a vial in the rotary evaporator, then further evaporated in the vacuum oven overnight to ensure all solvent

is evaporated. 100 microliters of pyridine were then added to dissolve leftover pyridine. 150 μL of HMDS and 80 μL of TMCS was added and placed in the shaking incubator for 15 minutes at 200 rpm. The solutions were left overnight and filtered into a GC vial and ready for GC analysis.

Preparation of HMR solution and curing of HMR, HMR-lignin, and HMR-pectin mix

HMR resin was prepared at a proportion of resorcinol/formaldehyde (F/R) 1.54 based on Vick, C. B., and co-workers .[1] The composition of HMR is shown in **Table 4.2**. The mixture was stirred with magnetic stirrer. Reaction was performed at room temperature for 4h under nitrogen blanket.

Table 4.2 HMR F/R 1.54 composition

HMR composition (g)	F/R 1.54
Water	90.43
Resorcinol	3.34
Formaldehyde	3.79
Sodium hydroxide	2.44

HMR and HMR/lignin – HMR/pectin Curing

HMR – approximately 10 grams of HMR was transferred into Teflon weighing boat and cured at 24.5°C with 50% relative humidity (RH) for approximately 16to 18 h.

HMR/lignin – approximately 1.0gram of HMR was mixed with 0.01-gram lignin in a glass vial and stirred with Teflon stirrer then transferred into medium square polystyrene weigh dish (3 ½ x 3 ½ x 1″ D) and cured 24.5°C with 50% relative humidity (RH) for approximately 20-24 h.

HMR/pectin – approximately 1.0-gram of HMR was mixed with 0.01-gram pectin in a glass vial and stirred with Teflon stirrer then transferred into Teflon weighing boat and cured 24.5°C with 50% relative humidity (RH) for approximately 24 h.

NMR sample preparation

For HMR and lignin, approximately 20-30 mg each was dissolved in 1.5mL DMSO-*d6* and transferred into NMR tubes for scanning. For HMR/lignin and HMR/pectin, cured samples were each dissolved in 1.5mL DMSO-*d6* and transferred into NMR tubes for NMR scanning. For pectin, approximately 30 mg pectin was dissolved in 1.5 mL D_2O and transferred into NMR tubes for HSQC scanning.

HSQC Measurement

HSQC spectra were acquired on Bruker Avance 600MHz spectrometer. Samples were analyzed as solution in DMSO-*d*6 at 25°C in thin-walled, borosilicate glass of 5 mm o.d x 7" L NMR tubes. HSQC spectra of lignin cured HMR resin, HMR-lignin mix, and HMR-pectin mix were referenced to (2.50,39.52) DMSO signal except for pectin which used D_2O solvent. Acquisition parameters for HSQC scanning are spectral width 0-10 ppm in ^{1}H using 2048 data points, 195 ms acquisition, spectral width 0-172 ppm in ^{13}C using 384 data points, increments of 64 scans, interscan delay 1.5 s total acquisition is 5h 53 min.

^{13}C-NMR Measurement

^{13}C-NMR spectra were acquired on Bruker Avance 500 MHz spectrometer (except for HMR resin ^{13}C-NMR was acquired on Bruker Avance 600MHz), Samples were analyzed as solution in DMSO-*d*6 at 25°C in thin-walled, borosilicate glass of 5 mm o.d x 7" L NMR tubes. ^{13}C-NMR spectra of HMR, HMR-lignin mix, and HMR-pectin mix were referenced to 39.52 center line DMSO peaks. 13C-NMR spectra were acquired using pulse program "zgpg30" with 64k data points, D1 of 0.5 s, AQ of 1.04 s, 6k scans, and a sweep width of 250 ppm with transmitter frequency offset of 105 ppm. Total acquisition time is 2h 45min.

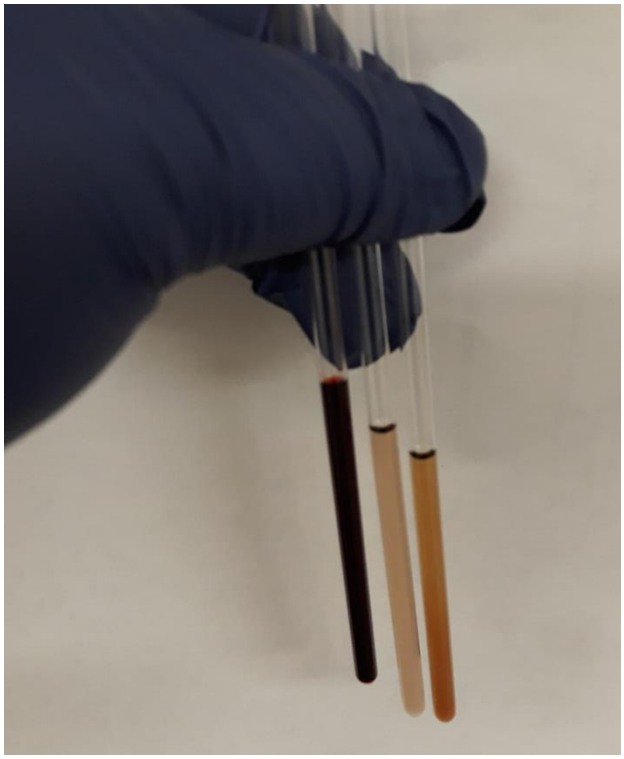

Figure 4.4 *NMR samples of cured HMR (left), HMR/pectin (middle) and HMR/cMWL (right)*

4.3. Results and Discussion

HMR resin cured for 16-18h resulted in soft gelled solid that still can be dissolved in DMSO-*d6* and thus can be run for solution state NMR analysis. Longer curing time will result in hard film that is not dissolved in any NMR solvents. The characteristics of cured HMR resin are shown in **Table 4.3**.

Table 4.3 HMR resin physical properties after curing.

Factor	F/R 1.54
Textured	Soft-gelled solid
Result image	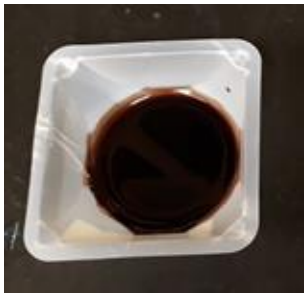
Dissolve in DMSO-d6	yes

Chemical compounds formed during the HMR resin synthesis are methylene glycols, methylene bridges (diarylmethanes) between resorcinolic rings, and hemiformal groups. Structures of compounds expected to appear on NMR spectra are shown in **Figure 4.5**. HSQC spectra of cured HMR is shown in **Figure 4.6**. At the aliphatic region, hemiformal showed at (3.27/55.62 ppm). β-hemiformals showed at chemical shift range (4.59-4.63/82.87-93.51) ppm. Methylols showed at (2-methylol, 4.50/54.10 ppm) and (4/6-methylol, 4.34/58.55 ppm). These methylols signals did not show in Yelle's cured HMR's HSQC spectra. One methylene signal shown (4,4'-methylene, 3,49/28.28 ppm), while in Yelle's work (2017)[11] 2,4-methylene was also observed at (3.44/25.1) ppm; but the 2,4-methylene signal is weak compared to 4,4'-methylene. At the aromatic region, C – H on resorcinolic rings observed at 2 and 4/6 position (6.21-6.31/101.92-107.01) ppm, while C – H on resorcinolic rings observed at 5 position (6.57-7.00/127.72-131.375) ppm.

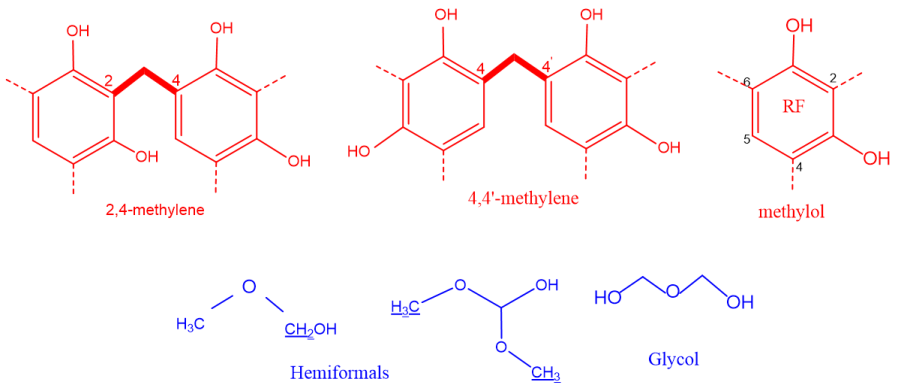

Figure 4.5 *Structure of methylenes and hemiformals expected to show on NMR spectra.*

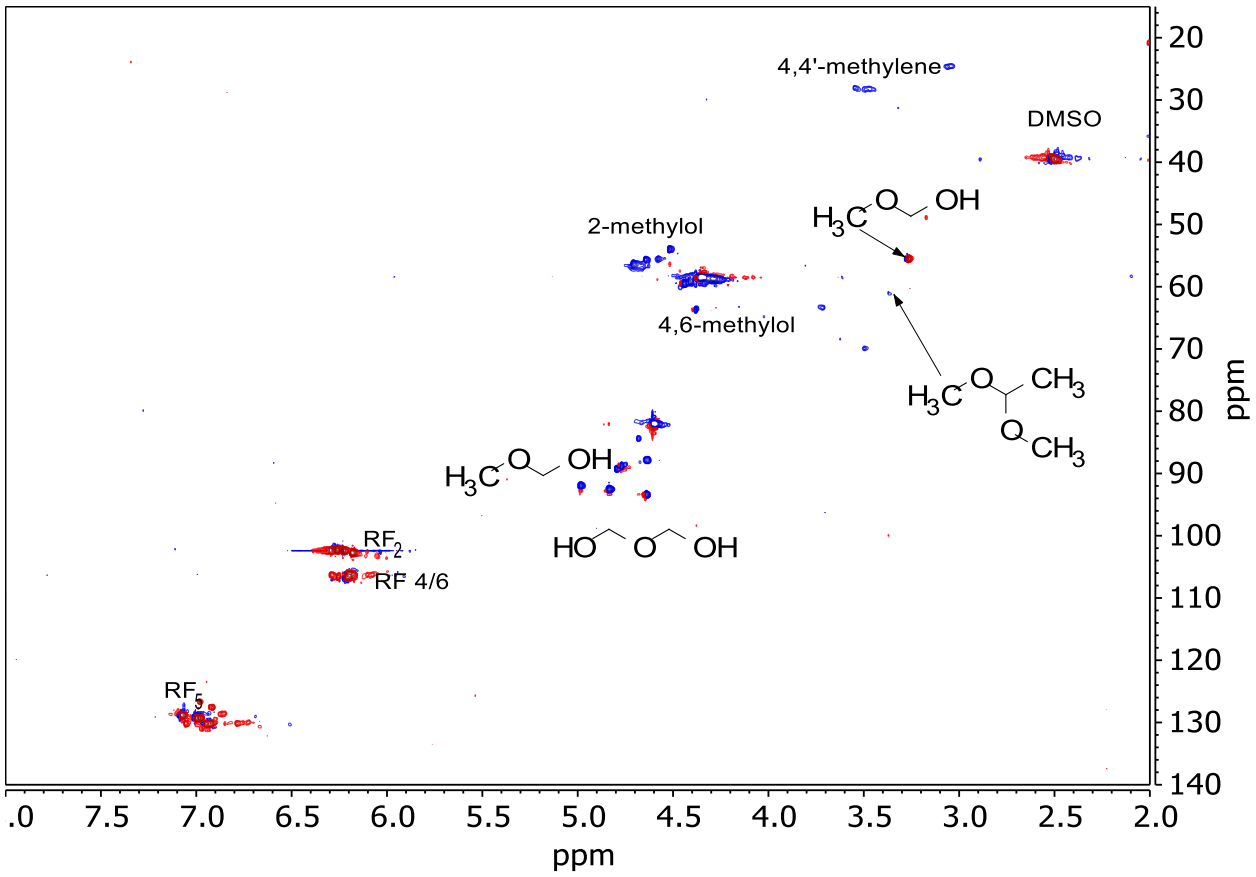

Figure 4.6 *HSQC spectra of HMR F/R 1.54*

The ^{13}C-NMR spectra of cured HMR resin is shown in Figure 4.7. ^{13}C-NMR spectra were assigned based on Christiansen (2000)[4] work for the late stage of resorcinol-formaldehyde reaction.[4] ^{13}C-NMR spectra of cured HMR showed signals of aromatic region confirmed the result of HSQC, while at the aliphatic region, carbon bonded to 2-methylol did not appear, only 4/6 substituted carbon was shown.

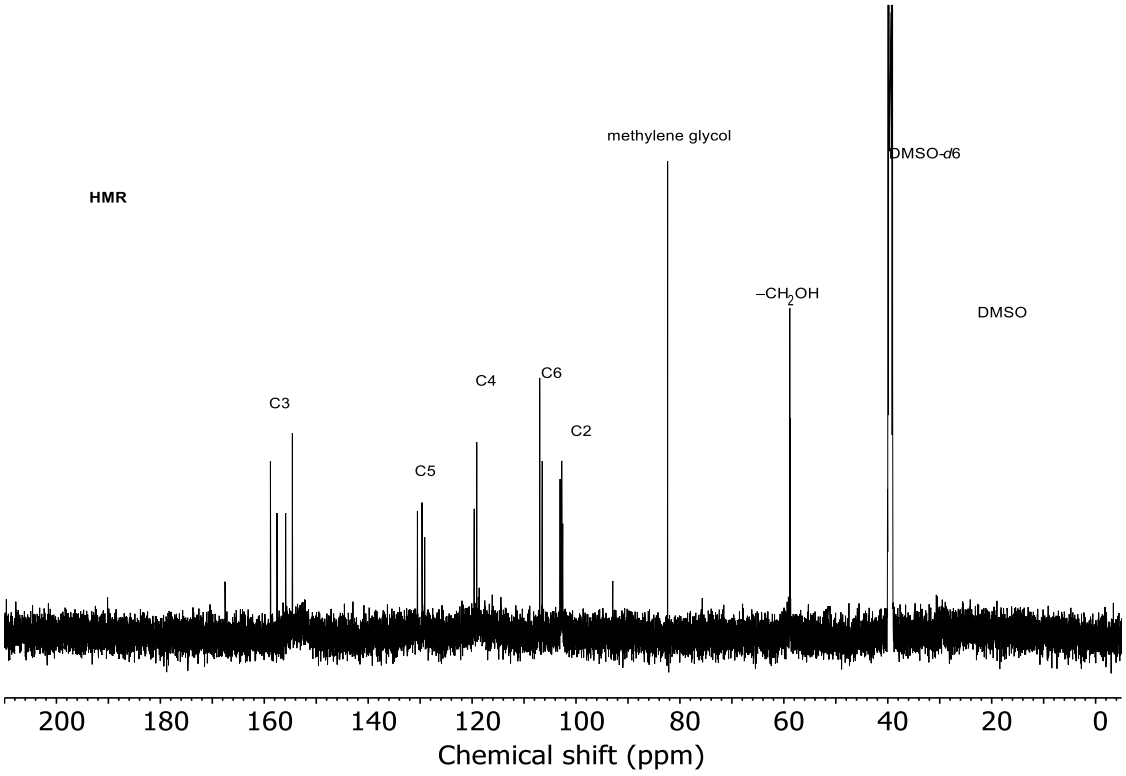

Figure 4.7 *^{13}C-NMR spectra of HMR F/R 1.54*

Important linkages in lignin are β-O-4, 5-5 biphenyl, β-5, β-1 and α-O-4.[26] The substructures to be seen in lignin extracted from Loblolly pine lignin have been reported to consist of β-aryl ether (**A**), phenylcoumaran (**B**), resinol (**C**), spirodienone, dibenzodioxocin, and guaiacyl (**G**). The

structure of each compound is shown in **Figure 4.8**.[11, 18, 19] We used Loblolly milled wood lignin which ball-milled for a total of 6h and extracted in aqueous dioxane.

The HSQC spectra of extracted lignin is shown in **Figure 4.9**. Lignin HSQC shows the domination of signal from β-aryl ether (**A**), phenylcoumaran (**B**) and guaiacyl (**G**), while signal from resinol (**C**) is not very strong, which has been reported by Sakakibara (1980)[26] that resinol β-β linkage is not abundant in softwood. Aliphatic region (3.0-5.5/50.0-90.0) ppm shows signal from β-aryl ether (**A**), phenylcoumaran (**B**) and resinol (**C**). The aromatic region shows signals from guaiacyl (**G**) carbons. Compared to sugar maple lignin spectra in Yelle's work (2017)[11], HSQC spectra of Loblolly pine lignin does not show xylan signal from O-acetyl-(4-O-methylglucuronoxylan) since softwood is low in xylan.

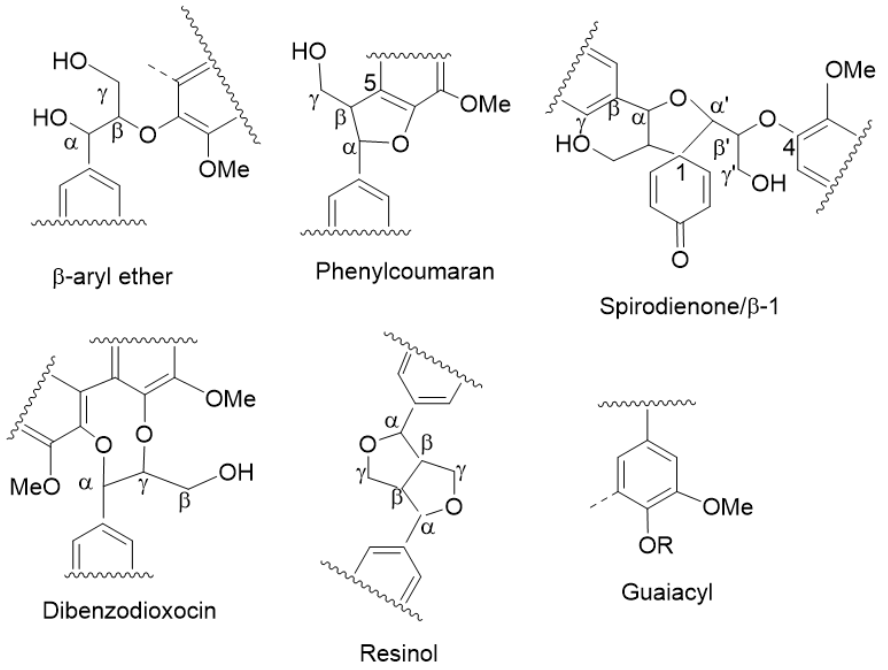

Figure 4.8 *Chemical compounds of Loblolly pine lignin substructures.*

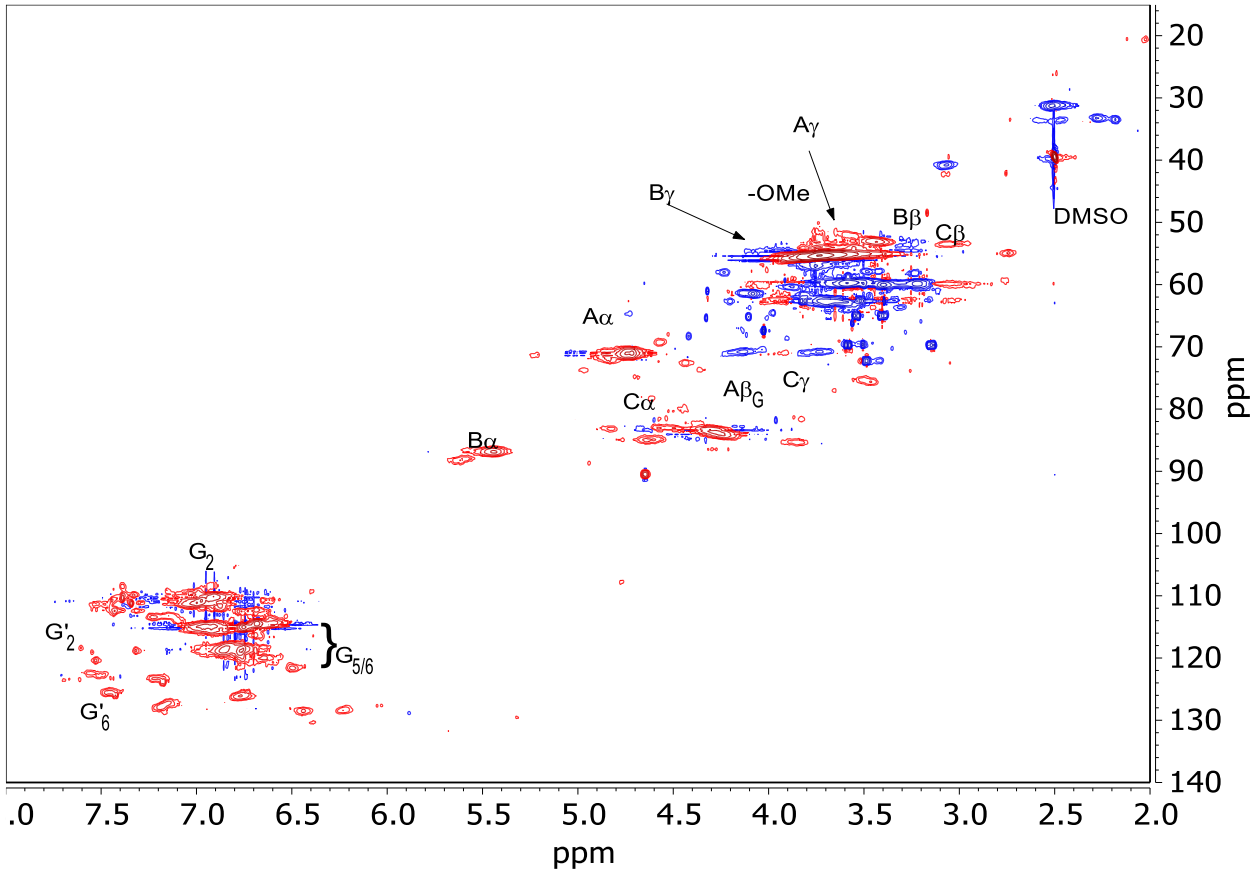

Figure 4.9 *HSQC spectra of Loblolly pine lignin in DMSO-d6*

The image of cured HMR resin in the presence of lignin is shown in **Figure 4.10.** Cured HMR-lignin resulted in a thin, brittle film. This film is slowly dissolved in DMSO-*d6* but produced enough signals for HSQC and ^{13}C-NMR scans. HSQC spectra of cured HMR/cMWL is shown in **Figure 4.11**. The spectra shows both signals from HMR and lignin. Two signals from HMR, 2,4-methylene and 4,4'-methylene signals are observed in cured HMR/cMWL aliphatic region at (3.58/25.29) and (3.47,28.01) ppm respectively, while 2,4-methylen is not observed in cured HMR. Meanwhile, Yelle's cured HMR-hardwood lignin only shows 4,4'-methylene signal. Methylols signals assigned for 2-methylol at (4.67/56.15) ppm and 4,6-methylol at (4.36/58.58) ppm is comparable to Yelle's spectra assignment for 2-methylol at (4.56/54) ppm and 4,6-methylol

at. Signals originated from lignin are observed at (3.0-5.5/55.0-70.00, weaker and narrower compared to the HSQC signal of lignin itself, but all lignin substructure units are shown.

Figure 4.10 *Cured HMR/cMWL.*

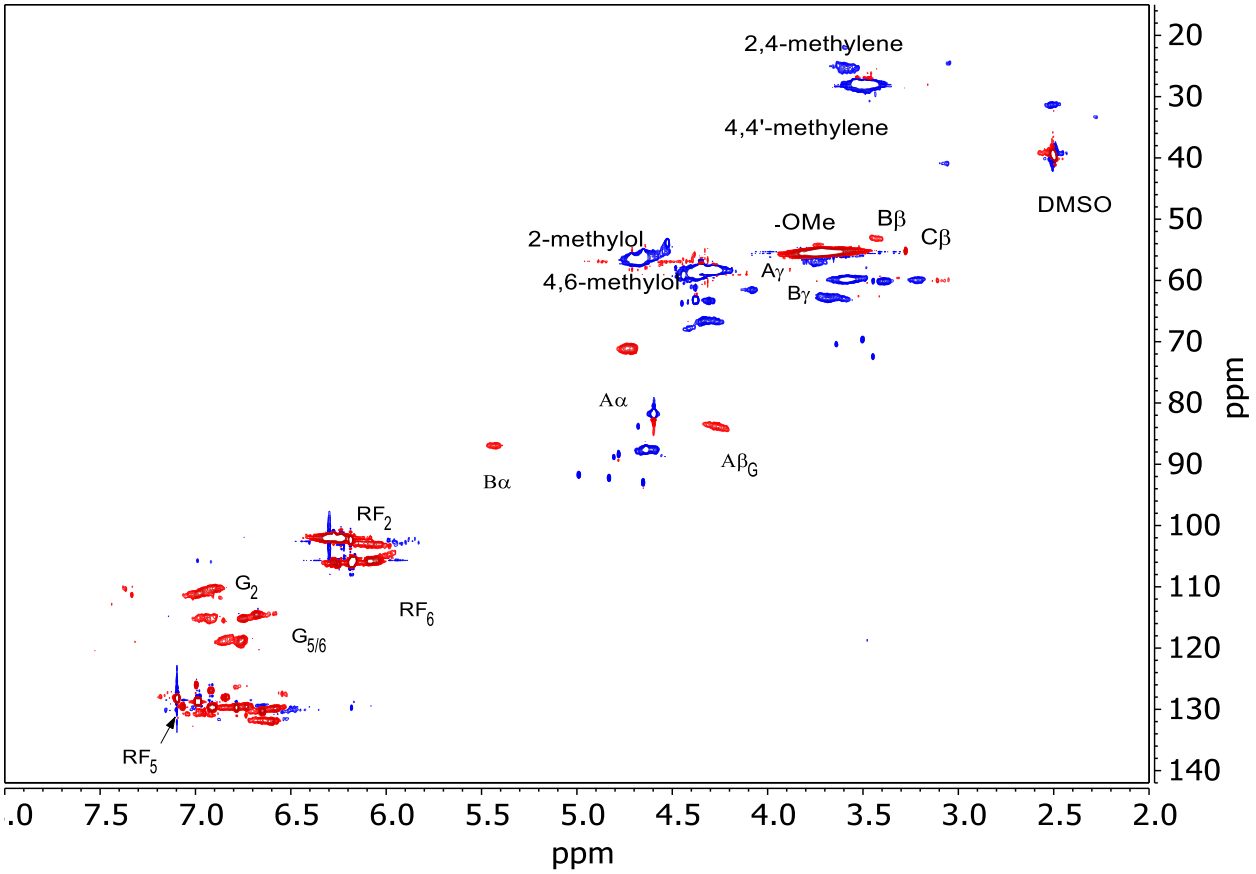

Figure 4.11 *HSQC spectra of HMR/cMWLin DMSO-d6*

The ^{13}C-NMR of cured HMR/cMWL spectra is shown in **Figure 4.12**. Based on Yelle[11] claimed, there are two ester carbonyls shown in the cured novolak-HMR in the presence of hardwood lignin at 172-174 ppm. Therefore, we expect to see the new ester carbonyl bond in this region. The^{13}C-NMR spectra of softwood lignin indicates the signals of carbonyl from benzaldehyde unit at 191 ppm and α-carbonyl signal from β-aryl ether at 194 ppm. Interestingly, these two carbonyl signals are not observed in the cured HMR-lignin ^{13}C-NMR spectra, but there is no signal that indicates new bond formation between the HMR resin and lignin. Signals from lignin major substructure unit linkages such as 5-5', β-O-4, β-1', 5-5/ β-O-4, α-O-4 at chemical shift 50-80 ppm are also weakened in the cured HMR-lignin, and this supports its HSQC spectra result (**Figure 4.11**) which show less strong signal from lignin substructures units.

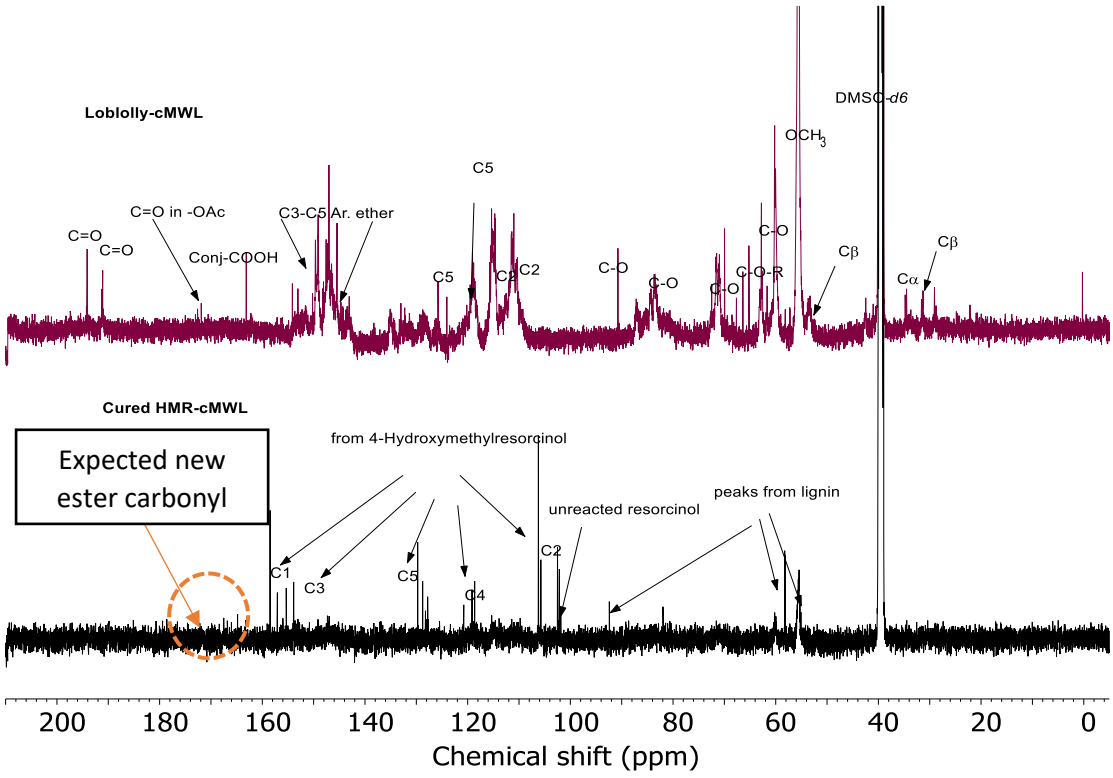

Figure 4.12 *^{13}C-NMR spectra of cMWL compared to cured HMR/cMWL*

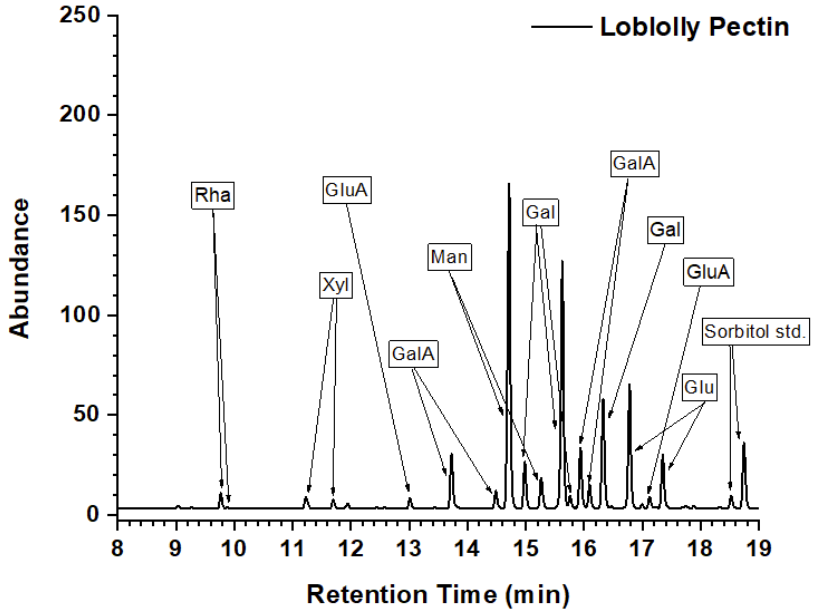

Figure 4.13 *GC spectra of Loblolly pectin*

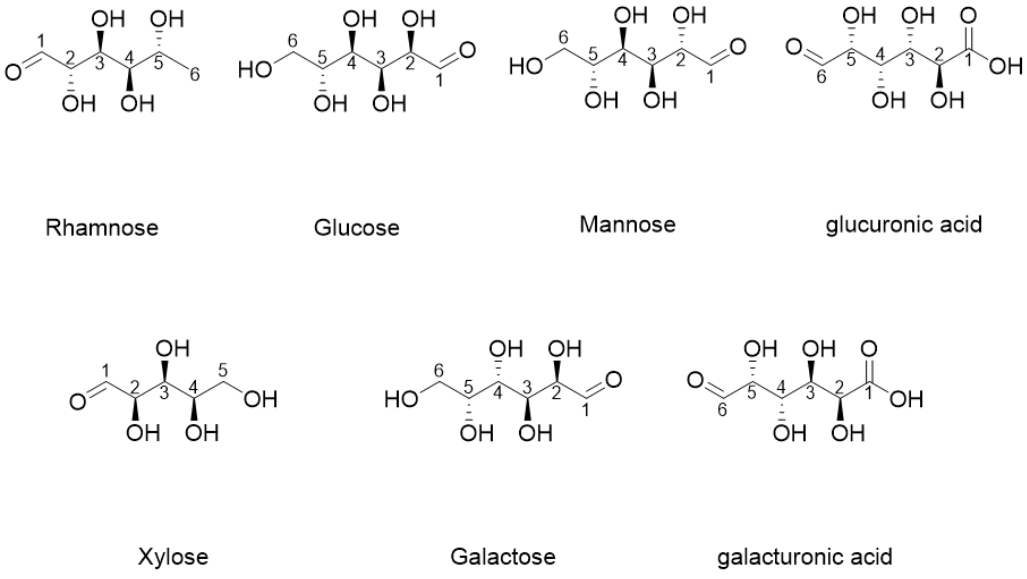

Figure 4.14 *Chemical structures of Loblolly pine pectin constituents.*

Pectic polysaccharide abundance in primary cell wall is approximately 30-50%.[27] Therefore, we looked at the possibility of HMR resin interactions with pectin. Pectin structure is different among sources, and we used gas chromatography (GC) to identify the constituent of pectin from Loblolly pine. The GC spectra of pectin is shown in **Figure 4.13**. Loblolly pectin has been identified to consist of rhamnose, glucose, mannose, glucuronic acid, xylose, galactose and galacturonic acids. Galactose and galacturonic acids are the two most abundant constituents in Loblolly pine pectin.

The HSQC spectra of loblolly pectin dissolved in D_2O solvent is shown in **Figure 4.15**. Since pectin alone is not well soluble in DMSO-*d6*, D_2O was used to obtain the HSQC spectra. The signals from esterified and non-esterified galactose and galacturonic acid residues are shown. The region in chemical shift (3.0-4.0/55.0-90.0) ppm are from C-2, 3, 4 and 5 of esterified and non-esterified galactose and galacturonic acid residues.

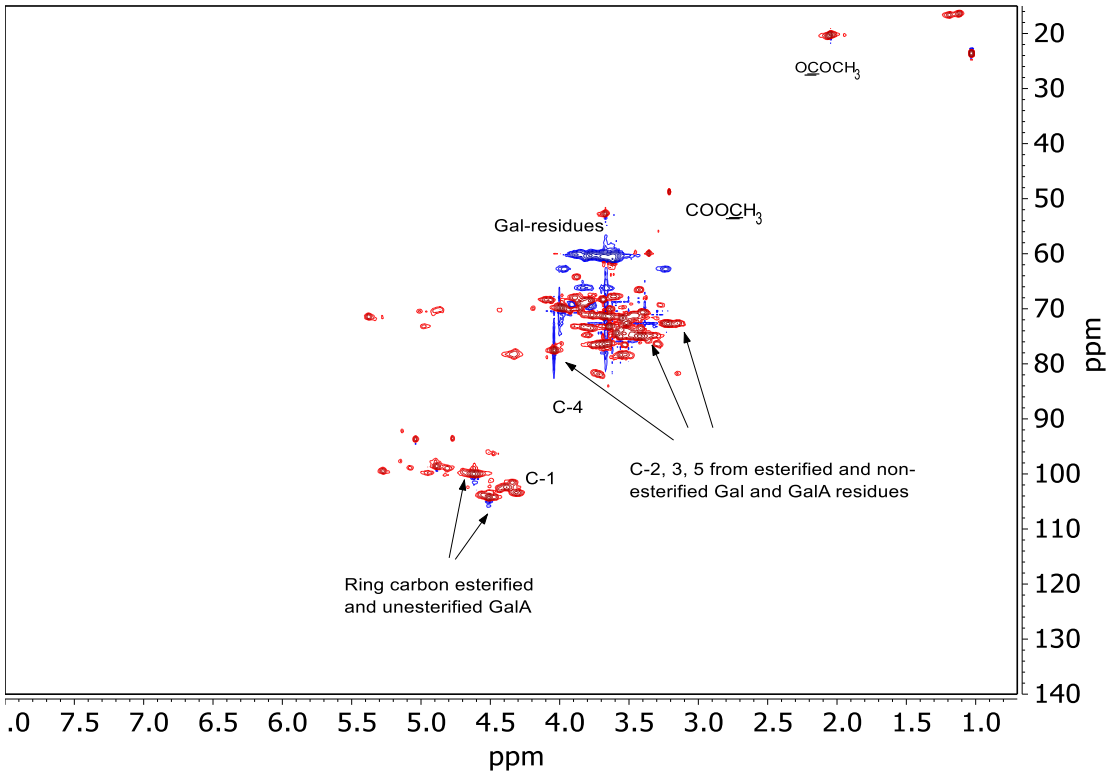

Figure 4.15 *HSQC spectra of Loblolly pectin in D_2O.*

Figure 4.16 *Cured HMR/pectin.*

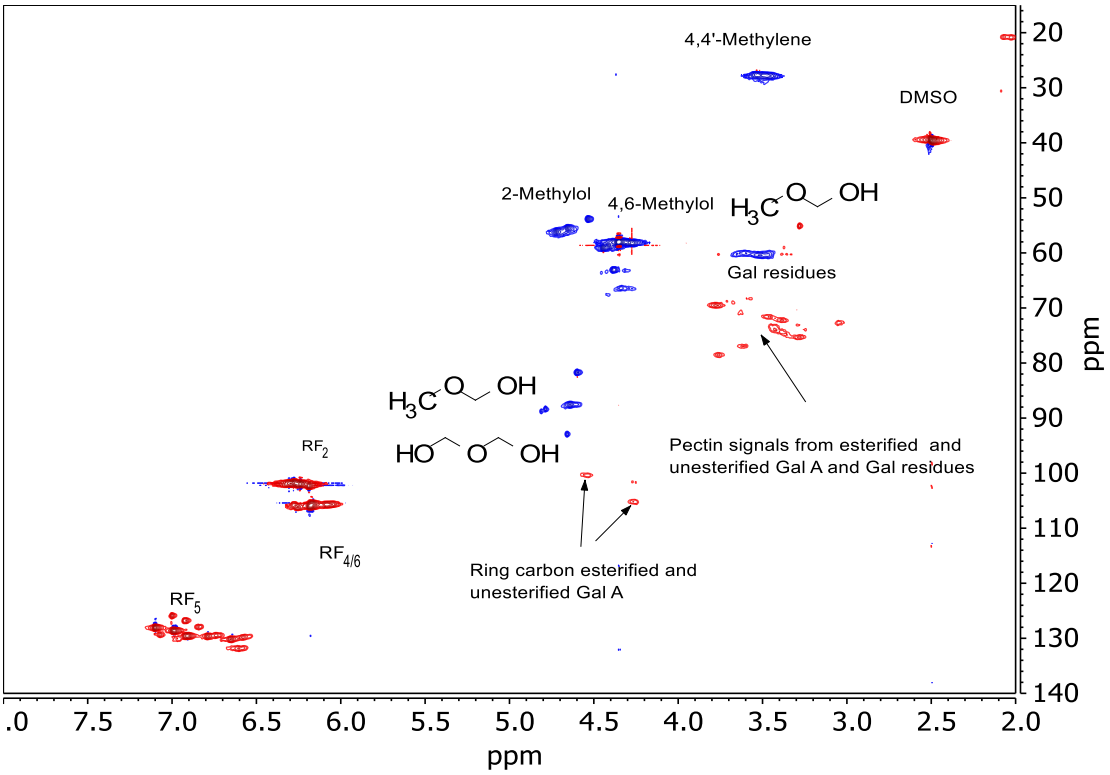

Figure 4.17 *HSQC spectra of cured HMR/pectin in DMSO-d6*

Cured HMR-pectin resulted in thin, brittle film (**Figure 4.16**). The HMR/pectin film is dissolved in DMSO-*d6* and therefore HSQC scan was performed using DMSO-*d6* solvent. The HSQC speactra of cured HMR is shown in **Figure 4.17**. Signals originated from HMR shown in aliphatic regions are 4,4'-methylene (3.52/27.78) ppm, 2-methylol at (4.67/56.15) ppm, and (4.37/58.67) ppm. The cured HMR/pectin do not show 2,4-methylene signals. At the aromatic region, signal from aromatic resorcinol formaldehyde (RF) ring were shown at the region (6.0-7.2/100-133) ppm. Signals originated from pectin were shown as residues of galacturonic acid and galactose at the aliphatic region of (3.1-3.7/59.0-82.0) ppm and ring carbon of esterified and non-esterified galacturonic acid at (4.3-4.6/105-110) ppm. Signal originated from esterified and non-esterified galactose and galacturonic acid residues are weakened in cured HMR-pectin.

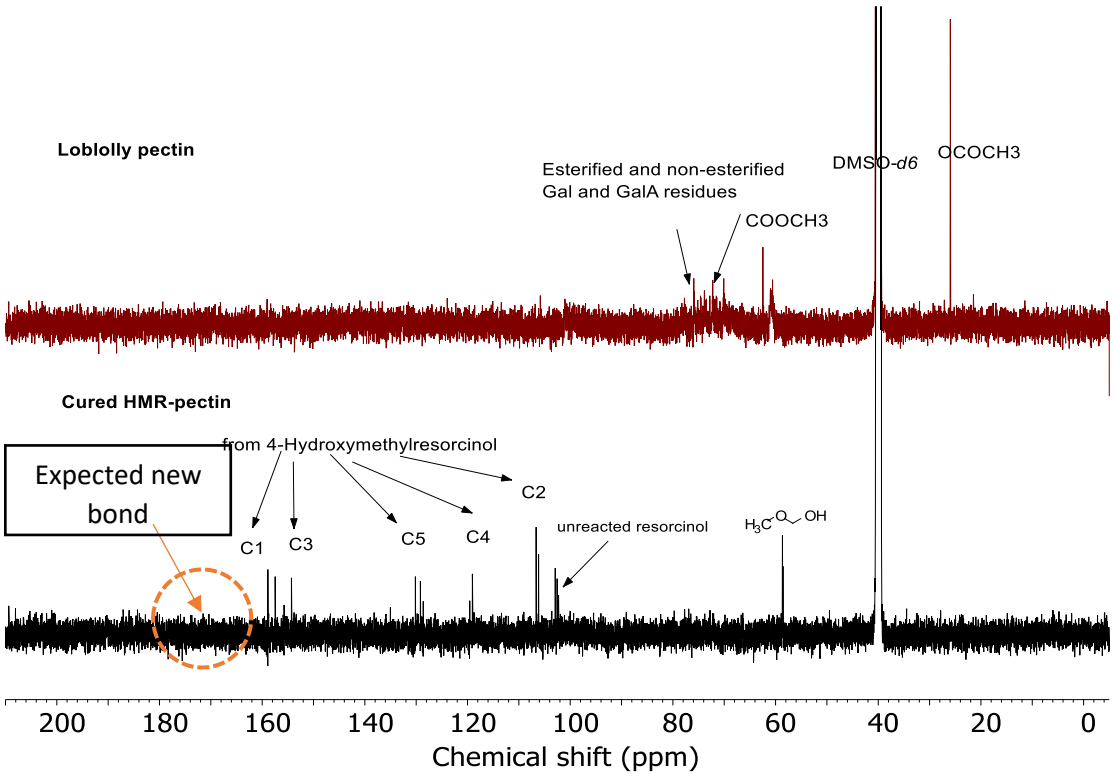

Figure 4.18 *^{13}C-NMR spectra of pectin compared to cured HMR/pectin.*

^{13}C-NMR spectra of pectin and cured HMR/pectin (**Figure 4.18**) are compared to see if there is new bond formed. The ^{13}C-NMR spectra of Loblolly pine pectin here was obtained in DMSO-*d6* to compare with the ^{13}C-NMR spectra of cured HMR/pectin. The cured HMR/pectin did not show any signals that originated from pectin. All signals in ^{13}C-NMR of cured HMR/pectin are showing HMR signals. We expect that the missing signal from pectin would be associated to the formation of new bond, but the cured HMR/pectin do not show any new signals corresponding to new ester carbonyl bond.

In Yelle's work[11], the cured HMR resin HSQC spectra of the HMR resin cured with hardwood lignin only shows 4,4'-methylene, while in the Novolak prepared-cured resin shows both 2,4-methylene and 4,4'-methylene bridges. Yelle claimed that the O-acetyl-(4-O-methylglucurono)xylan in hardwood avoids crosslinking at 2-position. We found that Yelle's HMR resin lack of formaldehyde due to stoichiometric error. The cured HMR resin prepared in this study does not show 2,4-methylene, but this is probably because we used HMR resin in the gel stage so it can be dissolved in NMR solvent.

The HSQC spectra cured HMR in the presence of softwood lignin shows both 2,4-methylene and 4,4'-methylene signals. Softwood is low in xylan, and thus crosslinking at C-2 position can occur. However, the HSQC spectra of the HMR resin cured with pectin, only 4,4-methylene was formed. Pectin is the source of O-acetyl group[28] and therefore it suggests that O-acetyl-(4-O-methylglucurono)xylan has stronger effect to block the crosslinking at 2-position.

^{13}C-NMR spectra for cured HMR-lignin indicates the missing of carbonyl signals at 191 and 194 ppm and the weakened signal in the lignin subunits region, while there is no new bond signal

shown. ^{13}C-NMR spectra for cured HMR-pectin are also missing the signal from esterified and non-esterified galactose and galacturonic acid residues. The HSQC spectra of cured HMR-lignin and cured HMR-pectin show the signal from HMR with weakened lignin subunits and galactose-galacturonic acid residues signals at the corresponding chemical shifts. This rejects Yelle's claim about the new ester carbonyl bond and suggests that HMR interaction with lignin/pectin occurs perhaps through permeation.

4.4 Conclusion

HSQC and ^{13}C-NMR scans were used to observe interaction between HMR resin with softwood cell wall constituent, lignin, and pectin. HSQC spectra of isolated lignin shows lignin's substructure unit signals at the aliphatic region is dominated by β-aryl ether (**A**), phenylcoumaran (**B**). The signal from guiacyl (**G**) unit is dominated the aromatic region. HSQC spectra obtained from the HMR resin cured in the presence of lignin showed both 2,4-methylene and 4,4'-methylene suggesting that softwood lignin, which low in xylan, does not hinder the crosslinking at C-2 position. Pectin isolated from Loblolly mainly consists of galactose and galacturonic acid, and therefore its HSQC spectra shows strong signal from esterified and non-esterified galactose and galacturonic acid residues. The HSQC spectra HMR cured in the presence of pectin was missing the 2,4-methylene. Pectin, which is the source of xylan, blocked crosslinking at C-2 position. HSQC spectra of cured HMR-lignin and HMR-pectin indicate weakened signals from lignin and pectin constituents that could be associated with HMR-lignin/pectin interaction through formation of new bond. However, ^{13}C-NMR spectra of both cured HMR-lignin and HMR-pectin do not show any evidence of formation new ester carbonyls linkage. The interaction of HMR with lignin or pectin perhaps occur via HMR permeation.

4.5 References

1. Vick, C. B.; Richter, K. H.; River, B. H. Hydroxymethylated Resorcinol for Coupling Agent and Method for Bonding Wood. 1996.

2. Vick, C. B. In *Hydroxymethylated Resorcinol Coupling Agent for Enhanced Adhesion of Epoxy and Other Thermosetting Adhesives to Wood*, Wood Adhesive, 1995.

3. Werstler, D. D., Quantitative 13C n.m.r. characterization of aqueous formaldehyde resins: 2. Resorcinolformaldehyde resins. *Polymer* **1986,** *27* (May), 757-764.

4. Christiansen, A. W., Resorcinol-Formaldehyde Reactions in Dilute Solution Observed by Carbon-13 NMR Spectroscopy. *J. Appl. Polym. Sci* **2000,** *75*, 1760-1768.

5. Christiansen, A. W.; Vick, C. B.; Okkonen, E. A. In *Enhanced Durability of One-Part Polyurethane Bonds to Wood Due to the Use of HMR Primer*, Forest Products Society Annual Meeting, South Lake Tahoe, NV, USA, South Lake Tahoe, NV, USA, 2000.

6. Vick, C. B.; Richter, K.; River, B. H.; Fried, A. R., Hydroxymethylated Resorcinol Coupling Agent for Enhanced Durability of Bisphenol-A Epoxy Bonds to Sitka Spruce *Wood and Fiber Science* **1995,** *27* (1), 2-12.

7. Okkonen, E. A.; Vick, C. B., Strength and Durability of One-Part Polyurethane Adhesive Bonds to Wood. *Forest Prod. J.* **1998,** *48* (11/12), 71-76.

8. Hunt, C. G.; Brandon, R.; Ibach, R. E.; Frihart, C. R. In *What does bonding to modified wood tell us about adhesion*, 5th COST E34 International Workshop, Bled, Slovenia, September, 6th; Ljubljana: Biotechnical Faculty, Dept. of Wood Science and Technology: Bled, Slovenia, 2007; pp 47-56.

9. Hill, C. A. S.; Papadopoulos, A. N.; Payne, D., Chemical modification employed as a means of probing the cell-wall micropore of pine sapwood. *Wood Science and Technology* **2004,** *37* (6), 475-488.

10. Son, J.; Tze, W. T. Y.; Gardner, D. J., Thermal Behavior of Hydroxymethylated Resorcinol Treated Maple Veneer. *Wood and Fiber Science* **2005,** *37*, 220-231.

11. Yelle, D. J., Solution-state NMR analysis of hydroxymethylated resorcinol cured in the presence of crude milled-wood lignin from Acer saccharum. *Journal of Applied Polymer Science* **2017,** *134* (41).

12. Fujimoto, A.; Matsumoto, Y.; Chang, H.-M.; Meshitsuka, G., Quantitative evaluation of milling effects on lignin structure during the isolation process of milled wood lignin. *Journal of Wood Science* **2005,** *51* (1), 89-91.

13. Crestini, C.; Melone, F.; Sette, M.; Saladino, R., Milled wood lignin: a linear oligomer. *Biomacromolecules* **2011,** *12* (11), 3928-35.

14. Bjorkman, A., Isolation of Lignin from Finely Divided Wood with Neutral Solvents. *Nature* **1954,** *174* (4440), 1057-1058.

15. Obst, J. R.; Laaducci, L. L., The Syringyl Content of Softwood Lignin. *Journal of Wood Chemistry and Technology* **1986,** *6* (3), 311-327.

16. Argyropoulos, D. S.; Jurasek, L.; Kristofova, L.; Xia, Z.; Sun, Y.; Palus, E., Abundance and Reactivity of Dibenzodioxocins in Softwood Lignin. *J. Agric. Food Chem.* **2002,** *50*, 658-666.

17. Kukkola, E. M.; Koutaniemi, S.; Gustafsson, M.; Karhunen, P.; Ruel, K.; Lundell, T. K.; Saranpaa, P.; Brunow, G.; Teeri, T. H.; Fagerstedt, K. V., Localization of dibenzodioxocin substructures in lignifying Norway spruce xylem by transmission electron microscopy-immunogold labeling. *Planta* **2003,** *217* (2), 229-37.

18. Min, D. Y.; Smith, S. W.; Chang, H. M.; Jameel, H., Influence of Isolation Condition on Structure of Milled Wood Lignin Characterized by Quantitative 13C Nuclear Magnetic Resonance Spectroscopy. *BioResources* **2013,** *8* (2), 1790-1800.

19. Huang, F.; Singh, P. M.; Ragauskas, A. J., Characterization of milled wood lignin (MWL) in Loblolly pine stem wood, residue, and bark. *J Agric Food Chem* **2011,** *59* (24), 12910-6.

20. Holtman, K. M.; Chang, H.; Jameel, H.; Kadla, J. F., Quantitative13C NMR Characterization of Milled Wood Lignins Isolated by Different Milling Techniques. *Journal of Wood Chemistry and Technology* **2006,** *26* (1), 21-34.

21. Vincken, J.-P.; Schols, H. A.; Oomen, R. J. F. J.; Beldman, G.; Visser, R. G. F.; Voragen, A. G. J., Pectin — the Hairy Thing. In *Advances in Pectin and Pectinase Research*, Voragen, F.; Schols, H.; Visser, R., Eds. Springer Netherlands: Dordrecht, 2003; pp 47-59.

22. Catoire, L.; Goldberg, R.; Pierron, M.; Morvan, C.; du Penhoat, C. H., Efficient procedure for studying pectin structure which combines limited depolymerization and 13C NMR. *Eur Biophys J.* **1998,** *27*, 127-136.

23. Mohnen, D., Pectin structure and biosynthesis. *Curr Opin Plant Biol* **2008,** *11* (3), 266-77.

24. Brauns, F. E., The Chemistry of lignin. *The Chemistry of lignin.* **1952**.

25. Gnanasambandam, R.; Proctor, A., Preparation of soy hull pectin. *Food Chem.* **1998,** *65*, 461-467.

26. Sakakibara, A., A structural model of softwood lignin. *Wood Sci. Technol.* **1980,** *14*, 89-100.

27. Cosgrove, D. J.; Jarvis, M. C., Comparative structure and biomechanics of plant primary and secondary cell walls. *Front Plant Sci* **2012,** *3*, 204.

28. Pawar, P. M.-A.; Koutaniemi, S.; Tenkanen, M.; Mellerowicz, E. J., Acetylation of woody lignocellulose: significance and regulation. *Frontiers in Plant Science* **2013,** *4*.

Chapter 5.

Summary and Future Work

This study used vanilla (*Vanilla planifolia*) seed coat and candlenut (*Aleurites moluccanus*) shell to represent tissues with catechyl (C)-lignin for studying C-lignin structure/property relationship in the context plant evolution. In Chapter 2, light and electron microscopy is used to study vanilla seed coat and candlenut shell morphology. Intact tissues are used to identify seed size, surface texture, and seed coat/nutshell thickness. A partially macerated technique is developed to identify cell type and size of seed coat and nutshell. Partially macerated technique is more useful for cell type and size determination, since it gives better cell's visualization than intact observation and it also prevents cell from overlapping as can be occurred in fully macerated cell.

In Chapter 3, C-lignin crystallinity is studied using X-ray diffraction. OriginLab analytical software is used to separate peaks in XRD diffractograms. We used wood's diffractogram as a reference to identify crystallographic plane in vanilla seed coat and candlenut shell. We use the peak deconvolution method to calculate % crystallinity. The peak deconvolution method is more useful to be used on highly amorphous material such as vanilla seed coat and candlenut shell since it can easily distinguish amorphous constituent from the crystalline constituent. However, in Southern Yellow Pine, which cellulose content is high, this method does not easily separate the amorphous constituent to crystalline constituent in cellulose.

Compressive-torsion DMA allows glass transition temperature (T_g) measurement of *in-situ* catechyl lignin. Solvent-submersion techniques allow T_g measurements within the non-damaging temperature. Due to vanilla seed coat and candlenut shell shape and size, specimen preparation must be taken very carefully, and specimens need to be saturated in plasticizer. Vanilla seed coat

needs to be separated from the embryo and endosperm, and candlenut shell needs to be cut/grind to fit 8 mm-parallel plate DMA. All specimens used in the measurement are saturated for at least 3 days, the minimum required saturation period which is determined using simple compression testing. These all steps ensure that vanilla seed coat and candlenut shell's T_gs can be measured using DMA instrument.

Overall, this dissertation has provided insights on newly discovered C-lignin's structure/property relationships. C-lignin has been known for its highly acid-resistant and projected as the ideal lignin for biorefinery. The use of combination approaches has facilitated this study to explain cellular, crystallinity and thermomechanical aspects of tissues which exhibit C-lignin. This research should initiate the effort to synthesize C-lignin and more exploration in other plants' sources of C-lignin.